

Dipl. Ing. Sigrid Egger

**From molecular mechanism to biocatalytic applications
of sugar oxidoreductases:**

Structure and catalytic mechanism of human UDP-glucose
dehydrogenase and development of whole-cell catalysts for
enantioselective synthesis of chiral alcohols

DISSERTATION

Zur Erlangung des akademischen Grades einer
Doktorin der technischen Wissenschaften

erreicht an der

Technischen Universität Graz

Univ. Prof. Dr. Bernd NIDETZKY

Institut für Biotechnologie und Bioprozesstechnik

Technische Universität Graz

2010

Deutsche Fassung:
Beschluss der Curricula-Kommission für Bachelor-, Master- und Diplomstudien vom 10.11.2008
Genehmigung des Senates am 1.12.2008

EIDESSTATTLICHE ERKLÄRUNG

Ich erkläre an Eides statt, dass ich die vorliegende Arbeit selbstständig verfasst, andere als die angegebenen Quellen/Hilfsmittel nicht benutzt, und die den benutzten Quellen wörtlich und inhaltlich entnommene Stellen als solche kenntlich gemacht habe.

Graz, am

.....
(Unterschrift)

Englische Fassung:

STATUTORY DECLARATION

I declare that I have authored this thesis independently, that I have not used other than the declared sources / resources, and that I have explicitly marked all material which has been quoted either literally or by content from the used sources.

.....
date

.....
(signature)

Acknowledgements

Most of all I want to thank my supervisor Prof. Bernd Nidetzky for sharing his enthusiasm for science and continuous encouragement even in challenging times. Lively discussions and inspiring ideas to overcome the obstacles on the way of the thesis project provided the optimal framework to develop my scientific and personal skills. Furthermore, I am very grateful for the constructive discussions with the members of my thesis committee, Prof. Albin Hermetter, Prof. Ulrike Wagner, and Dr. Harald Pichler.

I would like to thank all the members of the Institute of Biotechnology and Biochemical Engineering for the friendly work atmosphere and sharing their personal knowledge with various techniques and methods (especially Dr. Mario Klimacek, Dr. Christiane Luley). Special thanks to the very fruitful and motivating close collaboration with Dr. Regina Kratzer in the biotransformation project.

Special thanks to my past and present office colleagues Dr. Simone Pival, Dr. Malene Thomsen, Dr. Stefan Leitgeb and Dipl. Ing. Patricia Bubner for their support and stimulating discussions.

During my project I had the great opportunity for a 9 month research stay at University of Oxford, UK, at the Structural Genomics Consortium (SGC) in the group of Prof. Udo Oppermann. It was an outstanding, challenging and productive experience. Cordial thanks to the SGC collaborators for their professional and moral support, especially Dr. Kate Kavanagh, Dr. Apirat Chaikuad, Dr. Panagis Filippakopoulos and Dr. Ivan Alfano.

Financial support from the DK Molecular Enzymology W901-B05 is gratefully acknowledged. Thanks to Prof. Ellen Zechner, Dr. Michaela Hiden and Annemarie Portschy for the excellent cooperation. Additional thanks to all the graduate students within the DK for inspiring scientific discussions and fellowship.

Sincere thanks to my friends and family for their continuous support and faith.

Read, every day, something no one else is reading.

Think, every day, something no one else is thinking.

Do, every day, something no one else would be silly enough to do.

It is bad for the mind to be always part of unanimity.

Christopher Morley

Abstract

Oxidoreductive transformations of sugars are key steps of cellular metabolism and have numerous important applications in biotechnology. The research resulting in this thesis is divided into two parts. In the first part, structure and function of human UDP-glucose 6-dehydrogenase (hUGDH) was studied. In the second part, xylose reductase from the yeast *Candida tenuis* (CtXR) was applied in the development of whole-cell catalysts for synthesis of chiral alcohols.

hUGDH catalyzes in two successive NAD⁺-dependent oxidations the conversion of UDP-glucose into UDP-glucuronic acid, without release of the intermediate aldehyde. The enzyme thus combines an alcohol and aldehyde dehydrogenase activity in one catalytic centre. In mammals, the product serves as precursor for biosynthesis of glycosaminoglycans like heparin, hyaluronic acid and chondroitin sulphate. Elevated levels of hyaluronan are implicated in epithelial tumor progression and inhibition of hyaluronan synthesis restricts *in vivo* tumor growth. Recently, UGDH was proposed as novel biomarker for prostate cancer. A detailed structural portrayal of the reaction coordinate of hUGDH is presented that includes for the first time clear evidence of formation of a covalent thiohemiacetal reaction intermediate. Steady-state and transient kinetic analysis of reactions catalyzed by wild-type hUGDH and site-directed mutants thereof allowed assignment of catalytic function to active-site residues in each step of twofold oxidation. The crystallographic data and evidence from mechanistic studies provide information exploitable in the development of enzyme inhibitors in cancer therapy.

A special feature of CtXR is its extremely broad substrate scope, which includes in addition to the natural substrate xylose, various non-natural ketones that are precursors of industrially relevant (chiral) alcohols. CtXR converts these ketones with excellent enantioselectivity. However, the free enzyme is inactivated quickly in the presence of organic substrate. To obtain more robust reductase catalyst for technological application, whole-cell systems based on *Escherichia coli* and *Saccharomyces cerevisiae* were constructed. Ideally, these biocatalysts should combine the benefits of CtXR with the additional advantages of internal coenzyme regeneration, higher catalyst stability and simple catalyst preparation. Thus, whole-cell catalyzed production of chiral alcohols could outpace classical chemical synthesis or the use of isolated enzymes in terms of cost, optical purity, efficiency and environmental impact. Using a multi-level engineering approach based on

enzyme, strain and reaction engineering, both whole-cell catalyst systems were optimized for high yields and purities of >99% enantiomeric excess in the production of chiral secondary alcohols by preventing byproduct formation and enhanced cofactor regeneration within the cell.

Zusammenfassung

Oxidoreduktionen von Zuckersubstraten sind wesentliche Bestandteile des zellulären Metabolismus und finden zahlreiche Anwendungen in der Biotechnologie. Die Forschungsarbeiten dieser Dissertation sind in zwei Teile untergliedert. Der erste Teil beschäftigt sich mit Struktur und Funktion der menschlichen UDP-glucose 6-dehydrogenase (hUGDH). Im zweiten Teil wurde mit Xylose Reduktase aus der Hefe *Candida tenuis* (CtXR) die Anwendung von Ganz-zell Katalysatoren zur Synthese chiraler Alkohole optimiert.

UDP-glucose dehydrogenase (UGDH) katalysiert die NAD^+ abhängige Reaktion von UDP-glucose zu UDP-glucuronsäure. Das als Intermediat gebildete Aldehyd bleibt während der gesamten Umsetzung an das Enzym gebunden. Somit vereint das Protein eine Alkohol- und Aldehyd Dehydrogenase Aktivität in einem katalytischen Zentrum. Das Produkt der Reaktion, UDP-glucuronsäure spielt bei Säugetieren eine wichtige Rolle in der Bioynthese von Glycosaminoglykanen wie z.B. Heparin, Hyaluronsäure und Chondroitin Sulfat. Eine Erhöhung der Hyaluronanwerte im Gewebe von epithelialen Tumoren und Inhibierung der malignen Ausbreitung des Tumors durch gezielte Unterdrückung der Hyaluronan Synthese wurden festgestellt. Weiters wurde UGDH als neuer Biomarker für Prostatakrebs vorgeschlagen. Im Rahmen dieser Arbeit präsentieren wir die ersten Proteinstrukturen für eine Veranschaulichung der wichtigsten Schritte im Laufe der Reaktion, besonders das kovalent gebundene Intermediat. Transiente kinetische Analyse sowie Untersuchung von Mutanten ermöglichen eine Unterscheidung der zwei hintereinander ablaufenden Reaktionen. Das Verständnis des detaillierten Reaktionsmechanismus liefert die Grundlage für weiters Design von Inhibitoren in der Krebstherapie.

Eine Besonderheit der CtXR ist die breite Substratspezifität nicht nur vom natürlichen Substrat Xylose sondern auch vielen anderen wie z.B. α -Keto Estern zur Herstellung von chiralen Alkoholen für die pharmazeutische Industrie mit ausgezeichneter Enantioselektivität. Das freie Enzym wird rasch inaktiviert durch das organische Substrat. Biokatalysatoren aus ganzen Zellen kombinieren die Vorteile einer Reduktase mit internem Kofaktor Recyclingsystem, höherer Stabilität und einfacher Herstellung im Vergleich zu klassischer chemischer Synthese oder dem Einsatz isolierter Enzyme aufgrund von Kosten, optischer Reinheit, Effizienz und Umweltverträglichkeit. Das Ziel der Arbeit ist die Anwendung von CtXR in der

Biokatalyse von ganzen Zellen mit den populärsten Systemen *Saccharomyces cerevisiae* and *Escherichia coli*. Mit einer vielseitigen Optimierungsstrategie wurden beide Stämme verbessert um mit guter Ausbeute und hoher Enantiomerenreinheit (>99%) chirale sekundäre Alkohole herzustellen. Dabei wurde auf eine Unterdrückung von Nebenreaktionen und Optimierung des Kofaktor Recyclingsystems besonderes Augenmerk gelegt.

Table of contents

Part I

UDP-glucose dehydrogenase: structure and function of a potential drug target

Sigrid Egger, Apirat Chaikuad, Kathryn L. Kavanagh, Udo Oppermann, and Bernd Nidetzky

Biochem. Soc. Transact., submitted. 1

Structure and mechanism of human UDP-glucose dehydrogenase

Sigrid Egger, Apirat Chaikuad, Kathryn L. Kavanagh, Udo Oppermann and Bernd Nidetzky

Manuscript in preparation. 18

Supplementary Information 35

Part II

Integration of enzyme, strain and reaction engineering to overcome limitations of baker's yeast in the asymmetric reduction of α -keto esters

Regina Kratzer Sigrid Egger, Bernd Nidetzky

Biotechnology and Bioengineering, Vol. 101, No. 5, 2008. 52

Whole-cell bioreduction of aromatic α -keto esters using *Candida tenuis* xylose reductase and *Candida boidinii* formate dehydrogenase co-expressed in *Escherichia coli*

Regina Kratzer, Matej Pukl, Sigrid Egger and Bernd Nidetzky

Microbial Cell Factories 2008, 7:37. 60

Enzyme identification and development of a whole-cell biotransformation for asymmetric reduction of *o*-chloroacetophenone

Regina Kratzer, Matej Pukl, Sigrid Egger, Michael Vogl, Lothar Brecker and Bernd Nidetzky

Biotechnology and Bioengineering, submitted. 72

Curriculum vitae and list of publications 111

UDP-glucose dehydrogenase: structure and function of a potential drug target

Sigrid Egger¹, Apirat Chaikuad², Kathryn L. Kavanagh², Udo Oppermann², and Bernd Nidetzky¹

¹Institute of Biotechnology and Biochemical Engineering, Graz University of Technology, Petersgasse 12, A-8010 Graz, Austria

²Structural Genomics Consortium, University of Oxford, Old Road Campus Research Building, Roosevelt Drive, Headington, Oxford OX3 7DQ, United Kingdom

* Corresponding author; Tel. +43 316 873 8400; E-mail: bernd.nidetzky@tugraz.at

Keywords: UDP-glucose dehydrogenase, UDP-glucuronic acid, structure, catalytic mechanism, hyaluronan, cancer

Abbreviations: UGDH, UDP- α -D-glucose 6-dehydrogenase; UDP-GlcA, UDP- α -D-glucuronic acid; UDP-Glc, UDP- α -D-glucose; SpUGDH, *Streptococcus pyogenes* UGDH; CeUGDH, *Caenorhabditis elegans* UGDH

Abstract

Biosynthesis of the glycosaminoglycan precursor UDP- α -D-glucuronic acid occurs through a twofold oxidation of UDP- α -D-glucose that is catalysed by UDP- α -D-glucose 6-dehydrogenase (UGDH). Structure-function relationships for UGDH and proposals for the enzymatic reaction mechanism are reviewed. Structure-based sequence comparison is used for sub-classification of UGDH family members. The eukaryotic group of enzymes (UGDH-II) utilise an extended C-terminal domain for formation of complex homohexameric assemblies. The comparably simpler oligomerisation behaviour of the prokaryotic group of enzymes (UGDH-I), in which dimeric forms prevail, is traced back to the lack of relevant intersubunit contacts and trimmings within the C-terminal region. The active site of UGDH contains a highly conserved cysteine, which plays a key role in covalent catalysis. Elevated glycosaminoglycan formation is implicated in a variety of human diseases, including the progression of tumors. Inhibition of synthesis of UDP- α -D-glucuronic acid using UGDH antagonists might therefore be a useful strategy for therapy.

UDP- α -D-glucuronic acid (UDP-GlcA), the activated form of D-glucuronic acid in cellular metabolism, plays a central role in a variety of biosynthetic pathways as well as in detoxification processes. UDP-GlcA is the donor substrate for different UDP-glucuronosyltransferases, promoting the incorporation of D-glucuronosyl residues into nascent glycosaminoglycans such as hyaluronan [1] or catalysing O-glucuronidation of small molecules in xenobiotic metabolism [2]. In addition, UDP-GlcA functions as precursor in biosynthesis of different carbohydrates, UDP- α -D-xylose and L-ascorbate for example [3]. UDP- α -D-glucose 6-dehydrogenase (UGDH; EC 1.1.1.22) is the enzyme responsible for formation of UDP-GlcA in a multitude of organisms ranging from bacteria to mammals. UGDH catalyses a twofold oxidation of UDP- α -D-glucose (UDP-Glc) using a nicotinamide adenine dinucleotide, typically NAD⁺, as the oxidant. The overall reaction catalysed by UGDH is (Equation 1):



UGDH was first described [4, 5] and biochemically characterised [6-23] from bovine liver. The enzyme has since been reported from a variety of organisms [24-34] and UGDH-encoding genes have been found in members of all three domains of life, e.g. [24, 31, 34]. UGDH from mammals has recently attracted special interest as it was established that elevated levels of the matrix glycosaminoglycan hyaluronan are directly implicated in the progression of various forms of epithelial cancer [35-41]. Reduced formation of UDP-GlcA restricts hyaluronan production and this in turn was shown to slow tumor growth [42, 43]. UGDH was recently proposed as biomarker for prostate cancer [44]. Inhibition of UGDH therefore presents a potential target for novel therapeutic strategies. Well defined structure-function relationships for UGDH are instrumental in a rational development of enzyme antagonists. This review provides an update on the properties of UGDH and described proposals for the catalytic mechanism of the enzyme. Inhibition of UGDH is also discussed.

Sequence-based classification and structural analysis of UGDH

More than 1000 open-reading frames are retrieved from the UniProt database using the respective EC number for UGDH “EC:1.1.1.22” as search query. Figure S1 (supporting information) shows a multiple sequence alignment for a representative selection of UGDH enzymes. The crystal structures of UGDH from *Streptococcus pyogenes* (SpUGDH; PDB identifiers: 1DLI and 1DLJ) [45] and *Caenorhabditis elegans* (CeUGDH; PDB identifier: 2O3J) are used to obtain relevant structure-function assignments. In Figure S1, secondary structural elements of CeUGDH and SpUGDH are mapped on the corresponding linear sequence of each enzyme. UGDH folds into two domains that both adopt a highly similar α/β -fold with a β -sheet core flanked by several α -helices. The two domains are connected by a central α -helix

(*Ce*UGDH α 10 and *Sp*UGDH α 9), which is approximately 48 Å long and bridges the last strand of the N-terminal region and the first helix of a three-helical bundle of the C-terminal domain (Figure 1A) [45]. The N-terminal domain is responsible for binding NAD⁺ whereas the C-terminal domain primarily contributes residues for binding of the UDP moiety of UDP-Glc. Catalysis takes place at the interdomain cleft (see later), and the active site of the enzyme is situated on top of the central interdomain α -helix.

UGDH enzymes can be categorised according to molecular size into a group (UGDH-I) consisting of proteins whose length of ~ 380 - 460 amino acids is substantially shorter than that of proteins of the second group (UGDH-II; ~ 480 - 500 amino acids). Sub-classification of UGDHs into two groups appears to reflect the source of the enzymes. UGDH-I members are typically from lower organisms of the domains Prokaryota and Archaea whereas enzymes belonging to UGDH-II are from higher and lower Eukaryota. Membership to UGDH-I is also indicated by a conserved internal peptide whose consensus sequence is AExxK(Y/L)(F/A)xNX(F/Y)LAx(K/R)(I/V)(S/A)(F/Y)(I/F)N(E/D) where x is any amino acid and the amino acids in parenthesis may be substituted one by another at the same position (Figure S1). The characteristic signature for the corresponding internal region of UGDH-II is WS(S/A)ELSKLxANA(F/M)LAQRIS(I/V)N(S/A)xSA-(I/L/V)CEATGA, as shown in Figure S1. In each UGDH-I and UGDH-II, the conserved internal peptide is responsible for formation of the interdomain α helix (*Ce*UGDH α 10 and *Sp*UGDH α 9) that represents a key secondary structural component of enzyme subunit and serves as the core of the dimer interface in *Sp*UGDH (Figure 1A). The α 9 helix was shown to contribute 37% of the interface solvent-inaccessible surface area in the crystallographic dimer of *Sp*UGDH. The largest portion (52%) of this surface area is provided by the C-terminal domain (α 10 – α 12) and interestingly, differences between enzymes of UGDH-I and UGDH-II are most pronounced in the C-terminal region (Figure S1). Residues involved in making dimer contacts in *Sp*UGDH are relatively well conserved among UGDH-I members but differ compared to UGDH-II group. Figure S1 therefore supports a distinction between UGDH-I and UGDH-II based on the interactions responsible for dimer and higher oligomer contact formation. In *Sp*UGDH a network of 31 hydrogen bonds stabilise the dimer interface. Within UGDH-I, aromatic amino acids dominate the dimer interface, mainly residues of α 9 (Phe206, Tyr210, Tyr217, Tyr224) and α 11 (Tyr272) [45] as indicated in Figure S1. Corresponding residues involved in dimer formation in UGDH-II diverge from those seen in UGDH-I, for *Ce*UGDH on helices α 10 (Val229, Phe233, Ser240, Val247) and α 13 (Cys295). Furthermore, in *Ce*UGDH, a network of 34 hydrogen bonds stabilise the interface. Interestingly, amino acids playing a role in forming the hexameric arrangement in *Ce*UGDH are only

conserved within UGDH-II (13 out of 36 are strictly conserved) whereas in UGDH-I corresponding amino acids cannot be found (Figure S1).

Biochemical data for different members of the UGDH-I group corroborate the notion from the crystal structure of *Sp*UGDH that these enzymes have a homodimeric quaternary structural organisation [45]. Figure 1A shows that orientation of the *Sp*UGDH subunits is “back-to-back” (with the position of the active site considered to be the front side) and “head-to-tail”. However, liver UGDH and other members of group UGDH-II are reported to predominantly exist as homo-hexamers [21, 46]. “Half-the-sites” reactivity was proposed for the liver enzyme, arguably indicating that the enzyme could function as a trimer of dimers [19]. An unpublished crystal structure of UGDH from *Caenorhabditis elegans* (*Ce*UGDH; PDB identifier: 2O3J), a member of the UGDH-II group, shows a disc-shaped homo-hexamer, which is assembled from three dimers whose overall structural organisation is highly homologous to that of the *Sp*UGDH dimer (Figure 1B). More detailed structural comparison of *Sp*UGDH and *Ce*UGDH (Figure 1C) reveals that the N-terminal domains of the two proteins share a large amount of similarity whereas structural divergence is observed for the C-terminal domain. The extended C-terminus of *Ce*UGDH results in an increased number of β -strands in the core of the domain, as compared to *Sp*UGDH. The C-terminal region of the bacterial enzyme, by contrast, is more flexible than that of *Ce*UGDH and packs on top of the uridine moiety of bound substrate. The extended and structured C-terminus of *Ce*UGDH (Figure 1C) and by extension (Figure S1), that of other UGDH-II enzymes, seem to assist in dimer-dimer interaction within the hexameric arrangement. These higher oligomeric contacts leading to “trimerisation” of the dimers are not available to *Sp*UGDH and other UGDH-I enzymes. Despite recent investigations [47], the role of dimer oligomerisation for UGDH enzyme function is currently not clear. Although the assembly of *Sp*UGDH and *Ce*UGDH subunits into dimers is highly similar, the intersubunit contacts utilised in formation of this “core” UGDH oligomer are different in the two enzymes.

The structure of *Ce*UGDH was obtained from protein crystallised in the absence of ligands (PDB identifier: 2O3J). However, structural superimposition of *Ce*UGDH (apo-form) and *Sp*UGDH (ternary complex with UDP- α -D-xylose and NAD⁺) reveals that residues involved in binding of substrate and coenzyme are largely conserved in the two enzymes. Residue conservation in functional sites spans both UGDH-I and UGDH-II groups. Amino acid variations in the binding pockets for UDP-Glc and NAD⁺ are restricted primarily to non-polar residues, which are unlikely to be essential for UGDH enzymatic function. The structure of the enzyme active site appears to be highly conserved among members of UGDH-I and UGDH-II. First and second-shell residues that are essentially invariant across the entire UGDH family are Cys260, Asp264, Lys204, Asn208, Thr118, Glu141, and Glu145 (Figure S1). Of these, Cys260 plays a

central role in the enzymatic mechanism, participating as catalytic nucleophile of the reaction. Unless indicated otherwise, amino acid numbering is according to the sequence of *Sp*UGDH.

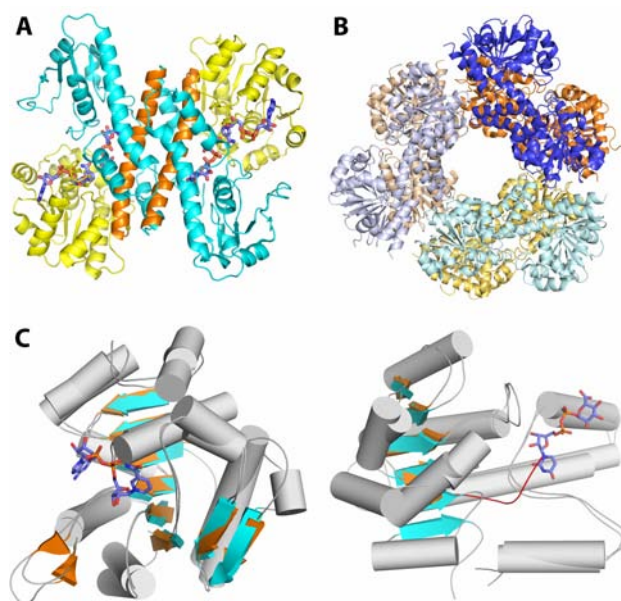


Figure 1: Structural comparison of UGDH-I and UGDH-II enzymes. **A.** Domain structure and mode of dimerisation of *Sp*UGDH. The N-terminal domain is displayed in yellow (“head”), the C-terminal domain in cyan (“tail”). The $\alpha 9$ helix connecting the two domains is shown in orange. Subunit orientation is indicated as “back-to-back” and “head-to-tail”. The structure of *Sp*UGDH bound to UDP- α -D-xylose and NAD^+ is shown (PDB identifier: 1DLI). **B.** The hexameric *Ce*UGDH is a trimer of dimers (PDB identifier: 2O3J). **C.** Topologies of the N-terminal domains (left) and C-terminal domains (right) of *Sp*UGDH and *Ce*UGDH. The flexible C-terminus of *Sp*UGDH is shown in red.

Mode of action of UGDH

Catalytic mechanism

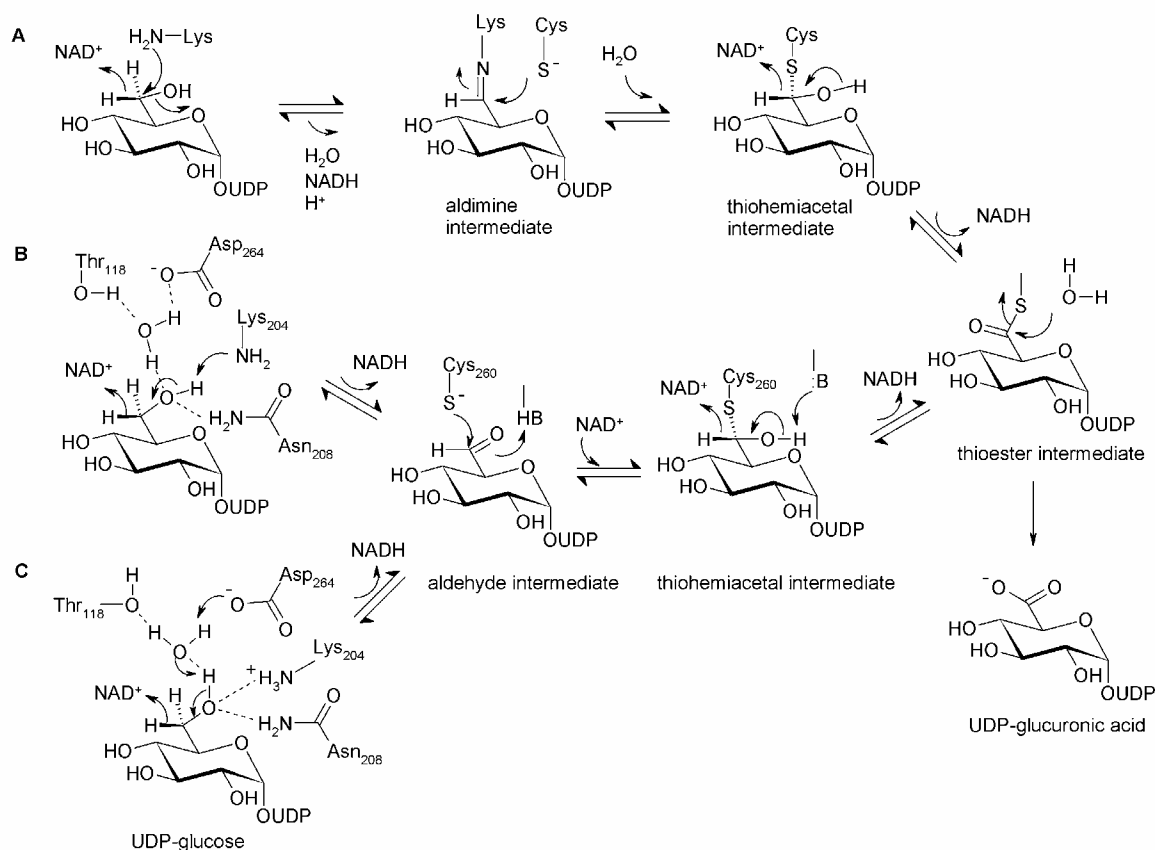
UGDH from bovine liver and *Sp*UGDH were subject to detailed mechanistic examination using elegant biochemical experiments. Mutagenesis studies were further used to interrogate the catalytic mechanism of *Sp*UGDH and human UGDH. It was established early that the stereochemical course of the reaction of UGDH involves transfer of the *pro*-R-C6 hydride of the substrate alcohol to the *si* face (B face) of NAD^+ [10, 48]. Two-step oxidation of UDP-Glc into UDP-GlcA was proposed to proceed in the absence of release into solution of an UDP- α -D-*gluco*-hexodialdose (UDP-aldehyde) intermediate [13, 14, 49]. The conclusion was based on the finding that aldehyde trapping reagents such as semicarbazide or hydroxylamine did not affect the distribution of products formed in the reaction catalysed by liver UGDH [4, 6, 50]. The requirement for a catalytic Cys in the reaction of UGDH was supported by a number of studies,

initially using chemical modification, and formation of covalent enzyme intermediate was common to the catalytic mechanisms considered [13, 24]. The mechanism of Kirkwood and co-workers (Scheme 1A) suggested initial trapping of the UDP-aldehyde by the catalytic side chain of an active-site Lys [16]. The Schiff base (aldimine) intermediate is thought to be hydrolysed while being attacked concomitantly from a nearby Cys side chain. The resulting thiohemiacetal would be further oxidised by a second NAD^+ to thioester, yielding UDP-GlcA upon hydrolysis. Evidence supporting the mechanism in Scheme 1A came from experiments employing tritium reduction of the aldimine formed from ^{14}C -labeled UDP-Glc substrate [16]. Scheme 1A is consistent with a Bi-Uni-Uni-Bi Ping-Pong steady-state kinetic mechanism as proposed for *Sp*UGDH and bovine liver UGDH [15, 24]. The absence of a primary kinetic isotope effect accompanying the reaction of *Sp*UGDH with UDP-[6",6"-di- ^2H]-D-glucose under V_{max} (substrate-saturating) conditions implies that hydride transfer to NAD^+ is not rate-determining overall. Generally, the final hydrolysis step was considered to be slowest step of the reaction catalysed by UGDH enzymes.

Tanner and co-workers re-examined participation of an aldimine intermediate in the reaction catalysed by UGDH [51]. They performed oxidation of UDP-Glc in H_2^{18}O solvent and measured ^{18}O incorporation into the UDP-GlcA product using *Sp*UGDH. If as proposed in Scheme 1A, reaction of UGDH involved an extra hydrolysis step at the level of the aldimine, one would expect that both oxygens of the carboxylate in UDP-GlcA become isotopically labeled from solvent. Observation that only a single ^{18}O atom was incorporated into product is inconsistent with the mechanism in Scheme 1A. A scenario was therefore proposed in which UDP-aldehyde immediately reacts with active-site Cys to generate the thiohemiacetal (Scheme 1B and 1C).

The UDP-aldehyde was chemically synthesised and examined as substrate of wild-type and mutated forms of *Sp*UGDH [52]. In assays carried out with wild-type enzyme, the aldehyde displayed similar reactivity and apparent binding affinity as did the natural substrate UDP-Glc, supporting the idea that UDP-aldehyde is a kinetically competent intermediate of the catalytic reaction of UGDH. Muteins of *Sp*UGDH having Cys260 replaced by Ala or Ser were strongly impaired in catalytic function for oxidation of UDP-Glc [53]. Reaction of the Cys260→Ser mutein with UDP-Glc or UDP-aldehyde led to the slow accumulation of an ester intermediate, in which the side chain of Ser260 had become acylated. Surprisingly, therefore, UDP-aldehyde was converted by the Cys260→Ala mutein with catalytic constants that were within one order of magnitude of the corresponding constants for the wild-type enzyme reacting with UDP-Glc. However, UDP-Glc was not a substrate of this mutein. Tanner and colleagues concluded that the Cys260→Ala mutein presumably recognises the hydrated form of the aldehyde which

resembles the “normal” thiohemiacetal intermediate of the reaction and converts it to the acid product. Earlier studies from Kirkwood and co-workers agree with these findings, showing that a variant of bovine liver UGDH in which the essential (active-site) Cys had been derivatised with cyanide also retained limited ability to catalyse the second oxidation step [13].



Scheme 1: Catalytic mechanism proposed for bovine liver UGDH (A) and *SpUGDH* (B,C). The identity of catalytic Lys and Cys in bovine liver UGDH was not reported in the studies of Kirkwood and co-workers [16]. Two mechanistic scenarios for *SpUGDH* were considered based on the crystal structure [51].

A very interesting property of the Cys260→Ala mutain was ability to reduce UDP-aldehyde back to UDP-Glc when NADH was present. The kinetic constants for this reaction ($k_{\text{cat}} = 1.9 \text{ s}^{-1}$; $K_{\text{M}} = 58 \text{ }\mu\text{M}$) were comparable to the kinetic constants of the wild-type enzyme for NAD⁺-dependent oxidation of UDP-Glc ($k_{\text{cat}} = 1.2 \text{ s}^{-1}$; $K_{\text{M}} = 14 \text{ }\mu\text{M}$). The observation of a reasonably rapid reductive conversion of UDP-aldehyde was interpreted to imply that Cys260 is not a key catalytic residue in the first step of UDP-Glc oxidation catalysed by the wild-type enzyme. The absence of measurable oxidation of UDP-Glc by the Cys260→Ala mutain was

explained by an unfavourable equilibrium for conversion of alcohol substrate into aldehyde product. Due to an enzymatic dismutation, in which aldehyde is transformed into both UDP-Glc and UDP-GlcA, conversion of UDP-aldehyde by wild-type *SpUGDH* could not be measured as consumption of NADH. A deuterium “wash-out” experiment was performed in which the Cys260→Ala mutein was incubated in the presence of UDP-[6”,6”-di-²H]-D-glucose, and 20 mM NADH and 4 mM NAD⁺ were added as coenzymes. If substrate was oxidised to UDP-aldehyde in this reaction, deuterated NADH would be formed. Now, if the NAD²H was exchanged by unlabeled NADH at the level of the ternary complex, UDP-aldehyde could be reduced back to starting material having the original *pro-R* deuterium replaced by hydrogen. Overall, therefore, the deuterium content of substrate would decrease. However, no significant loss of deuterium was observed upon prolonged incubation under the conditions just described. This finding might imply the absence of coenzyme exchange in the complex of enzyme, UDP-aldehyde and NADH, as proposed by Ge al. [51]. However, it could also indicate the absence of reaction catalysed by the Cys260→Ala mutein to give the aldehyde product. In any case, it seems probable that wild-type enzyme utilises a mechanism by which escape of UDP-aldehyde is prevented during reaction. One possibility is that the first-formed NADH is not released before the (ionised) side chain of Cys260 has added to the aldehyde, generating the thiohemiacetal intermediate, as shown in Scheme 1B and 1C.

Cys276 of human UGDH, which is homologous to Cys260 of *SpUGDH*, was substituted by Ser, and the resulting mutein showed no activity in a conventional steady-state assay [46]. However, it did perform a single step of oxidation on UDP-Glc, producing NADH in a concentration corresponding to the molar equivalent of enzyme present in the reaction. These findings suggest that nucleophilic catalysis by Cys is utilised by human UGDH and by extension (Figure S1), members of UGDH-I.

Role of active-site residues other than Cys

The crystal structure of *SpUGDH* has revealed residues potentially involved in catalysis to two-fold oxidation of UDP-Glc, as shown in Figure 2. Lys204 and water bonded to Asp264 were previously considered to have a catalytic base function in the first step of oxidation. Thr118 (by Ala; T118A), Glu141 and Glu145 (each by Gln; E141Q, E145Q) were replaced in *SpUGDH*. The T118A mutein showed a 164-fold lowered k_{cat} as compared to the k_{cat} of the wild-type enzyme, suggesting an auxiliary function of Thr-118 in the enzymatic reaction, perhaps as stabiliser (via active-site water; Figure 2) of negative charge developing on the reactive oxygen atom of substrate in the course of the reaction. E141Q and E145Q muteins showed only modestly decreased k_{cat} values that were within about one order of magnitude of the wild-type value.

Glu141 was proposed as candidate catalytic base facilitating attack of water during thioester hydrolysis. Muteins of *SpUGDH* at position Lys204 (K204A) and Asp264 (D264N) were not expressed as soluble proteins in *E. coli*. However, substitution of the corresponding Lys220 (by Ala, His, or Arg) and Asp280 (by Asn) in human UGDH very strongly impaired the enzyme activity [54]. Although different functions were considered, the exact role of these two residues in UGDH catalysis remains currently elusive. In addition to the abovementioned catalytic base facilitation of the “alcohol dehydrogenase” step of the reaction, deprotonation of Cys (by the couple of Asp264 and water) as well as oxyanion stabilisation (together with Asn208) during formation and breakdown of thiohemiacetal and thioester might be roles accomplished by the two (highly conserved) active-site residues, as shown for *SpUGDH*.

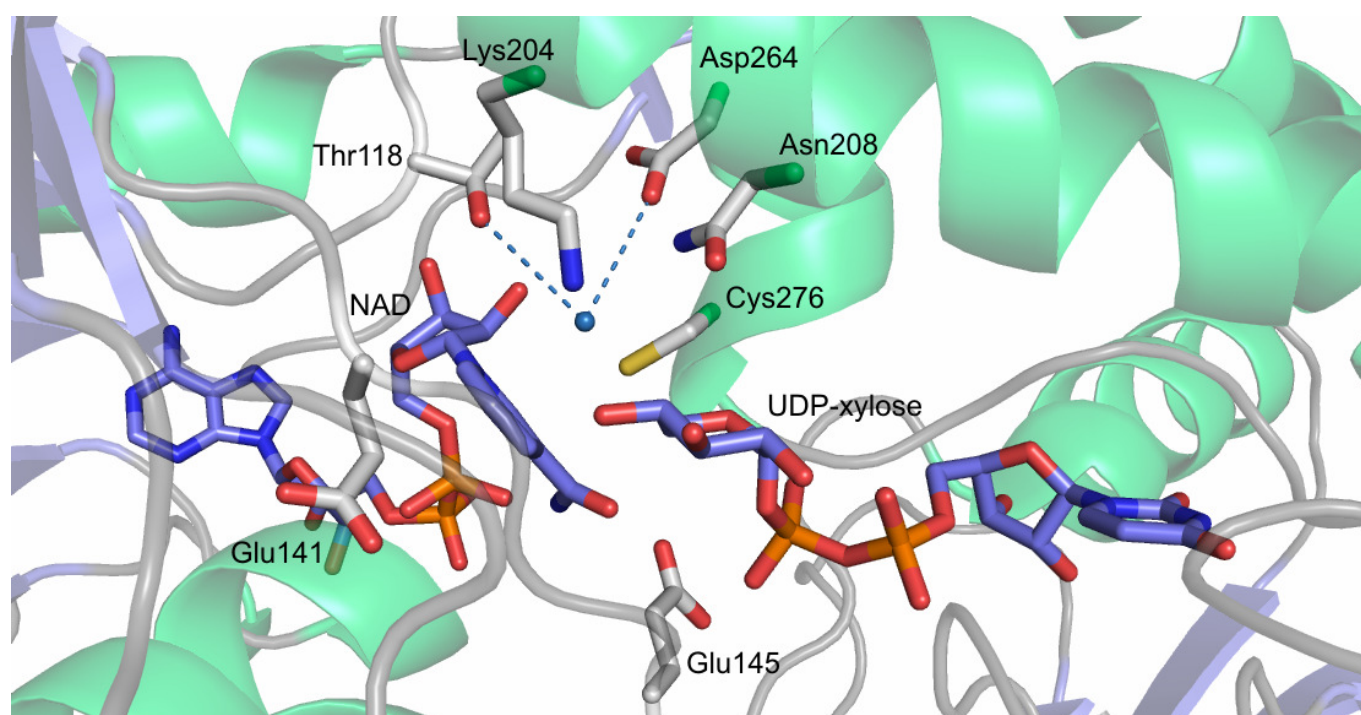


Figure 2: Close-up structure of the active site of *SpUGDH* (PDB: 1DLI) bound with UDP- α -D-xylose and NAD⁺ (indicated in blue) and water (sphere).

Kinetic cooperativity

Work by Feingold and co-workers focused on the occurrence of “half-of-the-sites” reactivity in the hexameric UGDH from bovine liver [14, 19, 20]. An assortment of biochemical methods were employed to measure substrate binding and determine protein conformational changes associated with the binding event. The liver enzyme was proposed to bind only 3 molecules of UDP-Glc and NAD⁺ per protein hexamer. The structure of *SpUGDH*, which is a dimeric UGDH, however, shows only weak “communication” between the active sites of adjacent protein subunits. The side chain of Arg-244 is contributed to the active site of the neighbouring subunit

where it provides hydrogen bonds to the hydroxyls at C2 and C3 of the glucosyl moiety of bound UDP-Glc. Arg-244 is conserved in members of both UGDH-I and UGDH-II. *Sp*UGDH exhibits only a weak allosterism with respect to UDP-Glc. It is currently not clear if the “half-of-the-sites” reactivity of the liver enzyme is a common feature of UGDH enzymes.

Possible role of UGDH in human pathophysiology

Hyaluronan is a linear polysaccharide composed of a $[\text{GlcA}\beta\text{-1-3GlcNAc}\beta\text{-1-4}]_n$ disaccharide unit. Unlike other members of the glycosaminoglycan class, hyaluronan is synthesised in the absence of a protein core at the inner face of the plasma membrane and it is not sulfated. The molecular size of hyaluronan can vary between 5×10^3 and 1×10^7 Da. Both the actual amount as well as the mass of the hyaluronan polymer determine its physiological function. In mammals, hyaluronan was implicated in numerous roles including development, tissue organisation, cell proliferation, and signaling processes [55, 56]. Interactions of hyaluronan with protein receptors such as CD44 and RHAMM have been linked to cell survival and motility under normal conditions but also under the pathophysiological conditions of cancer. It was shown that elevated concentrations of hyaluronan promote cancer progression and cell aging, both in animal models as well as in human patients. Work on tumors of breast [37], ovaries [36], colon [38] and prostate [57] collectively supports a strong correlation between the hyaluronan content in the connective tissue matrix (stroma) of the tissue and (negative) prediction of patient survival. Inhibition of hyaluronan synthesis in general [43, 58] and by restriction of the building block UDP-GlcA in particular [42] has been shown to slow down tumor growth. Recently, human UGDH has been proposed as a novel field-specific candidate biomarker for prostate cancer [44]. Limitation of UDP-GlcA in tumor cells by UGDH antagonism is a novel therapeutic target in combating cancer. Group-selective inhibition of UGDH is of an even more general interest in therapy because in many pathogenic bacteria (e.g. group A streptococci) UGDH-I provides UDP-GlcA for synthesis of antiphagocytotic capsular polysaccharides, which are known to constitute an important virulence factor. UGDH-I therefore is a target for new antibacterial drugs [59].

Development of UGDH antagonists is still in its infancy. UDP- α -D-xylose is a strong feedback inhibitor of UGDH enzymes from different sources (Note: UDP- α -D-xylose is produced from UDP-GlcA by oxidoreductive decarboxylation). It exhibits a K_i of $\sim 2.7 \mu\text{M}$ against *Sp*UGDH [24]. Previously described irreversible inhibitors, for example, UDP-chloroacetol and others that are directed against the active-site Cys, are probably not useful. However, Tanner and co-workers synthesised UDP-7-deoxy- α -D-gluco-hept-6-ulopyranose as an UDP-Glc mimic and showed reversible inhibition of *Sp*UGDH by this substrate analogue with a K_i of $\sim 6.7 \mu\text{M}$ [48].

The polyphenols gallic acid and quercetin were recently shown to inhibit human UGDH [60]. Both compounds were also demonstrated to reduce proliferation of MCF-7 human breast cancer cells *in vitro* [60]. In addition to binding efficacy and inhibition potency, future design of UGDH inhibitors will need to focus on selectivity (UGDH-I vs. UGDH-II) and cell targeting. Mechanistic details of the human enzyme would be useful to advance in this goal.

Funding

Funding by the Austrian Science Fund [DK Molecular Enzymology, W901-B05] is gratefully acknowledged.

References

- 1 Lee, J.Y. and Spicer, A.P. (2000) Hyaluronan: a multifunctional, megaDalton, stealth molecule. *Curr. Opin. Cell. Biol.* 12, 581-586
- 2 Gueraud, F. and Paris, A. (1998) Glucuronidation: a dual control. *Gen. Pharmacol.* 31, 683-688
- 3 Linster, C.L. and Van Schaftingen, E. (2007) Vitamin C. Biosynthesis, recycling and degradation in mammals. *Febs. J.* 274, 1-22
- 4 Strominger, J.L., Kalckar, H.M., Axelrod, J. and Maxwell, E.S. (1954) Enzymatic oxidation of uridine diphosphate glucose to uridine diphosphate glucuronic acid. *J. Am. Chem. Soc.* 76, 6411-6412
- 5 Kalckar, H.M., Maxwell, E.S. and Strominger, J.L. (1956) Some properties of uridine diphosphoglucose dehydrogenase. *Arch. Biochem. Biophys.* 65, 2-10
- 6 Nelsestuen, G.L. and Kirkwood, S. (1971) The mechanism of action of uridine diphosphoglucose dehydrogenase. Uridine diphosphohexodialdoses as intermediates. *J. Biol. Chem.* 246, 3824-3834
- 7 Gainey, P.A., Pestell, T.C. and Phelps, C.F. (1972) A study of the subunit structure and the thiol reactivity of bovine liver uridine diphosphate glucose dehydrogenase. *Biochem. J.* 129, 821-830
- 8 Schiller, J.G., Bowser, A.M. and Feingold, D.S. (1972) Studies on the mechanism of action of UDP-D-glucose dehydrogenase from beef liver. *Carbohydr. Res.* 21, 249-253
- 9 Franzen, J.S., Kuo, I., Eichler, A.J. and Feingold, D.S. (1973) UDP-glucose dehydrogenase: substrate binding stoichiometry and affinity. *Biochem. Biophys. Res. Commun.* 50, 517-523
- 10 Ridley, W.P. and Kirkwood, S. (1973) The stereospecificity of hydrogen abstraction by uridine diphosphoglucose dehydrogenase. *Biochem. Biophys. Res. Commun.* 54, 955-960
- 11 Chen, A., Marchetti, P., Weingarten, M., Franzen, J. and Feingold, D.S. (1974) Binding studies with bovine liver UPD-D-glucose dehydrogenase. *Carbohydr. Res.* 37, 155-165
- 12 Gainey, P.A. and Phelps, C.F. (1974) The binding of oxidized and reduced nicotinamide--adenine dinucleotides to bovine liver uridine diphosphate glucose dehydrogenase. *Biochem. J.* 141, 667-673
- 13 Ridley, W.P., Houchins, J.P. and Kirkwood, S. (1975) Mechanism of action of uridine diphosphoglucose dehydrogenase. Evidence for a second reversible dehydrogenation step involving an essential thiol group. *J. Biol. Chem.* 250, 8761-8767
- 14 Franzen, J.S., Ishman, R. and Feingold, D.S. (1976) Half-of-the-sites reactivity of bovine liver uridine diphosphoglucose dehydrogenase toward iodoacetate and iodoacetamide. *Biochemistry* 15, 5665-5671
- 15 Ordman, A.B. and Kirkwood, S. (1977) UDPglucose dehydrogenase. Kinetics and their mechanistic implications. *Biochim. Biophys. Acta* 481, 25-32

- 16 Ordman, A.B. and Kirkwood, S. (1977) Mechanism of action of uridine diphoglucose dehydrogenase. Evidence for an essential lysine residue at the active site. *J. Biol. Chem.* 252, 1320-1326
- 17 Eccleston, E.D., Thayer, M.L. and Kirkwood, S. (1979) Mechanisms of action of histidinol dehydrogenase and UDP-Glc dehydrogenase. Evidence that the half-reactions proceed on separate subunits. *J. Biol. Chem.* 254, 11399-11404
- 18 Prihar, H.S. and Feingold, D.S. (1979) Loss of C-5 hydrogen during oxidation of UDP-D-glucose by UDP-D-glucose dehydrogenase. *FEBS Lett.* 99, 106-108
- 19 Franzen, J.S., Ashcom, J., Marchetti, P., Cardamone, J.J., Jr. and Feingold, D.S. (1980) Induced versus pre-existing asymmetry models for the half-of-the-sites reactivity effect in bovine liver uridine diphosphoglucose dehydrogenase. *Biochim. Biophys. Acta* 614, 242-255
- 20 Franzen, J.S., Marchetti, P.S. and Feingold, D.S. (1980) Resonance energy transfer between catalytic sites of bovine liver uridine diphosphoglucose dehydrogenase. *Biochemistry* 19, 6080-6089
- 21 Feingold, D.S. and Franzen, J.S. (1981) Pyridine nucleotide-linked four-electron transfer dehydrogenases. *Trends Biochem. Sci.* 6, 103-105
- 22 Franzen, J.S., Marchetti, P.S., Lockhart, A.H. and Feingold, D.S. (1983) Special effects of UDP-sugar binding to bovine liver uridine diphosphoglucose dehydrogenase. *Biochim. Biophys. Acta* 746, 146-153
- 23 Jaenicke, R., Rudolph, R. and Feingold, D.S. (1986) Dissociation and in vitro reconstitution of bovine liver uridine diphosphoglucose dehydrogenase. The paired subunit nature of the enzyme. *Biochemistry* 25, 7283-7287
- 24 Campbell, R.E., Sala, R.F., van de Rijn, I. and Tanner, M.E. (1997) Properties and kinetic analysis of UDP-glucose dehydrogenase from group A streptococci. Irreversible inhibition by UDP-chloroacetol. *J. Biol. Chem.* 272, 3416-3422
- 25 Hung, R.J., Chien, H.S., Lin, R.Z., Lin, C.T., Vatsyayan, J., Peng, H.L. and Chang, H.Y. (2007) Comparative analysis of two UDP-glucose dehydrogenases in *Pseudomonas aeruginosa* PAO1. *J. Biol. Chem.* 282, 17738-17748
- 26 Sieberth, V., Rigg, G.P., Roberts, I.S. and Jann, K. (1995) Expression and characterization of UDPGlc dehydrogenase (KfiD), which is encoded in the type-specific region 2 of the *Escherichia coli* K5 capsule genes. *J. Bacteriol.* 177, 4562-4565
- 27 Vigetti, D., Ori, M., Viola, M., Genasetti, A., Karousou, E., Rizzi, M., Pallotti, F., Nardi, I., Hascall, V.C., De Luca, G. and Passi, A. (2006) Molecular cloning and characterization of UDP-glucose dehydrogenase from the amphibian *Xenopus laevis* and its involvement in hyaluronan synthesis. *J. Biol. Chem.* 281, 8254-8263
- 28 Hwang, H.Y. and Horvitz, H.R. (2002) The *Caenorhabditis elegans* vulval morphogenesis gene sqv-4 encodes a UDP-glucose dehydrogenase that is temporally and spatially regulated. *Proceedings of the Proc Natl Acad Sci U S A* 99, 14224-14229
- 29 Klinghammer, M. and Tenhaken, R. (2007) Genome-wide analysis of the UDP-glucose dehydrogenase gene family in Arabidopsis, a key enzyme for matrix polysaccharides in cell walls. *J. Exp. Bot.* 58, 3609-3621
- 30 Blanch, M., Legaz, M.E. and Vicente, C. (2008) Purification and properties of an unusual UDP-glucose dehydrogenase, NADPH-dependent, from *Xanthomonas albilineans*. *Microbiol. Res.* 163, 362-371
- 31 Spicer, A.P., Kaback, L.A., Smith, T.J. and Seldin, M.F. (1998) Molecular cloning and characterization of the human and mouse UDP-glucose dehydrogenase genes. *J. Biol. Chem.* 273, 25117-25124
- 32 Stewart, D.C. and Copeland, L. (1998) Uridine 5'-diphosphate-glucose dehydrogenase from soybean nodules *Plant. Physiol.* 116, 349-355
- 33 Turner, W. and Botha, F.C. (2002) Purification and kinetic properties of UDP-glucose dehydrogenase from sugarcane. *Arch. Biochem. Biophys.* 407, 209-216

- 34 Yurist-Doutsch, S., Magidovich, H., Ventura, V.V., Hitchen, P.G., Dell, A. and Eichler, J. (2010) N-glycosylation in Archaea: On the coordinated actions of *Haloferax volcanii* AglF and AglM. *Molecular microbiology* 75, 1047–1058
- 35 Aaltomaa, S., Lipponen, P., Tammi, R., Tammi, M., Viitanen, J., Kankkunen, J.P. and Kosma, V.M. (2002) Strong stromal hyaluronan expression is associated with PSA recurrence in local prostate cancer. *Urologia internationalis* 69, 266-272
- 36 Anttila, M.A., Tammi, R.H., Tammi, M.I., Syrjanen, K.J., Saarikoski, S.V. and Kosma, V.M. (2000) High levels of stromal hyaluronan predict poor disease outcome in epithelial ovarian cancer. *Cancer Res.* 60, 150-155
- 37 Auvinen, P., Tammi, R., Parkkinen, J., Tammi, M., Agren, U., Johansson, R., Hirvikoski, P., Eskelinen, M. and Kosma, V.M. (2000) Hyaluronan in peritumoral stroma and malignant cells associates with breast cancer spreading and predicts survival. *Am. J. Pathol.* 156, 529-536
- 38 Ropponen, K., Tammi, M., Parkkinen, J., Eskelinen, M., Tammi, R., Lipponen, P., Agren, U., Alhava, E. and Kosma, V.M. (1998) Tumor cell-associated hyaluronan as an unfavorable prognostic factor in colorectal cancer. *Cancer Res.* 58, 342-347
- 39 Stern, R. (2008) Hyaluronidases in cancer biology. *Semin Cancer Biol* 18, 275-280
- 40 Tammi, R.H., Kultti, A., Kosma, V.M., Pirinen, R., Auvinen, P. and Tammi, M.I. (2008) Hyaluronan in human tumors: pathobiological and prognostic messages from cell-associated and stromal hyaluronan. *Semin Cancer Biol* 18, 288-295
- 41 Toole, B.P. and Hascall, V.C. (2002) Hyaluronan and tumor growth. *Am. J. Pathol.* 161, 745-747
- 42 Huh, J.W., Choi, M.M., Yang, S.J., Yoon, S.Y., Choi, S.Y. and Cho, S.W. (2005) Inhibition of human UDP-glucose dehydrogenase expression using siRNA expression vector in breast cancer cells. *Biotechnol. Lett.* 27, 1229-1232
- 43 Simpson, M.A., Wilson, C.M. and McCarthy, J.B. (2002) Inhibition of prostate tumor cell hyaluronan synthesis impairs subcutaneous growth and vascularization in immunocompromised mice. *Am. J. Pathol.* 161, 849-857
- 44 Huang, D., Casale, G.P., Tian, J., Lele, S.M., Pisarev, V.M., Simpson, M.A. and Hemstreet, G.P., 3rd (2010) UDP-glucose dehydrogenase as a novel field-specific candidate biomarker of prostate cancer. *Int. J. Cancer* 126, 315-327
- 45 Campbell, R.E., Mosimann, S.C., van De Rijn, I., Tanner, M.E. and Strynadka, N.C. (2000) The first structure of UDP-glucose dehydrogenase reveals the catalytic residues necessary for the two-fold oxidation. *Biochemistry* 39, 7012-7023
- 46 Sommer, B.J., Barycki, J.J. and Simpson, M.A. (2004) Characterization of human UDP-glucose dehydrogenase. CYS-276 is required for the second of two successive oxidations. *J. Biol. Chem.* 279, 23590-23596
- 47 Lee, H.S., Son, Y.J., Chong, S.H., Bae, J.Y., Leem, C.H., Jang, Y.J. and Choe, H. (2009) Computational analysis of the quaternary structural changes induced by point mutations in human UDP-glucose dehydrogenase. *Arch. Biochem. Biophys.* 486, 35-43
- 48 Campbell, R.E. and Tanner, M.E. (1999) UDP-glucose analogues as inhibitors and mechanistic probes of UDP-glucose dehydrogenase. *Journal of organic chemistry* 64, 9487-9492
- 49 Franzen, B., Carrubba, C., Feingold, D.S., Ashcom, J. and Franzen, J.S. (1981) Amino acid sequence of the tryptic peptide containing the catalytic-site thiol group of bovine liver uridine diphosphate glucose dehydrogenase. *Biochem. J.* 199, 599-602
- 50 Axelrod, J., Kalckar, H.M., Maxwell, E.S. and Strominger, J.L. (1957) Enzymatic formation of uridine diphosphoglucuronic acid. *J. Biol. Chem.* 224, 79-90
- 51 Ge, X., Penney, L.C., van de Rijn, I. and Tanner, M.E. (2004) Active site residues and mechanism of UDP-glucose dehydrogenase. *Eur. J. Biochem.* 271, 14-22
- 52 Campbell, R.E. and Tanner, M.E. (1997) Uridine diphospho- α -D-glucopyranose: Synthesis and kinetic competence in the reaction catalyzed by UDP-glucose dehydrogenase. *Angew. Chem. Int. Ed. Engl.* 36, 3

- 53 Ge, X., Campbell, R.E., van de Rijn, I. and Tanner, M.E. (1998) Covalent adduct formation with a mutated enzyme: Evidence for a thioester intermediate in the reaction catalyzed by UDP-glucose dehydrogenase. *J. Am. Chem. Soc.* 120, 6613-6614
- 54 Easley, K.E., Sommer, B.J., Boanca, G., Barycki, J.J. and Simpson, M.A. (2007) Characterization of human UDP-glucose dehydrogenase reveals critical catalytic roles for lysine 220 and aspartate 280. *Biochemistry* 46, 369-378
- 55 Turley, E.A., Noble, P.W. and Bourguignon, L.Y. (2002) Signaling properties of hyaluronan receptors. *J. Biol. Chem.* 277, 4589-4592
- 56 Viola, M., Vigetti, D., Genasetti, A., Rizzi, M., Karousou, E., Moretto, P., Clerici, M., Bartolini, B., Pallotti, F., De Luca, G. and Passi, A. (2008) Molecular control of the hyaluronan biosynthesis. *Connect. Tissue. Res.* 49, 111-114
- 57 Lin, S.L., Chang, D. and Ying, S.Y. (2007) Hyaluronan stimulates transformation of androgen-independent prostate cancer. *Carcinogenesis* 28, 310-320
- 58 Bharadwaj, A.G., Rector, K. and Simpson, M.A. (2007) Inducible hyaluronan production reveals differential effects on prostate tumor cell growth and tumor angiogenesis. *J. Biol. Chem.* 282, 20561-20572
- 59 Dougherty, B.A. and van de Rijn, I. (1993) Molecular characterization of hasB from an operon required for hyaluronic acid synthesis in group A streptococci. Demonstration of UDP-glucose dehydrogenase activity. *J. Biol. Chem.* 268, 7118-7124
- 60 Hwang, E.Y., Huh, J.W., Choi, M.M., Choi, S.Y., Hong, H.N. and Cho, S.W. (2008) Inhibitory effects of gallic acid and quercetin on UDP-glucose dehydrogenase activity. *FEBS letters* 582, 3793-3797

Supplementary Information:

Figure S1: Multiple alignment of selected UGDH sequences. UGDH-II from higher and lower eukaryotes: CaeEle: (Q19905/1-481 *Caenorhabditis elegans*), Human (O60701/1-494 *Homo sapiens*), Bovine (P12378/1-494 *Bos taurus*), XenLae (Q56R95/1-494 *Xenopus laevis*), DrosMe (O02373/1-476 *Drosophila melanogaster*), AraTha (Q9LIA8/1-480 *Arabidopsis thaliana*), CryNeo (Q5K899/1-468 *Cryptococcus neoformans*). Underneath the black line representatives of UGDH-I from archaea: HaloVo (C3W971/1-430 *Halobacterium volcanii*), and prokaryotes: EColi (P76373/1-388 *Escherichia coli* (strain K12)), and StrPyo (P0C0F4/1-402 *Streptococcus pyogenes*) are shown. The black vertical line divides UGDH-II and UGDH-I. Secondary structure elements for CeUGDH (based on PDB: 2O3J) on top of the alignment and SpUGDH (based on PDB: 1DLI) underneath. Helices are numbered H1-H15/20 and strands by their sheets A-C/D. Motifs are indicated as beta turn (β), gamma turn (γ) and beta hairpin (\equiv). Positions in the sequence that are highlighted with white text on black background are conserved active-site residues. Conserved motifs of the Rossmann fold domain at the N-terminus are highlighted in grey ($GxGxxG$) for all UGDH members. The internal peptide used for classification into UGDH-I ($\alpha 9$) and UGDH-II ($\alpha 10$) is indicated in grey. Residues responsible for dimerisation in SpUGDH and CeUGDH are highlighted as white text and dark grey background. Amino acids assisting in higher oligomerisation in CeUGDH, namely Lys99, Tyr101, Gly102, Arg103, Ala108, Pro109, Asp110, Leu111, Lys112, Glu115, Arg119, Ser144, Cys147, Ile148, Glu151, Tyr293, Arg319, Asp323, Ile326, Ala327, Phe330, Asn331, Thr332, Thr334, Lys336, Glu366, Glu367, His368, His414, His434, Gln438, His439, Pro440, Ala441, Gly459, and Arg461 are indicated as boxed and in light grey.

CaeEle : MTDQVFGKVSQVVCVAGYVGGPTCAMIAHKCPHITVTVVDMNTAKIAEWNSSDKLPYIEPGLDEIVFAARGNLFSSDI : 80

 Human : -----MFEIKKICCIAGYVGGPTCSVIAHMCPEIRVTVVDVNESRINAWNSPTLPIYEPGLKEVVESCRGKNLFFSTNI : 75

 Bovine : -----MFEIKKICCIAGYVGGPTCSVIAHMCPEIRVTVVDINESRINAWNSPTLPIYEPGLKEVVESCRGKNLFFSTNI : 75

 XenLae : -----MFQIKKICCIAGYVGGPTCSVIAQMCPDIKVTVDVQARINAWNSDTPYIEPGLKEVVESCRGKNLFFSTDI : 75

 DrosMe : -----MKVCCIAGYVGGPTCAVMALKCPDIVITLVDKSSERIAQWNSDKLPYIEPGLDEVVKKCRNVNLFSTDI : 71

 AraTha : -----MVKICCIAGYVGGPTMAVIALKCPDEVAVVDISVPRINAWNSDTPYIEPGLDDVVVKQCRGNLFFSTDV : 72

 CryNeo : ---MAPITVKKICCIAGYVGGPTCAVIALKCPQIQVTVVDLNOQRIDAWNSDNLPIYEPGLDEVVKATRGNLFFSTDV : 77

 HaloVo : -----MELSTIGSGYVGTIIAACFAELG--HDVVNVDDIDEDIVASLNDGQAPIHEPGLAELVERYAGDRLRATTDY : 69

 EColi : -----MKITISGTGYVGLSNGLLIAQNH---EVVALDILPSRVAMLNDRISPIVDKEIQQLQSDK-IHFNATLTK : 67

 StrPyo : -----MKIAVAGSGYVGLSLGVLVLSLQN---EVTIVDILPSKVDKINNGLSPIQDEYIEYLLKSKQ-LSIKATLDS : 67

CaeEle : PKAIAEADLFIISVNTPTKTYGGRGKGMADPLKLVSVSPTIAQYAGGPKIVVEKSTVPVRAAESIRRIFFDANTK--PNLN : 160

 Human : DDAIKADLVFIISVNTPTKTYGGRGKGMADPLKLVSVSPTIAQYAGGPKIVVEKSTVPVRAAESIRRIFFDANTK--PNLN : 153

 Bovine : DDAIKADLVFIISVNTPTKTYGGRGKGMADPLKLVSVSPTIAQYAGGPKIVVEKSTVPVRAAESIRRIFFDANTK--PNLN : 153

 XenLae : DDAIKADLVFIISVNTPTKTYGGRGKGMADPLKLVSVSPTIAQYAGGPKIVVEKSTVPVRAAESIRRIFFDANTK--PNLN : 153

 DrosMe : ETAIKADLVFIISVNTPTKTYGGRGKGMADPLKLVSVSPTIAQYAGGPKIVVEKSTVPVRAAESIRRIFFDANTK--PNLN : 149

 AraTha : EKHVREADLVFIISVNTPTKTYGGRGKGMADPLKLVSVSPTIAQYAGGPKIVVEKSTVPVRAAESIRRIFFDANTK--PNLN : 149

 CryNeo : DKGIEDADLVFIISVNTPTKTYGGRGKGMADPLKLVSVSPTIAQYAGGPKIVVEKSTVPVRAAESIRRIFFDANTK--PNLN : 155

 HaloVo : D-EILDTDATFLALPTPSTDDG-SIDLGMKTAATSLGETLARKDDSHLVVTKSTVVPRTTVDVIGPRIEASGRVGDG : 147

 EColi : NEAYRDADYVIATPTDYPD---KTNFYNTSSVESVIKDVVEIN-PYAVMVIKSTVPVGFATAMHKKYRTENI----- : 136

 StrPyo : KAAAYKEAELVIATPTNYS---RINYPTDQHVETVIVEVLSVN-SHATLTIKSTVPVGFATAMHKKYRTENI----- : 136

CaeEle : FQVLSNPEFLAEGTAMKDLANPDRVIGGESSPEGL--QAVAELVRIYENWVPRN---RITTTNTWSSELSKLVANAFLA : 235

 Human : LQVLSNPEFLAEGTAMKDLANPDRVIGGESSPEGL--QAVAELVRIYENWVPRN---RITTTNTWSSELSKLVANAFLA : 228

 Bovine : LQVLSNPEFLAEGTAMKDLANPDRVIGGESSPEGL--QAVAELVRIYENWVPRN---RITTTNTWSSELSKLVANAFLA : 228

 XenLae : LQVLSNPEFLAEGTAMKDLANPDRVIGGESSPEGL--QAVAELVRIYENWVPRN---RITTTNTWSSELSKLVANAFLA : 228

 DrosMe : YDILSNPEFLAEGTAMKDLANPDRVIGGESSPEGL--QAVAELVRIYENWVPRN---RITTTNTWSSELSKLVANAFLA : 224

 AraTha : YDILSNPEFLAEGTAMKDLANPDRVIGGESSPEGL--QAVAELVRIYENWVPRN---RITTTNTWSSELSKLVANAFLA : 224

 CryNeo : YDILSNPEFLAEGTAMKDLANPDRVIGGESSPEGL--QAVAELVRIYENWVPRN---RITTTNTWSSELSKLVANAFLA : 230

 HaloVo : LDIAMNPEFLAEGTAMKDLANPDRVIGGESSPEGL--QAVAELVRIYENWVPRN---RITTTNTWSSELSKLVANAFLA : 221

 EColi : ---IFSPPEFLAEGTAMKDLANPDRVIGGESSPEGL--QAVAELVRIYENWVPRN---RITTTNTWSSELSKLVANAFLA : 205

 StrPyo : ---IFSPPEFLAEGTAMKDLANPDRVIGGESSPEGL--QAVAELVRIYENWVPRN---RITTTNTWSSELSKLVANAFLA : 212

CaeEle : QRISINSISALCEATGADVEEVATAIGMDQIRIGNKFLKASVGFSGSCFQKDVLSLVVLCESLNPOVADYVQGVINLNN : 315

 Human : QRISINSISALCEATGADVEEVATAIGMDQIRIGNKFLKASVGFSGSCFQKDVLSLVVLCESLNPOVADYVQGVINLNN : 308

 Bovine : QRISINSISALCEATGADVEEVATAIGMDQIRIGNKFLKASVGFSGSCFQKDVLSLVVLCESLNPOVADYVQGVINLNN : 308

 XenLae : QRISINSISALCEATGADVEEVATAIGMDQIRIGNKFLKASVGFSGSCFQKDVLSLVVLCESLNPOVADYVQGVINLNN : 308

 DrosMe : QRISINSISALCEATGADVEEVATAIGMDQIRIGNKFLKASVGFSGSCFQKDVLSLVVLCESLNPOVADYVQGVINLNN : 304

 AraTha : QRISINSISALCEATGADVEEVATAIGMDQIRIGNKFLKASVGFSGSCFQKDVLSLVVLCESLNPOVADYVQGVINLNN : 304

 CryNeo : QRISINSISALCEATGADVEEVATAIGMDQIRIGNKFLKASVGFSGSCFQKDVLSLVVLCESLNPOVADYVQGVINLNN : 310

 HaloVo : SKISLANDLANIKVGFVDSAEVLESIGLDSRIGSAFLGAGLVGSGSCFQKDVLSLVVLCESLNPOVADYVQGVINLNN : 299

 EColi : MRVAYFNELDSYAESLGLNSROIIEGVCLDPRIGNHNNPFSFGYGGYCLPKDITKOLLANYQSVPN----NLISAIVDANR : 281

 StrPyo : LRVAYFNELDSYAESLGLNSROIIEGVCLDPRIGNHNNPFSFGYGGYCLPKDITKOLLANYQSVPN----NLISAIVDANR : 288

CaeEle : WQRSRFAKTIKAELENTVTD--KKAIFGFQAFKKTGDTRESSAIHVIKHLMEEAKLSVYDPKVQKSQLNDLAS----- : 389

 Human : YQRRFASRIIDSLFNTVTD--KKAIFGFQAFKKTGDTRESSSIYISKYLMDEGAHLHIYDPKVPREQIVVDLSH----- : 382

 Bovine : YQRRFASRIIDSLFNTVTD--KKAIFGFQAFKKTGDTRESSSIYISKYLMDEGAHLHIYDPKVPREQIVVDLSH----- : 382

 XenLae : YQRRFASRIIDSLFNTVTD--KKAIFGFQAFKKTGDTRESSSIYISKYLMDEGAHLHIYDPKVPREQIVVDLSH----- : 382

 DrosMe : YQRRFASRIIDSLFNTVTD--KKAIFGFQAFKKTGDTRESSSIYISKYLMDEGAHLHIYDPKVPREQIVVDLSH----- : 378


 AraTha : YQRRFASRIIDSLFNTVTD--KKAIFGFQAFKKTGDTRESSSIYISKYLMDEGAHLHIYDPKVPREQIVVDLSH----- : 383

 CryNeo : YQRRFASRIIDSLFNTVTD--KKAIFGFQAFKKTGDTRESSSIYISKYLMDEGAHLHIYDPKVPREQIVVDLSH----- : 384

 HaloVo : GQPERMLDLRERFDLQDGR---VAVLGLFAFKPGTDDIRKSRAILLIQALLDAGADVGYDPAVATENMRER----- : 367

 EColi : TRKDFIADAILNSRKPQ-----VVGIRYIMKSGSDNFRASSIQGIMKRIKAKGVEVIYEPVM-KEDSFF----- : 345

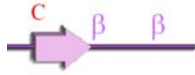
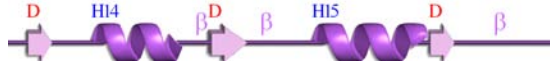
 StrPyo : WRKSMATKOTITNSLKRQSPVKKVYVYRITMKSNSDNFRFRSATKDVTDITLTKSKDITKTIYEPVMIKRIKAKGVEVIYEPVM-KEDSFF----- : 359



```

CaeEle : ---V TSAQD---VERLITVESDPYAAARGAIAIVVLT EWDFVELNYSQIINDMQHPAIFDGRLLID--QKALREIEF : 461
Human  : ---PGVSED-DQVSR LVTISKDPYEACDGAHAVVICTEWDMFKELDYERIHKKMLKPAFIFDGRRLDGLHNELQTI GFQ : 458
Bovine : ---PGVSKD-DQVARLVTISKDPYEACDGAHAVVICTEWDMFKELDYERIHKKMLKPAFIFDGRRLDGLHNELQTI GFQ : 458
XenLae : ---PGVAAD-DRVSQLVHISTDLYEACENAHAMVICTEWDMFKELDFNRIHRMMLKPAFIFDGRRLDELHGELQNI GFQ : 458
DrosMe : ---PSVTESPEKVKKAVQIHSDPYSAVRATHALVICTEWDEFVLDLDFKRIYQSMMPAYIFDGRKILD--HERLQQI GFH : 453
AraTha : DHPLHLQPMSPTTVKQVTVTWDAYEATKDAHGICIMTEWDEFKNLDFQKIFDNMQKPAFVFDGRNIMN--LQKLREI GF I : 461
CryNeo : YGEIPAEPIQP---HLTICKSVEEACANAEIAIVICTEWDEFKTLDWKKIYDNCPRPAFVFDGRLLILN--RQELTNI GFK : 458
HaloVo : -----FPDIDYADSAADALANADAALVATDWDEFAALDD---EFDAMRERIVIDGRRIVT-----RREGLD : 425
EColi  : -----NSRLERDLATFKQQADVIIISNRMAEELKDVADKVYTRDLFGSD----- : 388
StrPyo : -----OSVLVNDLENFKKOANIIVTNRYDNELODVKNKVYSRDI FG RD----- : 402

```



```

CaeEle : TFAIGTSPDQAYNLFGTAGY-----* : 481
Human  : IETIGKKVSSKRIPYAPSGEIPKFSLQDPPNKKPKV : 494
Bovine : IETIGKKVSSKRIPYAPSGEIPKFSLQDMPNKKPRV : 494
XenLae : VETIGKKVASKRIPFPTADIPKFGLDLPHKKQRV : 494
DrosMe : VQTIGKKYQRTGLLRS-WGIVPQL----- : 476
AraTha : VYSIGKPLDDWLKDMPAVA----- : 480
CryNeo : VVTIGT--GDRI----- : 468
HaloVo : YESLV----- : 430
EColi  : ----- : -
StrPyo : ----- : -

```

Structure and mechanism of human UDP-glucose dehydrogenase

Sigrid Egger¹, Apirat Chaikuad², Kathryn L. Kavanagh², Udo Oppermann² and Bernd Nidetzky¹

¹Institute of Biotechnology and Biochemical Engineering, Graz University of Technology, Petersgasse 12, A-8010 Graz, Austria

²Structural Genomics Consortium, University of Oxford, Old Road Campus Research Building, Roosevelt Drive, Headington, Oxford OX3 7DQ, United Kingdom

* Corresponding author; Tel. +43 316 873 8400; E-mail: bernd.nidetzky@tugraz.at

Keywords: UDP-glucose dehydrogenase, UDP-glucuronic acid, structure, catalytic mechanism

Abbreviations: UGDH, UDP- α -D-glucose 6-dehydrogenase; UDP-GlcA, UDP- α -D-glucuronic acid; UDP-Glc, UDP- α -D-glucose

Abstract

Elevated production of the matrix glucosaminoglycan hyaluronan is strongly implicated in epithelial tumor progression. Inhibition of synthesis of the hyaluronan precursor UDP-glucuronic acid (UDP-GlcA) therefore presents a potential target for cancer therapy. Human UDP-glucose 6-dehydrogenase (hUGDH) catalyzes, in two successive NAD⁺-dependent steps without release of the intermediate aldehyde, the biosynthetic oxidation of UDP-glucose (UDP-Glc) to UDP-GlcA. Herein we delineate the reaction coordinate of hUGDH using crystal structures of apo-enzyme, two ternary complexes (enzyme/UDP-Glc/NADH, enzyme/UDP-GlcA/NAD⁺), and a trapped thiohemiacetal intermediate in Glu161→Gln mutated enzyme. The quaternary structure of hUGDH is a disc-shaped trimer of homodimers whose subunits consist of two discrete α/β domains and an active site located in the interdomain cleft. Ternary complex formation is accompanied by rigid body and restrained movement of the N-terminal NAD⁺ binding domain, sequestering substrate and coenzyme in their reactive positions through interdomain closure. By alternating between conformations in and out of the active site during domain motion, Tyr14, Glu161, and Glu165 participate in control of coenzyme binding and release during two-fold oxidation. The thiohemiacetal intermediate structure identifies Cys276 as catalytic nucleophile of the reaction. Based on structural and kinetic evidence for wild-type and mutated enzymes, a catalytic mechanism is proposed where Lys220 is the general base for oxidation of UDP-glucose and together with Asn224, functions as oxyanion stabilizer during

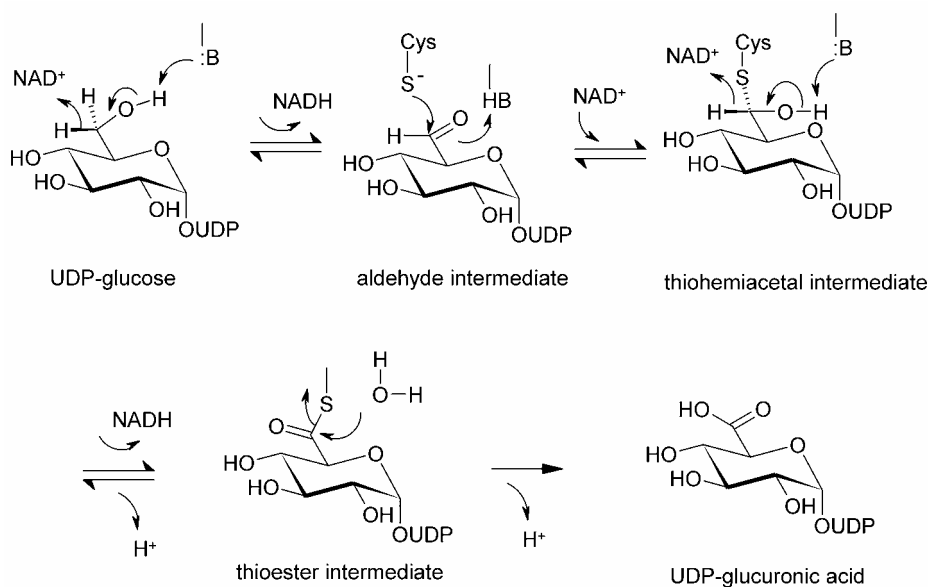
formation and breakdown of thiohemiacetal and thioester intermediates. Water bonded to Asp280 activates Cys276 for acting as aldehyde trap and contributes to oxyanion stabilization. Glu161 seems to facilitate water attack on thioester in the final hydrolytic step of the overall catalytic cycle.

Introduction

UDP-glucuronic acid (UDP-GlcA) fulfils a range of vitally important functions in human physiology. It serves as precursor for synthesis of extracellular matrix glycosaminoglycans (heparin, hyaluronan, chondroitin sulphate), which in turn play significant roles in diverse cellular processes like signaling, wound healing, inflammation, morphogenesis and matrix organization as well as in the pathobiology of cancer (1-3). UDP-GlcA is the substrate for enzymatic glucuronidation, a key step in numerous detoxification pathways carried out in liver and intestine (4). Biosynthetic routes toward various UDP-sugars involve UDP-GlcA as the central intermediate. UDP-GlcA is derived from UDP-glucose (UDP-Glc) whereby UDP-glucose 6-dehydrogenase (UGDH; EC 1.1.1.22) catalyzes, in two successive NAD⁺-dependent steps without release of the intermediate aldehyde, the four-electron oxidation of the substrate C6 alcohol into the corresponding carboxylic acid (5, 6). Elevated production of hyaluronan strongly promotes epithelial cancer progression, and it was shown that limitation of hyaluronan synthesis at the level of UDP-GlcA has significant potential in slowing tumor growth (7-9). Moreover, UGDH was recently proposed as novel biomarker for prostate cancer (10). Therefore, restriction of UDP-GlcA availability in cancer cells through inhibition of human UGDH (hUGDH) presents a novel target for therapy. Design of useful antagonists for hUGDH would greatly benefit from known relationships between enzyme structure and function.

Previous biochemical and mechanistic studies of UGDH have focused mainly on enzyme orthologs from bovine liver (5, 11-24) and *Streptococcus pyogenes* (*SpUGDH*) (6, 25-29). The catalytic reaction of UGDH is thought to occur in three steps via thiohemiacetal and thioester intermediates, as shown in Scheme 1. Crystal structures of *SpUGDH* were determined for enzyme complexes with UDP-GlcA/NAD(H) (PDB: 1DLJ for Cys260Ser) and UDP-xylose/NAD⁺ (PDB:1DLI for wild-type). These structures suggest that Lys220, Cys276 and active-site water bonded to Asp280 (amino acid numbering of the human enzyme is used) fulfill key roles in catalysis, with the cysteine being a clear candidate nucleophile (6, 25, 29). Site-directed mutagenesis of relevant residues in hUGDH confirmed the importance of the triad Lys/Cys/Asp for enzyme function (30, 31). However, it is currently unclear how each of the conserved active-site groups participates in the different steps of the UGDH catalytic cycle, and no experimentally determined high-resolution structure of the human enzyme has been reported. Due to the low

level of sequence identity (23%) between hUGDH and *Sp*UGDH, one cannot simply infer properties of the human enzyme from structure-function relationship data for the bacterial ortholog. For example, hUGDH differs from *Sp*UGDH, which is a homodimer, because it functions in a more complex hexameric assembly of protein subunits.



Scheme 1: Proposed catalytic mechanism of UDP-glucose 6-dehydrogenase (6).

Herein we report the first crystal structures of hUGDH presenting new insights into the structural basis for the particular quaternary organization of the human enzyme. We also provide crystallographic structure snapshots along the reaction coordinate of hUGDH which delineate the basic enzymatic mechanism. Detailed kinetic comparison of wild-type enzyme and relevant site-directed mutants thereof allows assignment of catalytic function to individual active-site groups. Localization of the rate-limiting step in native UGDH potentially informs the development of inhibitors for the enzyme.

Results and discussion

Overall structure of the functional hUGDH hexamer

Crystal structures of a truncated form of hUGDH (residues 1 – 466) were determined (Table S2, Supporting Information) because crystallization of the full-length enzyme (residues 1 – 494) had failed. However, the C-terminal deletion did not affect the enzyme activity, as demonstrated in initial-rate assays using purified hUGDH preparations (Table S4, Supporting Information). Figure 1A depicts the tertiary fold of the enzyme protomer with UDP-Glc and NAD⁺ bound. Superimposition of the dimeric ortholog from *Sp*UGDH and hUGDH reveals a highly conserved

overall fold (rmsd of 1.5 Å for 351 equivalent C α atoms; Figure 1B). Minor differences among the two enzymes are observed at the C-terminal domain where in the shorter bacterial enzyme (residue 1 - 402) the floppy tail packs on top of the substrate binding pocket (Figure 1B). For a detailed comparative analysis of *SpUGDH* and hUGDH structures see Supporting Information. Assembly of the subunits to form the dimer (Figure 1C) and the functional hexamer (trimer of dimers) of hUGDH is shown in Figure 1D. The subunit of hUGDH consists of two domains, each of which adopts a highly similar α/β fold whereby a six-stranded parallel β -sheet core is flanked by α -helices on both sides (Figure 1A).

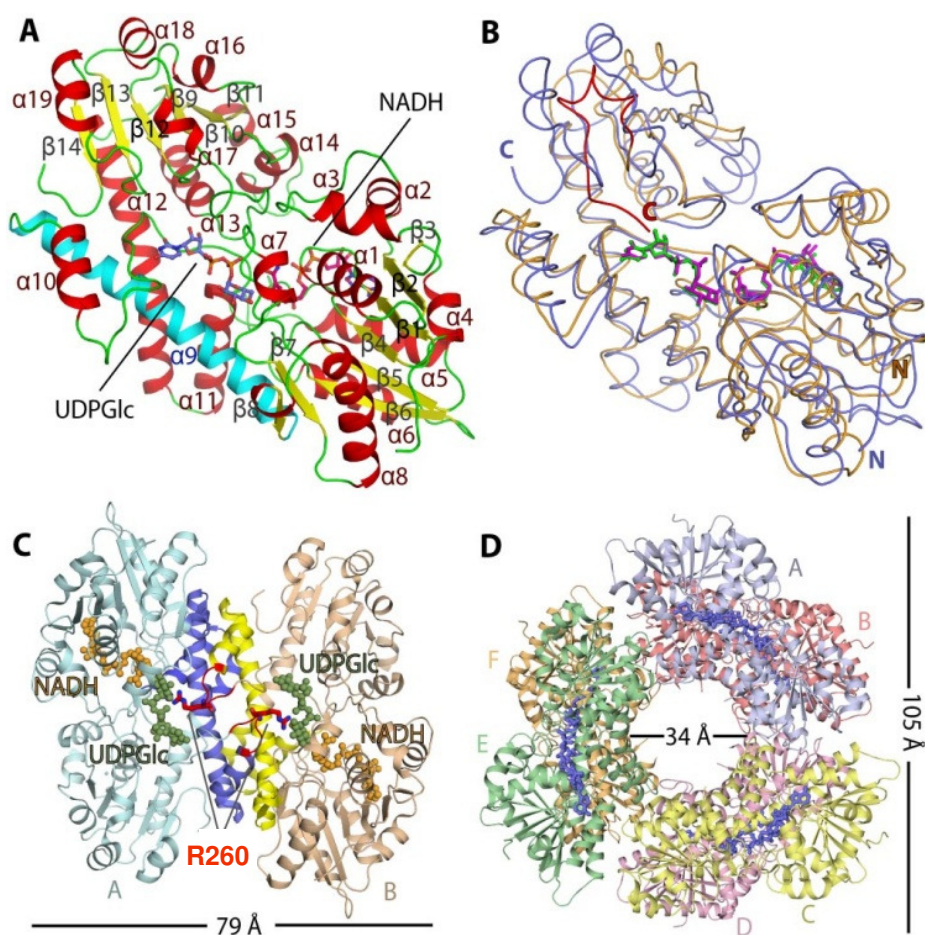


Figure 1: Structure overview. **A.** monomer of hUGDH with numbering of α -helices shown in red (with the central interdomain α_9 helix in cyan) and β -strands (yellow). **B.** superimposition of hUGDH (blue) and *SpUGDH* (orange) – red region of *SpUGDH* shows shorter C-terminus that packs on top of substrate binding pocket. **C.** dimeric assembly – all interacting regions are highlight in blue and yellow with Arg260 (red) from the loop that connects α_{10} and α_{11} shown in stick representation. **D.** hexameric quaternary structure of hUGDH.

The N-terminal domain (residues 1 – 212) has the familiar Rossmann fold. We describe below crystal structures of hUGDH in complex with UDP-Glc/NADH (PDB: 2Q3E) and UDP-GlcA/NAD⁺ (PDB: 2QG4), see Figure 1B, blue α -carbon trace. These structures reveal that the N-terminal domain is primarily responsible for binding of the NAD⁺ cofactor. The C-terminal domain, by contrast, provides residues required for binding of UDP-Glc. The domain interface is located in the central region of the subunit and consists mainly of interdomain helix α 9 (residues 213 – 244), which bridges the last β -strand (β 8) of the N-terminal domain and the first helix of the three helices (α 10 – α 12) of the C-terminal domain. Crystallographic observation of occupancy of the NAD(H) site with UDP-Glc substrate (PDB: 3KHU) (Figure S1, Supporting Information) underscores the interdomain pseudo-symmetry within the hUGDH subunit.

hUGDH forms a disc-shaped double-layer hexameric structure assembled from a trimer of dimers. Each dimer pair is related by a three-fold symmetry axis running through a central channel, perpendicular to the view in Figure 1D. The dimer interface is located adjacent to the UDP-Glc binding pocket and is created through “head-to-tail” arrangement of the individual subunits approaching each other in a “back-to-back” orientation (Figure 1C). Dimer contacts mainly in the form of hydrophobic interactions and hydrogen bond networks are provided by the interdomain helix as well as by the helices α 10 – α 12. In spite of global similarity, dimerization in hUGDH and *Sp*UGDH differs due to sequence variation (32). The hydrogen bond network in the central region of the dimer interface, for example, appears to be stronger in hUGDH where Ser233, Tyr299, and Gln229 substitute for the corresponding residues (Tyr217, Leu279, and Leu213) in *Sp*UGDH, respectively.

Intersubunit contacts between adjacent dimer pairs forming the enzyme hexamer are distinct from the ones involved in dimerization (32). They exploit a completely different oligomeric interface, which has ~48% less contact area than the dimer interface (~2673 Å²). The loop connecting β 4 and α 5 (residues 88 – 105) in the N-terminal domain of subunit A is located close to the central channel and extends to the C-terminal edge of subunit C where it forms intersubunit contacts with the loop between β 11 and α 12 (residues 322 – 330). Dimer-dimer interactions include hydrogen bonds of Lys94^(A) with Glu360^(C) and Asn324^(C), Tyr96^(A) with Tyr327^(C), Met98^(A) with Glu360^(C), and Asp105^(A) with Thr325^(C). Further stabilization of the hexamer is derived from a salt bridge between Glu110^(A) and Lys329^(C) as well as from a hydrogen bond network involving Arg114^(A), Lys343^(C), and Asn147^(A). Site-directed mutagenesis data were previously interpreted to support a critical role of Lys279, Ala222, and Ser223 in hUGDH hexameric assembly (31, 33). However, due to their positions in the structure remote from the relevant interface, stabilization of the enzyme hexamer by these residues must

be indirect. The importance of Lys279 is plausibly linked to structural stabilization of the β 4- α 12 loop and to formation of the NAD⁺ binding pocket. Stabilization by Ala222 and Gly223 would seem to facilitate stability of the hUGDH dimer, prior to formation of the “trimer of dimers”. Structural and sequence comparisons reveal that interactions of residues leading to higher-order oligomerization in hUGDH, which are mainly conserved in enzymes from higher phylogenetic lineages, are completely absent in dimeric enzymes from bacteria (32).

Binding of substrate and coenzyme

The structures of ternary complexes of hUGDH bound with UDP-Glc/NADH (PDB: 2Q3E) and UDP-GlcA/NAD⁺ (PDB: 2QG4), reveal how substrate and coenzyme (Figure 2A and 2B) are accommodated by the enzyme. The binding pocket for UDP-Glc is built from amino acids of both domains whereby, as in *SpUGDH* (25), anchoring the substrate is achieved primarily by residues from C-terminal domain (UMP) and assistance of some N-terminal domain residues interacting with the α -glucose 1-phosphate portion of the substrate.

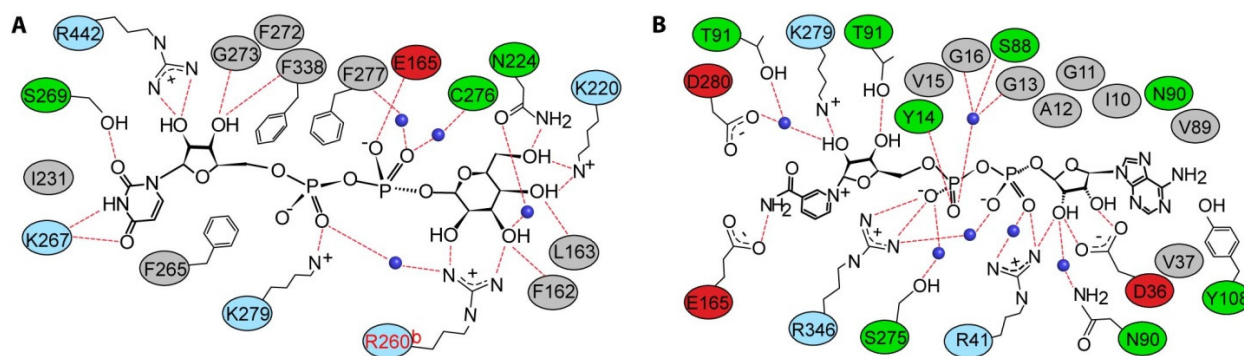


Figure 2. Binding pockets of hUGDH. Schematic diagrams of A. substrate and B. cofactor binding sites. Amino acids lining the pockets are presented in colors according to their charge properties; red for acidic, blue for basic, grey for non-polar, green for uncharged polar, and water molecules are shown in blue spheres. Interactions between substrate/cofactor formed either to main chains or, if shown, side chains of these residues and are shown in dashed red lines.

The active site is situated in a cleft at the domain interface, with six highly conserved residues presumably being involved in catalysis (see later and Figure S1, Supporting Information): Thr131, Glu161, Lys220, Asn224, Cys276, and Asp280. A water molecule forming hydrogen bonds (~ 2.6 Å) to the carboxyl group of Asp280 and Thr131 is conserved in all structures. Its position in the active site immediately suggests a possible function in acid-base

catalysis. The water is likewise a candidate nucleophile for the final hydrolysis step of the catalytic cycle (Scheme 1), as discussed later. It also forms a hydrogen bond with the C2 ribose hydroxyl of NAD⁺ (2.9 Å), arguably facilitating the approximation of the reactive groups of substrate and coenzyme in the active site.

Contribution of the loop connecting helices α 10 and α 11 to subunit-subunit interactions (Figure 1C) positions Arg260 to the UDP-Glc binding pocket of the adjacent subunit. The guanidinium group of Arg260 forms a bidentate hydrogen bond with glucopyranosyl hydroxy groups at C2 and C3 (Figure 2A). This indicates a possible communication between the two active sites during substrate binding. However, steady-state analysis of NAD⁺-dependent oxidation of UDP-Glc by hUGDH did not support substrate kinetic cooperativity in the enzymatic reaction (see later). There was also no indication for half-of-the-sites binding of UDP-Glc in the structure because all active sites were occupied with substrate. In any case, the structural features seen in Figure 2A strongly support a role of dimerization for enzyme function.

Detailed structural comparison of the subunit of apo-hUGDH with that of the UDP-Glc/NAD⁺ ternary complex (Figure 3A) demonstrates significant structural alterations among them, emphasized on the angular variation between the two domains. Detailed analysis of the structures and biochemical data provides evidence (see later) that UDP-Glc binds to hUGDH and the C-terminal domain is fixed in place. Subsequent nucleotide cofactor binding is accompanied by $\sim 13^\circ$ rotation of the Rossmann-fold domain toward the fixed C-terminal domain. This “domain-closure” conformational change results from a combination of rigid body and restrained movements of the N-terminal domain and involves Leu218-Leu227 from the α 9 helix as hinge region (Figure 3A, close up) as confirmed by protein domain motion analysis program DynDom (<http://fizz.cmp.uea.ac.uk/dyndom/>).

In accordance with the bi-uni-uni-bi ping-pong mechanism proposed for *Sp*UGDH (26), this observation has two important consequences for the catalytic mechanism of hUGDH. First, substrate and coenzyme are sequestered in their reactive positions and the active site is closed up. Second, exchange of NADH by NAD⁺ in the course of the two-step oxidation requires intermittent domain opening. Interestingly, the structure of a thiohemiacetal intermediate (PDB: 3KHU) to be described below, in which UDP-Glc occupies the site where normally NAD⁺ binds, shows a “semi-open” domain orientation that is only 3° different from the fully “open” conformation seen for apo-hUGDH. Superimposition of all three structures in Figure 3A therefore provides strong support in favor of the notion that NAD(H) exchange steps in the catalytic cycle of hUGDH are coupled to “opening” and “closing” motions of the N-terminal domain. The structural trajectory from the “open” to the “closed” conformation of hUGDH is also traceable as a change of residue occupancy within the coenzyme binding site whereby Tyr14

and Glu161 alternate with Glu165 between conformations in and outside of the binding pocket (Figure 3B).

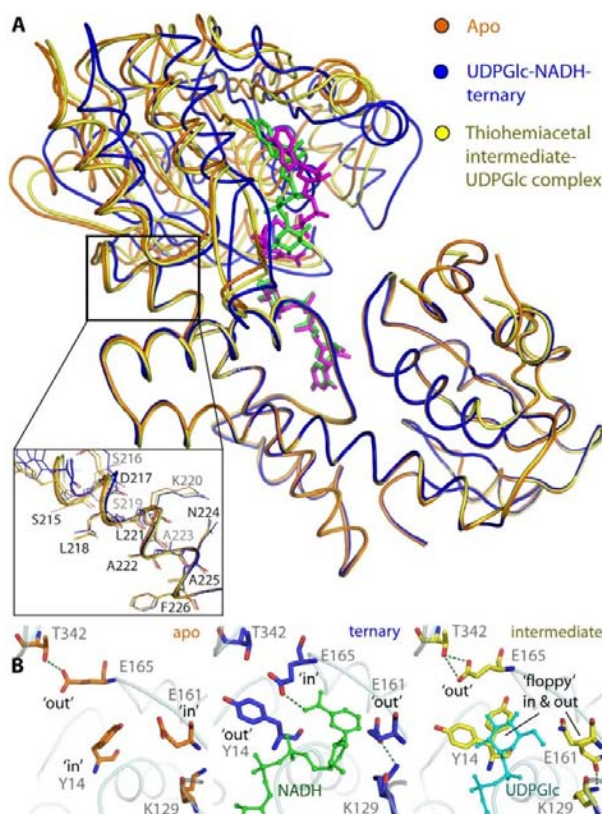


Figure 3: Closure of N-terminal domain upon cofactor binding. A) Superimposition of apo, UDPGlc-NADH ternary, and thiohemiacetal-intermediate-UDPGlc complex reveals significant movement of N-terminal lobe, corresponding to enclosure of the active site upon cofactor binding. Inset shows the ‘hinge’ region at 218-221 residues of $\alpha 9$. **B)** Conformational changes of residues in the cofactor binding pocket at the domain interface. Note two modes of Y14, E165 and E161, which are related to catalytic states of the enzyme and the presence of the cofactor in the binding pocket.

Interactions with Thr342 and Lys129 stabilize Glu165 and Glu161 in their respective “out” conformations. Bonding of Glu165 with the carboxamide of NAD^+ brings the *si* face of the nicotinamide ring into a suitable position for pro-*S* stereospecific hydride transfer to its C4 atom, implying that global structural rearrangements of hUGDH in response to substrate/coenzyme binding are precisely relayed into the active site where they appear to be directly conducive to catalysis. The “semi-open” conformation of the thiohemiacetal intermediate has Glu165 pointing toward Thr342 away from the binding pocket whereas Tyr14 and Gln161 adopt flexible conformations. The “in” conformation of Glu(n)161 would generate a steric conflict with the nicotinamide ring of NAD^+ , indicating that “out” \rightarrow “in” movement of Glu161 could serve as trigger

for release of NADH at the steps prior to the formation of thiohemiacetal and thioester intermediate. Interestingly, Tyr14, Glu161 and Glu165 are conserved across UGDH primary structures but their roles were previously not known.

Biophysical and biochemical characterization

Here we provide further insight into binding of substrate and coenzyme to hUGDH. Using differential scanning fluorimetry we determined apparent melting temperatures (T_m) of hUGDH alone and in the presence of different ligands. Substrate (product) and coenzyme acted synergistically in enhancing the stability of the apo-enzyme ($T_m \approx 50$ °C), the observed increase in T_m being as large as 15 ± 1 °C when either UDP-Glc/NADH or UDP-GlcA/NAD⁺ was added to the enzyme solution (Table S3, Supporting Information). Considering that the apo-hexamer has ~12% more exposed surface area than the average surface area of the also hexameric ternary complex (103170 vs. 91880 Å²), it is plausible that conformational rearrangement of hUGDH upon ternary complex formation confers this extra stability to the protein structure.

Using isothermal titration calorimetry (ITC) we showed that UDP-Glc binds to apo-enzyme of wild-type hUGDH with a dissociation constant (K_d) of 17 ± 2 μM and a large favorable free enthalpy of -6.2 kcal/mol ($\Delta H = -3.3 \pm 0.5$ kcal/mol; $T\Delta S = 2.9$ kcal/mol). The observed K_d is in close agreement with the kinetically determined Michaelis constant for UDP-Glc (Table S4, Supporting Information). Addition of NAD⁺ to apo-enzyme failed to produce a heat signal under otherwise identical conditions, suggesting that NAD⁺ does not bind to hUGDH unless the enzyme-substrate complex has formed. We employed a Cys276Ala mutant of hUGDH that showed negligible activity toward substrate conversion in the timespan of the ITC experiment, to determine a K_d of 1.6 ± 0.3 μM for binding of NAD⁺ to the complex of enzyme and UDP-Glc ($\Delta G = -7.5$ kcal/mol; $\Delta H = -8.6 \pm 0.5$ kcal/mol; $T\Delta S = -1.1$ kcal/mol). Comparison of this K_d with the relevant K_m (Table S4, Supporting Information) reveals that the affinity of Cys276Ala for binding NAD⁺ in the first round of the two-fold oxidation ($\sim 1/K_d$) was about two orders of magnitude larger than the kinetically determined apparent affinity for NAD⁺ ($\sim 1/K_m$). UDP-Glc binding stoichiometry in wild-type apo-enzyme was lower than unity (0.4 ± 0.1), possibly hinting at a cooperative effect of NAD⁺ concentrations (in the range of K_d) on substrate binding. However, no evidence for substrate/coenzyme kinetic cooperativity was observed in all initial-rate experiments that used NAD⁺ in a physiologically relevant concentration range (~ 0.5 mM, equaling $0.7 \times K_m$; see Figure S2, Supporting Information).

Kinetic dissection of catalytic steps during two-fold oxidation of UDP-Glc

Stopped-flow experiments were performed with the aim of analyzing oxidation of substrate alcohol and aldehyde as kinetically separated reaction steps. Time courses of UDP-Glc conversion by wild-type hUGDH (Figure 4A) were characterized by a transient “burst” of NADH formation that was followed by the linear steady-state phase. From appropriate fit of the data, we determined the portion of the total molar enzyme concentration that was turned over in the “burst” and found (Figure 4B) that it decreased as the concentration of NAD^+ was raised. This result implies that there is a slow step in the enzymatic reaction that occurs after the formation of NADH and the contribution of this step to overall rate limitation decreases at high NAD^+ concentration. In the case of the scenario proposed for *SpUGDH* that hydrolysis of thioester is rate-determining overall, the molar ratio of NADH produced in the “burst” and enzyme present has a limiting value of 2 (6). Using substrate and NAD^+ concentrations that saturate the enzyme in the steady state, one would therefore expect that the observable ratio be at least 1 or greater. In hUGDH, the “burst” ratio at high NAD^+ is only ~ 0.25 , strongly suggesting that a step prior to oxidation of aldehyde is slow.

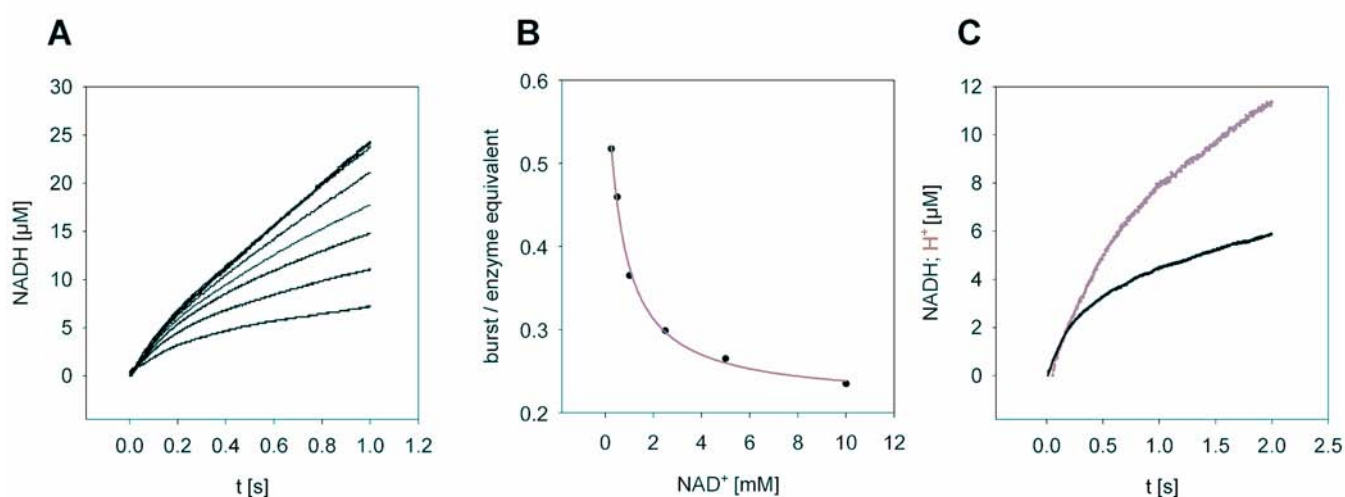


Figure 4: Fast kinetic analysis of wild-type hUGDH. **A.** Stopped flow traces of UDP-glucose conversion by hUGDH wild-type. Increasing NAD^+ concentrations (0.1 mM, 0.25 mM, 0.5 mM, 1 mM, 2.5 mM, 5 mM, 10 mM) enhance steady state rate constant. The initial burst phase separating the ADH from the ALDH reaction is distinct in all conditions. **B.** Stopped flow traces of UDP-glucose conversion by UGDH wild-type. Evaluation of μM NADH produced during the initial burst phase related to enzyme equivalent present with increasing and saturating concentrations of NAD^+ . **C.** Stopped flow traces of UDP-glucose conversion by UGDH wild-type under subsaturating conditions of 0.1 mM NAD^+ and a saturating concentration of 1 mM UDP-glucose. Comparison of proton release (grey line) and hydride transfer (black line).

The presteady-state rate constant of NADH formation increased only 2.5-fold, to a limiting value of 10 s^{-1} , in response to an increase in the NAD^+ concentration from 0.1 to 10 mM while there was a 20-fold change in the steady-state rate constant within the same NAD^+ range. Together with the observation (for Cys276Ala) that the K_d for NAD^+ is smaller than the corresponding K_m , these data provide strong support in favor of the notion that in the presence of physiological concentrations of NAD^+ ($\leq 1 \text{ mM}$) the slowest part of the reaction of wild-type hUGDH is binding of the second cofactor molecule required for aldehyde oxidation.

The enzymatic reaction of hUGDH, $\text{UDP-Glc} + 2 \text{ NAD}^+ + \text{H}_2\text{O} \rightarrow \text{UDP-GlcA} + 2 \text{ NADH} + 2 \text{ H}^+$, implies, that two protons are released as result of substrate oxidation. At neutral pH, a third proton will appear due to ionization of UDP-GlcA. A molar ratio of 2/3 for NADH and proton formed in the steady state was confirmed (data not shown). Because the relative timing of the transfer of hydride and proton in the kinetic transient potentially contains important mechanistic information, we performed the stopped-flow experiments depicted in Figure 4C and found that in the in the “burst” phase, the change in total proton concentration was twice (1.9 ± 0.1) the molar equivalent of NADH formed. In other words, two protons were released prior to the rate-limiting step (see later).

Trapped thiohemiacetal intermediate in Glu161Gln mutant

In order to bring the nicotinamide ring of NAD^+ into hydride transfer position Glu161 must move away from its original place in the active site of the apo-enzyme. We speculated that replacement of Glu161 by Gln might destabilize a reactive conformation represented by the structure of the UDP-Glc/NADH complex where Glu161 is drawn away by stabilizing contacts to Lys129. The Glu161Gln mutant displayed a 500-fold decrease in specific activity as compared to wild-type hUGDH, partly caused by a strongly reduced NAD^+ binding affinity ($K_m > 10 \text{ mM}$; not saturable, Table S4, Supporting information). Transient kinetic data for Glu161Gln (Figure S3, Supporting Information) reveal that under conditions of NAD^+ being present in large excess (15 mM), there was a large pre-steady state “burst” of NADH formation that corresponded to exactly one molar equivalent of enzyme used in the reaction. When compared to the relevant rates for the wild-type enzyme, the disruptive effect of the mutation was about 30-fold higher on the steady-state rate than it was on the transient rate (15-fold decrease).

The immediate suggestion from the kinetic properties of Glu161Gln that a covalent enzyme intermediate might accumulate under steady-state reaction conditions is supported by a time-resolved MS experiment and the crystal structure. Thereby we identified of a molecular species displaying the mass increase relative to apo-enzyme that would be expected if a catalytically competent hemiacetal intermediate of Glu161Gln (apo-enzyme: $52019 \pm 1 \text{ g/mol}$;

putative intermediate: 52581 ± 1 g/mol; experimental Δ_{mass} : 562 ± 2 g/mol calculated Δ_{mass} : 564 g/mol) was formed as a first step of conversion of UDP-Glc and NAD^+ (data not shown).

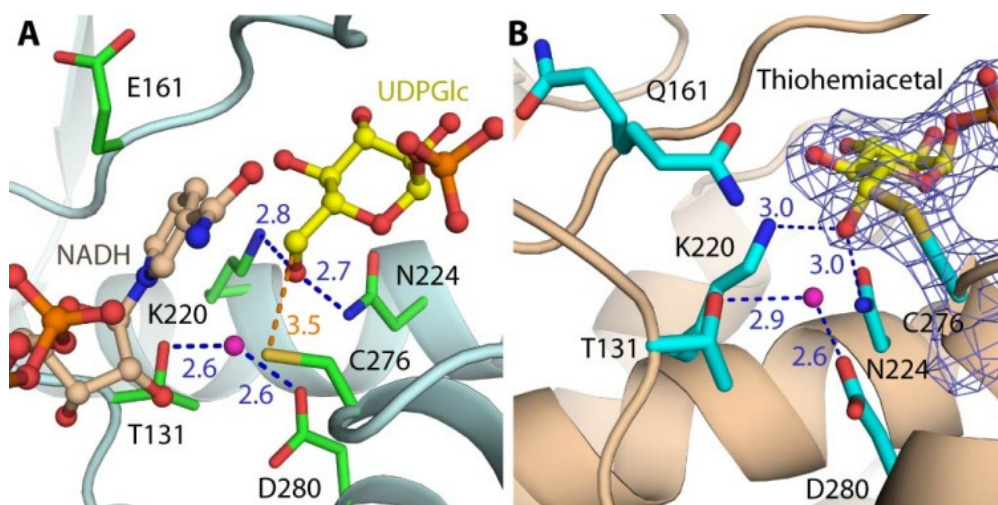


Figure 5. Active sites of hUGDH. **A)** The active site of UDPGlc-NADH-hUGDH complex unveils positions of six key residues, with a potential nucleophilic water molecule shown in magenta sphere. **B)** Electron density map (contour at 1.0σ) confirms the presence of the trapped thiohemiacetal intermediate. Active site residues and nucleophilic water molecule are in similar positions as in the ternary complex except two conformations of the mutated Q161.

Figure 5B shows a close-up of the Glu161Gln active site derived from the structure of the mutant in which this covalent thiohemiacetal intermediate has been trapped in the crystal. Structural comparison to the UDP-Glc/NADH complex (Figure 5A) reveals that except for Cys276, the spatial arrangement of active-site residues was hardly affected by formation of the intermediate (Figure 5B). The position of the glucopyranosyl ring in the substrate binding pocket was unchanged in the intermediate structure as compared to the ternary complex structure. Electron density for the covalently bound ligand in Figure 5B is best compatible with a tetrahedral (sp^3 hybridized) reactive carbon on substrate, corroborating kinetic data in the suggestion that the intermediate is truly a thiohemiacetal, not a thioester. Gln161 is seen to adopt two different conformations in and out of the active site, as shown in Figure 5B. A structural overlay of the ternary complex and the thiohemiacetal intermediate (having Gln161 in the “out” conformation) shows that the C6 of covalently bound UDP-gluco-hexodialdose would be in suitable hydride transfer distance (2.9 \AA) to nicotinamide ring C4 of NAD^+ (data not shown). Extremely low affinity of Glu161Gln for binding NAD^+ to perform the second oxidation plausibly explains accumulation of the thiohemiacetal intermediate in this mutant.

Proposed catalytic mechanism of hUGDH, and its implication

Structure snapshots along the enzymatic reaction coordinate combined with results of kinetic data from site-directed mutants (Table S4, Supporting Information) suggest a catalytic mechanism for hUGDH which is summarized in Scheme 2. In this mechanism, Lys220 functions as a general base for alcohol oxidation. In support of this catalytic role, a Lys220Ala mutant was 1.4×10^4 -fold less active than the wild-type enzyme. Addition of primary amines resulted in partial complementation of the catalytic defect in Lys220Ala, and the pH dependence of this “chemical rescue” was consistent with catalytic participation from the unprotonated amine. The time course of NADH formation upon oxidation of UDP-Glc by Lys220Ala displayed a presteady-state lag phase of several minutes (Figure S4B, Supporting Information). This transient lag, which indicates the occurrence of a slow step prior to the first hydride transfer step, was eliminated completely in the presence of external amine so that the reaction time course eventually became linear (Figure S4A, Supporting Information, trace V in dark grey). Deprotonation of Lys220 to solvent regenerates the uncharged ϵ -amino side chain which is exploited, together with the carboxamide side chain of Asn224, as oxyanion stabilizer in the following steps of the catalytic cycle.

The role of Cys276 as catalytic nucleophile of the reaction is established by crystallography. However, there is the mechanistically important question of the relative timing of hydride transfer from the alcohol substrate and formation of the thiohemiacetal intermediate. A Cys276Ser mutant was about 6000-fold less active than the wild-type enzyme. The time course of NADH formation by this mutant was characterized by an initial release of product in amounts corresponding to precisely one molar equivalent of enzyme used, followed by a very slow steady-state phase of reaction (Figure S4A, Supporting Information, trace II in grey). ESI-MS analysis of a sample taken from the reaction mixture revealed that the mass of Cys276Ser had increased by 561 ± 2 g/mol (data not shown). Considering the expected mass increase for a covalent adduct between Ser276 and the UDP-gluco-hexodialdose resulting from one-step oxidation of UDP-Glc (564 g/mol), the kinetic behavior of Cys276Ser, like that of an analogous mutant of *SpUGDH* (29), is explained by formation and very slow breakdown of a hemiacetal intermediate. The Cys276Ala mutant, by contrast, converted UDP-Glc continuously in the absence of a transient “burst” of product formation. This result suggests that complete removal of a catalytic nucleophile from the enzyme does not specifically disrupt the second step of the twofold oxidation of UDP-Glc, as one might expect for a stepwise reaction in which formation and covalent trapping of substrate aldehyde are kinetically uncoupled one from another.

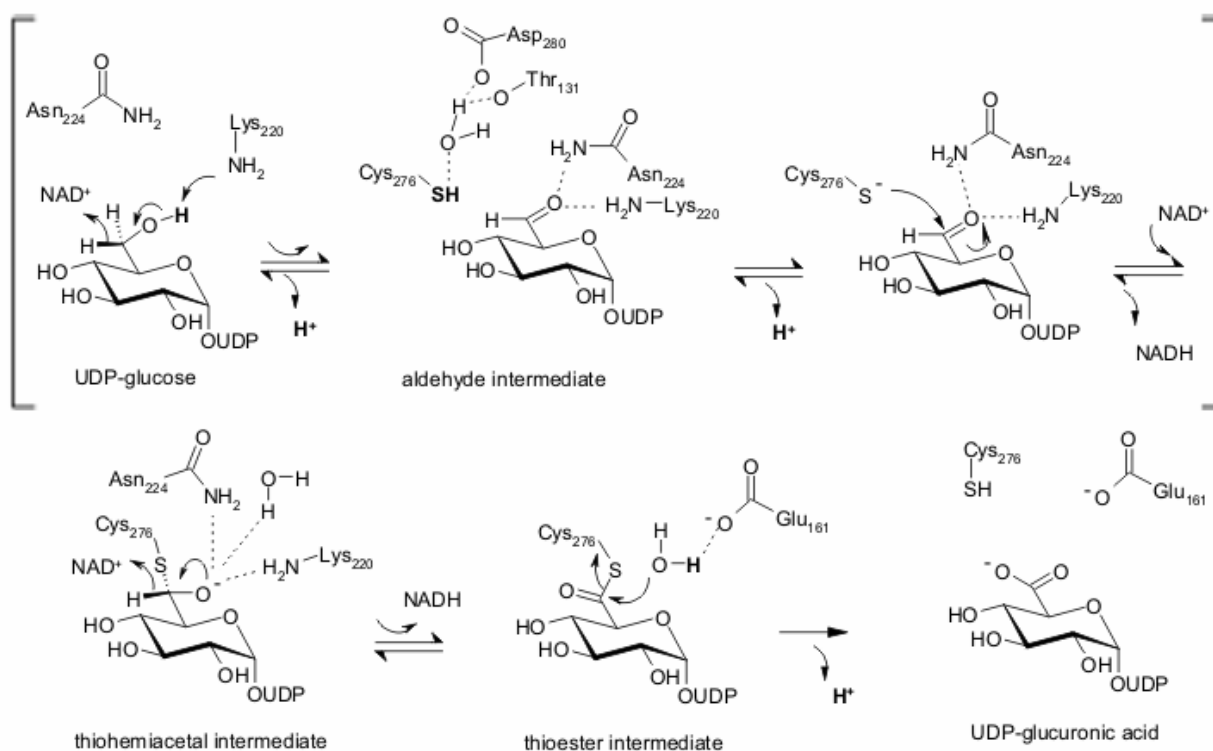
We therefore propose that nucleophilic attack from Cys276 takes place in a concerted manner with hydride transfer from alcohol. Kinetic data showing that two protons are released to

bulk solvent in the course of the first oxidation step are consistent with coupling of chemical reaction and “activation” of Cys276 through deprotonation. Active-site water bonded to Asp280 is ideally positioned to pull off the proton. Loss of catalytic participation from Cys276 explains the large disruptive effect of an Asp280Ala mutation on enzyme activity (Table S4, Supporting Information and Scheme 2). Comparison of the conformations of Cys276 in ternary complex (Figure 5A) and thiohemiacetal intermediate (Figure 5B) reveals that minimal side chain rotation (~ 2 Å) is required for the cysteine to adopt a position not only suitable for attack on carbon, but arguably also conducive to the hydride transfer via a back-side nucleophilic “push”. The proposed action of Cys276 fulfils the principle of least nuclear motion in catalysis because it avoids structural rearrangement of substrate and enzyme groups required for accommodating a stepwise reaction coordinate with the associated multiple changes in hybridization of the reactive carbon ($sp^3 \rightarrow sp^2 \rightarrow sp^3$). The thiohemiacetal formed in the proposed reaction of hUGDH is an oxyanion, suitably stabilized by strong hydrogen bonding interactions with Lys220 (3.0 Å), Asn224 (2.9 Å), and water (2.8 Å).

Reloading the active site with NAD^+ for the second oxidation to occur requires a full round of domain opening and closing, accompanied by the described conformational changes of Glu161 and Glu165. In the presence of physiological concentrations of NAD^+ , this is the slowest step of the overall reaction. At steady state under these conditions, therefore, a substantial fraction of the enzyme will be present as thiohemiacetal intermediate. Search for selective inhibitors of hUGDH could explore ligand binding to the N-terminal coenzyme binding domain of the covalently modified enzyme. The thiohemiacetal intermediate structure showing occupancy of the NAD^+ binding pocket with UDP-Glc in all monomers could provide a useful basis for inhibitor design (Figure S1, Supporting Information). Because NAD^+ binds about $4 \cdot 10^2$ -fold less tightly to the intermediate than it binds to the enzyme-substrate complex, competition between a suitable inhibitor and NAD^+ should be best available for exploitation in the covalent intermediate.

NAD^+ -dependent conversion of thiohemiacetal to thioester, release of NADH from the active site, and hydrolysis of thioester followed by UDP-GlcA product dissociation complete the reaction coordinate of hUGDH. The structure of enzyme bound with UDP-GlcA shows that half of the subunits bound an NAD^+ molecule, but Glu161 has adopted the “out” conformation. The other monomers revealed Glu161 in the “in” conformation displacing the nicotinamide ring of coenzyme from the active site. Irrespective of whether NADH is actually dissociated from hUGDH at the time of the hydrolysis step, we believe, in agreement with interpretation of structural evidence for *Sp*UGDH, that the presence of Glu161 in the catalytic center is conducive to breakdown of the thioester. One possibility is that Glu161 provides catalytic

assistance (3.1 Å) to the attack of the water molecule in the plane below the reactive substrate carbon in the structure of the thiohemiacetal intermediate (Figure S1, Supporting Information) on the thioester (3.6 Å). An attractive feature of this scenario is that hydrolysis would be achieved through a tetrahedral intermediate geometrically analogous to the thiohemiacetal. An alternative possibility is that active-site water functions as nucleophile (distance to reactive carbon: 3.8 Å), and Asp280 (2.5 Å) and Thr131 (2.9 Å) would be well positioned for providing base catalytic assistance to its reaction. There is a chain of water molecules connecting active-site water to bulk solvent, providing a plausible route through which the catalytic site could recruit a fresh water molecule post-hydrolysis. Glu161 is too far away from nucleophilic water (~4 Å) to fulfill a catalytic role but its presence could generate a favorable electrostatic environment. UDP-GlcA would be the last product to dissociate from the enzyme, completing the catalytic cycle. Summarizing, therefore, this paper presents a comprehensive structural characterization of structure of hUGDH and delineates the first complete reaction coordinate for any member of this class of enzymes. Considering the roles of hUGDH as cancer biomarker and potential drug target, the results are relevant for exploitation in the development of novel inhibitors for this enzyme.



Scheme 2. Proposed catalytic mechanism. The alcohol dehydrogenase part of the reaction (Lys220 as catalytic base abstracts the proton from C6 hydroxyl and hydride transfer to the first NAD⁺) proceeds in a concerted manner without the release of the intermediate aldehyde,

indicated as []. Two protons are released (indicated in bold letters) before the rate limiting step which is the exchange of NADH with the second NAD⁺ cofactor needed for the subsequent aldehyde dehydrogenase part of the reaction accompanied by domain motion and conformational changes of Glu161 and Tyr14 in- and outwards the active site. The aldehyde intermediate is subjected to the second hydride transfer to NAD⁺, the oxyanion is stabilized by Lys220, Asn224 and the catalytic site water. Conformational rearrangement of Glu161 towards the thioester intermediate leads to release of NADH due to steric hindrance and activates the water molecule in close vicinity (3.1 Å) to Glu161 for the final hydrolysis step. Release of the last proton due to ionization of the product UDP-GlcA takes place and the product dissociates.

Methods summary

A clone encoding human UGDH residues 1-467 in a pBEN derived vector with an N-terminal solubility enhancement and Streptavidin tag followed by a tobacco etch virus (TEV) protease cleavage site was used. As expression strain the phage-resistant *E. coli* BL21(DE3)-R3 was employed. Cells were lysed with a high-pressure cell disruptor and purified to homogeneity using a sequence of streptavidin, gel filtration (Superdex 200 16/60 HiLoad, GE/Amersham Biosciences) and anion exchange (HiTrap-Q HP) chromatography. The 10 kDa tag was removed by incubation with TEV protease prior to size exclusion chromatography step even though it did not affect activity (data not shown). Site-directed mutagenesis was performed using QuikChange Site-Directed Mutagenesis Kit (Stratagene, La Jolla, CA) according to the manufacturer's protocol. Oligonucleotides are listed in supplementary information. Crystal structures of WT and mutant hUGDH were determined by molecular replacement of *C. elegans* UGDH (PDB ID: 2O3J) as search model. Kinetic characterization of hUGDH was carried out by measuring initial rates of NAD⁺ dependent oxidation of UDP-Glc at 25°C in potassium phosphate buffer (50mM, pH 7.5). For detailed description see supplementary information.

References

1. Fraser, J. R., Laurent, T. C., & Laurent, U. B. (1997) *J. Intern. Med.* **242**, 27-33.
2. Bharadwaj, A. G., Rector, K., & Simpson, M. A. (2007) *J. Biol. Chem.* **282**, 20561-20572.
3. Stern, R. (2008) *Semin Cancer Biol* **18**, 237.
4. Gueraud, F. & Paris, A. (1998) *Gen. Pharmacol.* **31**, 683-688.
5. Feingold, D. S. & Franzen, J. S. (1981) *Trends Biochem. Sci.* **6**, 103-105
6. Ge, X., Penney, L. C., van de Rijn, I., & Tanner, M. E. (2004) *Eur. J. Biochem.* **271**, 14-22.
7. Simpson, M. A., Wilson, C. M., & McCarthy, J. B. (2002) *Am. J. Pathol.* **161**, 849-857.
8. Huh, J. W., Choi, M. M., Yang, S. J., Yoon, S. Y., Choi, S. Y., & Cho, S. W. (2005) *Biotechnol. Lett.* **27**, 1229-1232.
9. Auvinen, P., Tammi, R., Parkkinen, J., Tammi, M., Agren, U., Johansson, R., Hirvikoski, P., Eskelinen, M., & Kosma, V. M. (2000) *Am. J. Pathol.* **156**, 529-536.
10. Huang, D., Casale, G. P., Tian, J., Lele, S. M., Pisarev, V. M., Simpson, M. A., & Hemstreet, G. P., 3rd (2010) *Int. J. Cancer* **126**, 315-327.
11. Franzen, J. S., Kuo, I., Eichler, A. J., & Feingold, D. S. (1973) *Biochem. Biophys. Res. Commun.* **50**, 517-523.
12. Franzen, J. S., Ashcom, J., Marchetti, P., Cardamone, J. J., Jr., & Feingold, D. S. (1980) *Biochim. Biophys. Acta* **614**, 242-255.
13. Franzen, J. S., Ishman, R., & Feingold, D. S. (1976) *Biochemistry* **15**, 5665-5671.
14. Franzen, J. S., Marchetti, P. S., & Feingold, D. S. (1980) *Biochemistry* **19**, 6080-6089.
15. Franzen, J. S., Marchetti, P. S., Lockhart, A. H., & Feingold, D. S. (1983) *Biochim. Biophys. Acta* **746**, 146-153.
16. Eccleston, E. D., Thayer, M. L., & Kirkwood, S. (1979) *J. Biol. Chem.* **254**, 11399-11404.
17. Hempel, J., Perozich, J., Romovacek, H., Hinich, A., Kuo, I., & Feingold, D. S. (1994) *Protein Sci.* **3**, 1074-1080.
18. Ordman, A. B. & Kirkwood, S. (1977) *Biochim. Biophys. Acta* **481**, 25-32.
19. Ordman, A. B. & Kirkwood, S. (1977) *J. Biol. Chem.* **252**, 1320-1326.
20. Prihar, H. S. & Feingold, D. S. (1979) *FEBS Lett.* **99**, 106-108.
21. Ridley, W. P., Houchins, J. P., & Kirkwood, S. (1975) *J. Biol. Chem.* **250**, 8761-8767.
22. Ridley, W. P. & Kirkwood, S. (1973) *Biochem. Biophys. Res. Commun.* **54**, 955-960.
23. Schiller, J. G., Bowser, A. M., & Feingold, D. S. (1972) *Carbohydr. Res.* **25**, 403-410.
24. Schiller, J. G., Bowser, A. M., & Feingold, D. S. (1972) *Carbohydr. Res.* **21**, 249-253.
25. Campbell, R. E., Mosimann, S. C., van De Rijn, I., Tanner, M. E., & Strynadka, N. C. (2000) *Biochemistry* **39**, 7012-7023.
26. Campbell, R. E., Sala, R. F., van de Rijn, I., & Tanner, M. E. (1997) *J. Biol. Chem.* **272**, 3416-3422.
27. Campbell, R. E. & Tanner, M. E. (1997) *Angew. Chem. Int. Ed. Engl.* **36**, 3.
28. Campbell, R. E. & Tanner, M. E. (1999) *Journal of organic chemistry* **64**, 9487-9492.
29. Ge, X., Campbell, R. E., van de Rijn, I., & Tanner, M. E. (1998) *J. Am. Chem. Soc.* **120**, 6613-6614.
30. Easley, K. E., Sommer, B. J., Boanca, G., Barycki, J. J., & Simpson, M. A. (2007) *Biochemistry* **46**, 369-378.
31. Sommer, B. J., Barycki, J. J., & Simpson, M. A. (2004) *J. Biol. Chem.* **279**, 23590-23596.
32. Egger, S., Chaikuad, A., K.L., K., Oppermann, U., & Nidetzky, B. (2010) *Biochem. Soc. Trans.* **submitted**.
33. Huh, J. W., Yang, S. J., Hwang, E. Y., Choi, M. M., Lee, H. J., Kim, E. A., Choi, S. Y., Choi, J., Hong, H. N., & Cho, S. W. (2007) *J. Biochem. Mol. Biol.* **40**, 690-696.

Supporting information

I MATERIAL AND METHODS

Materials and enzymes

Unless stated otherwise, all materials were of highest purity available from Sigma-Aldrich (St. Louis, MO, U.S.A.). NAD⁺ was obtained from Roth (Karlsruhe, Germany) of a purity of >98.

Expression and purification of recombinant human UGDH

The constructs of human UDP-glucose dehydrogenase (EC 1.1.1.22), wild-type and mutants thereof, contain the C-terminal truncated (27 amino acids) sequence (residues 1-467) in pBEN derived vector in-frame with N-terminal SET1 and SBP tags, followed by a tobacco etch virus (TEV) protease cleavage site. The constructs were expressed in the phage-resistant *E. coli* expression strain BL21(DE3)-R3 harboring the pRARE2 plasmid for rare codon expression in LB or TB media supplemented with 50 µg/ml kanamycin and 34 µg/ml chloramphenicol. The starter culture was grown overnight at 37°C and used to inoculate the main culture to a beginning OD₆₀₀ of 0.01. The culture was grown at 37°C to an OD₆₀₀ of ~ 0.8. High-level soluble protein production was performed at 18°C at an IPTG concentration of 0.2 mM overnight. Cells were harvested by centrifugation at 5000 rpm for 20 minutes and the pellet was resuspended in 150 ml Streptavidin binding buffer (100 mM Tris, 150 mM NaCl, pH 8) supplemented with Complete Protease Inhibitors (Complete, EDTA-free Protease Inhibitor Cocktail, Roche Diagnostics Ltd.) and stored at -20°C. Cells were lysed using an EmulsiFlex-C5 high pressure homogenizer (Avestin) at 4 °C. Affinity purification via Strep-Tactin affinity columns was performed according to manufacturer's protocol. Buffer exchange to 50 mM Hepes, 300 mM NaCl and 0.5 mM TCEP was carried out using a NAP-10 (GE Healthcare) desalting column. The 10 kDa SET1 and SBP tag was cleaved by TEV protease even though the tag did not affect protein activity (data not shown). Further purification by size-exclusion chromatography (Superdex 200 16/60 HiLoad, GE/Amersham Biosciences) and anion-exchange chromatography (HiTrap-Q HP) using a linear gradient (50 mM Hepes, to 50 mM Hepes 1 M NaCl) was performed. UGDH eluted as a hexamer in size-exclusion chromatography as confirmed by dynamic light scattering (data not shown). Purified protein was concentrated to 20 mg/ml using 30,000 kDa MW cutoff Amicon Ultra concentration device (Millipore, Bedford, MA) resulting in a homogenous and pure protein preparation. The expected molecular mass

was verified by electrospray mass ionization time-of-flight mass spectrometry (Agilent LC/MSD). Molar protein concentrations were determined by absorbance at 280 nm using an extinction coefficient of $48360 \text{ M}^{-1} \text{ cm}^{-1}$ based on amino acid analysis for UGDH and verified using BCA protein assay (ThermoScientific, Rockford, U.S.A.) according to manufacturer's protocol. In a control experiment the construct of the full length human UGDH (residues 1-494) in pLIC-SGC1 vector as an N-terminally His₆-tagged fusion protein with a TEV cleavage site was expressed as described previously and purified using a sequence of IMAC with Ni²⁺ nitrilotriacetate resin according to manufacturer's protocol. Buffer exchange to 50 mM Hepes, 300 mM NaCl and 0.5 mM TCEP using a NAP-10 (GE Healthcare) desalting column and subsequent gel filtration (Superdex 200 16/60 HiLoad, GE/Amersham Biosciences) yielded the purified protein. The expected molecular mass was verified by electrospray mass ionization time-of-flight mass spectrometry (Agilent LC/MSD). The molar extinction coefficient of the full length construct was determined as $51340 \text{ M}^{-1} \text{ cm}^{-1}$ with the poly-His-tag and $49850 \text{ M}^{-1} \text{ cm}^{-1}$ without tag, respectively. Biochemical and biophysical properties of the wild-type were not affected compared to the 27 amino acid C-terminal truncated version (see Table 1).

Mutagenesis

Site-directed mutagenesis was performed using QuikChange Site-Directed Mutagenesis Kit (Stratagene, La Jolla, CA) according to the manufacturer's protocol. The oligonucleotides used are listed in Table S1 in 5'-3' direction and mutated codons are underlined. Plasmid miniprep DNA of all mutants was subjected to dideoxy sequencing to verify the introduction of the desired mutations and to prove that no misincorporations of nucleotides had occurred.

Protein Crystallization and Structural Determination

WT-UGDH at 20 mg/ml was incubated with 5mM NAD⁺ and 1mM UDP-glucuronate (UGDH-NAD⁺-UDPGlcA) or 5mM NADH and 10mM UDP-glucose (UGDH-NADH-UDPGlc). Crystals of ternary complexes grew at 4°C in 150nl sitting drops, equilibrated against mother liquor containing 16%-20% PEG3350, 10% Ethylene glycol, 0.1M Bis-Tris propane pH 6.5 and 0.08-0.2 mM NaBr. Two UGDH mutants were used in crystallization of apo (T131A) and thiohemiacetal-intermediate-bound (E161Q) forms. Viable apo crystals were obtained with the optimized condition containing 15% PEG smears, 0.1M MES pH 6.0 at 20°C. Crystals of the intermediate-UGDH complex were obtained by mixing the protein (15 mg/ml) with 4mM NAD⁺

and 2mM UDP-Glc, followed by crystallization using 18% PEG smears, 0.1M HEPES pH 7.5 and 5% ethylene glycol as precipitant at 4°C.

Diffraction data were collected at 100 K at Swiss Light Source station X10SA or Diamond beamline I03. Data were processed with MOSFLM and subsequently scaled using the programme SCALA. Structures were solved by molecular replacement using the Phaser programme and the *C. elegans* UGDH (PDB ID: 2o3j) as a model. The structures were manually rebuilt in COOT and restrained refinement with appropriate TLS groups was performed using REFMAC5. Data collection and refinement statistics are summarised in Table S2.

Steady-state kinetic analysis

All absorbance measurements were performed on a Beckman Coulter DU 800 UV/Vis spectrophotometer equipped with a temperature controlled cell holder, results were recorded at 25°C. Steady-state kinetic parameters (k_{cat} , k_{cat}/K_m) for two-fold NAD⁺-dependent oxidation of UDP-glucose to UDP-glucuronic acid were monitored spectrophotometrically by initial rate analysis of NADH production at 340 nm ($\epsilon_{\text{NADH}} = 6220 \text{ M}^{-1} \text{ cm}^{-1}$). If not indicated otherwise, 50 mM potassium phosphate buffer, pH 7.5, was used. Enzyme concentrations in the assays were chosen such that the observed rates were in the range 0.001–0.1 $\Delta A/\text{min}$ and constant for at least 3 min. Therefore, molar enzyme concentrations in all steady state assays were in the range 0.05–0.20 μM for wild-type UGDH and 0.5–100 μM for the mutated enzymes. Reactions were started by the addition of enzyme. Apparent kinetic parameters were obtained from initial-rate measurements under conditions in which one reactant was varied, typically at 6 different levels, over a concentration range of 0.5–10 times the apparent K_m , and the other reactant was present at a constant and saturating concentration. Appropriate controls containing the enzyme and NAD⁺, or UDP-glucose and NAD⁺ were recorded and verified that blank rates were not significant under conditions used or, if significant, were subtracted. Functional complementation of K220A (mutated UGDH in which Lys220 was substituted by alanine) by external primary amines was assayed essentially as described elsewhere (1) at a constant and saturating concentration of methylamine of 500 mM.

Transient kinetic analysis

An applied Photophysics SX.18MV Stopped-flow Reaction Analyzer equipped with a 20 μl flow cell of 1 cm path length was used. Rapid-mixing stopped-flow experiments were performed at

25 ± 0.1 °C. All reactions were started by mixing a buffered substrate solution (20 mM NAD⁺, 1 mM UDP-glucose) with an equal volume of a buffered enzyme solution, containing 1 mM UDP-glucose. Unless stated otherwise, a 50 mM potassium phosphate buffer (pH 7.5) was used. Reaction was monitored from the increase in NADH absorbance at 340 nm. Absorbance traces were recorded in triplicate and averaged [wild-type UGDH, E161Q (mutated UGDH in which Glu161 was substituted by glutamine)]. Kinetic measurements of proton release by the wild-type enzyme during NAD⁺-dependent oxidation of UDP-glucose were carried out using the pH indicator Phenol Red, whose absorbance at 556 nm was recorded. The response of the pH indicator was calibrated by titration with HCl and the model reaction of *Candida tenuis* Xylose reductase (*CtXR*, AKR2B5). As shown previously the reaction involves release of 1 mol proton per 1 mol NAD⁺ (2). Enzymes were gel-filtered twice into a reaction buffer containing 0.5 mM Tris buffer (pH 7.5) and 30 μM Phenol Red. The ionic strength of the buffer was adjusted with NaCl to 100 mM. All reactions were started with enzyme solution to a final concentration of 1.7 μM *CtXR* in a buffered substrate solution (10 mM NAD⁺, 1 M xylitol) and a final concentration of 0.2 μM UGDH to a buffered substrate solution of 10 mM NAD⁺ and 1 mM UDP-glucose, respectively. Steady state kinetic data were recorded at 556 nm to detect the proton release and at 340 nm to monitor hydride transfer. The difference in the rate constant between the traces was used as frame of reference to calibrate the UGDH traces.

Data processing

Results were fitted to equation (1) using unweighted non-linear least-squares regression analysis with the Sigmaplot program version 9 (Jandel). Initial rates that were recorded under conditions in which a single substrate concentration was varied and that gave linear double-reciprocal plots were fitted to the expression:

$$v = k_{\text{cat}} [E][A] / (K_m + [A]) \quad \text{eq.1}$$

where v is the initial rate, $[E]$ the molar concentration of the enzyme subunit (52 kDa), $[A]$ the substrate or coenzyme concentration, k_{cat} the turnover number [s^{-1}] and K_m the apparent Michaelis constant. Unless otherwise stated, the estimated kinetic parameters have standard errors of < 15%.

Isothermal titration calorimetry

Isothermal Calorimetry - Isothermal titration calorimetry was carried out on a VP-ITC titration microcalorimeter from MicroCal™, LLC (Northampton, MA) equipped with a ThermoVac module, with a cell volume of 1.4189 ml and a 250 μl microsyringe. All experiments were carried

out at 10°C while stirring at 295 rpm, in 10 mM HEPES pH 7.5 (at 25°C), 150 mM NaCl. Solutions were degassed (gentle swirling under vacuum) before loading to the microcalorimeter. The microsyringe was loaded with a solution of the ligand (0.5 and 1 mM UDP-glucose and NAD⁺ respectively, in 10 mM HEPES, pH 7.5, 150 mM NaCl) and was carefully inserted into the calorimetric cell which was filled with an amount of the protein sample (2.1 ml, 30 – 50 μM in 10 mM HEPES, pH 7.5, 150 mM NaCl). The system was first allowed to equilibrate until the cell temperature reached 10°C and an additional delay of 120 sec was applied. All titrations were conducted using an initial control injection of 2 μl followed by 29 identical injections of 8 μl with a duration of 16 sec (per injection) and a spacing of 200 sec between injections. The titration experiments were designed in such a fashion to ensure complete saturation of the enzymes before the final injection. The heat of dilution for the ligands was independent of their concentration and corresponded to the heat observed from the last injection, following the saturation of the enzyme, thus facilitating the estimation of the baseline of each titration from the last injection. The collected data were corrected for ligand heats of dilution (measured on separate experiments by titrating the ligands into 10 mM HEPES, pH 7.5, 150 mM NaCl) and deconvoluted using the MicroCal™ Origin software supplied with the instrument to yield enthalpies of binding (ΔH) and binding constants (K_d). This methodology has been previously described in detail by Wiseman and coworkers (2). Thermodynamic parameters were calculated using the basic equation of thermodynamics ($\Delta G = \Delta H - T\Delta S = -RT\ln KB$, where ΔG , ΔH and ΔS are the changes in free energy, enthalpy and entropy of binding respectively). A single binding site model was employed, supplied with the MicroCal™ Origin software package. Detailed background information is described elsewhere (3, 4).

Differential scanning fluorimetry

A thermal stability shift assay was employed to rapidly screen stabilization upon substrate binding. Thermal melting experiments were carried out using the Mx3005p real-time polymerase chain reaction machine (Agilent) and employing a protein concentration of 2 μM in 10 mM Hepes, 150 mM NaCl pH 7.5. Substrates were added to a final concentration of 1 mM for nucleotide sugars and 2 mM for cofactors tested. SYPRO Orange (Molecular Probes; dilution, 1:1000) was added as a fluorescence probe. Excitation and emission filters for the SYPRO-Orange dye were set at 465 and 590 nm, respectively. The temperature was raised at 1 °C/min from 25°C to 96°C and fluorescence readings were taken at each interval. Blank rates were not significant under conditions used or, if significant, were subtracted. The assay and data evaluation were carried out as described elsewhere (5).

ESI-MS analysis

All purified proteins were shown to have expected masses by electrospray ionization mass spectrometry. LC-MS analysis was performed using an LC/MSD TOF electrospray ionisation time-of-flight mass spectrometer coupled to an 1100 series HPLC (Agilent Technologies). Protein samples at 1 mg/ml were diluted 1:50 (v/v) in H₂O, 0.1 % formic acid. Sample volumes of 10 µL were loaded on to a Zorbax 300SB-C3 column, 4.6 x 500 mm, 5 µm particles at a flow rate of 0.5 ml/min. A gradient was developed from 5 - 95 % (B:A) over 6 minutes, where solvent A was H₂O, 0.1 % formic acid and solvent B was MeOH, 0.1 % formic acid. The mass spectrometer was operated in positive ion mode using a standard ESI source. Data analysis and spectral deconvolution was performed using the Protein / MagTrans analysis software package (Agilent Technologies). The setup to investigate the covalently attached intermediate followed the conversion of the E161Q mutant at a final concentration of 20 µM and saturating substrate concentrations (15 mM NAD⁺, 1 mM UDP-glucose) in 50 mM phosphate buffer pH 7.5. Representative samples were taken for 24 hours and analysed as described above.

II DETAILED STRUCTURAL ANALYSIS

Conserved active site in human UGDH compared to SpUGDH

The active site of UGDH is situated at the cleft at the domain interface, where catalytic residues from both domains are found and the nicotinamide group of the cofactor and the sugar moiety of the substrate are positioned. The crystal structures allow precise identification of residues that are in proximity to this region, including Cys276, Asp280, Lys220, Asn224, Thr131 and Glu161 (numbering according to hUGDH). An NAD⁺ molecule is oriented in a cleft between β_1 and β_4 , similarly as previously described for UGDH structures and other enzymes of this class. The substrate binds adjacent to the loop that links α_{10} and α_{11} of the C-terminal domain, which primarily contributes to a large area of UDP-Glc binding pocket. Even though most of residues in the binding pockets are remarkably similar to that previously described for SpUGDH, some interactions between residues and cofactor/substrate as well as properties of the binding sites are observed due to amino acid substitutions and structural alterations between the two orthologs.

Anchoring the NAD⁺ within the pocket is achieved mainly through the N-terminal ₁₁GXGXXG₁₅ glycine-rich region – a signature motif of the Rossmann fold – which accommodates the pyrophosphate portion of the cofactor. Several residues form direct or water-mediated H-bond contacts with the cofactor. Some important interactions include Asp36 and the adenylyl ribose, Arg41 and Arg346 and both phosphate groups and Thr91 and Lys279 and the nicotinamide ribose. By comparison to the bacterial enzyme, two major substitutions in the pocket are noted by Ile79 and Ser275 in hUGDH with Tyr71 and Tyr259, respectively, in SpUGDH. Tyr 71 is located at a lipophilic pocket that is responsible for the binding site of the adenylyl ring. With Ile79 in hUGDH the ring is localised in this pocket without forming any direct interaction to the protein. In contrast, a water-mediated H-bond interaction is formed to Tyr71 in the bacterial enzyme. The second substitution is in proximity to the nicotinamide ribose and phosphate groups. Although both residues do not directly participate in stabilization of the cofactor binding, the change leads to a considerable structural alteration in this pocket. As a result of the larger side chain of Tyr259 in SpUGDH the surrounding region of these groups of the cofactor is more tightly constrained in bacterial enzyme. In contrast, with the corresponding residue Ser275, there are four ordered water molecules in the human form. Structural evidence from the hUGDH thiohemiacetal-intermediate-complex suggests that this additional space in the NAD⁺ pocket may enable binding of UDP-Glc, which could be discouraged in the bacterial

enzyme due to steric hindrance between the bulky side chain of Tyr259 and the glucose ring of the substrate.

In the substrate binding pocket of hUGDH, the uridine is oriented by Ser269 and the main-chain of Lys267 with pyrophosphate moieties forming polar interactions to Lys339 and the main-chain amine of Glu165. This pocket is adjacent to the dimer interface and Arg260 from the neighbouring molecule also aids positioning of the glucose moiety of the substrate in the active site by forming hydrogen bonds with hydroxyls on C2' and C3'. In contrast to the cofactor pocket, differences in the UDP-Glc binding pocket between the bacterial and human orthologs are created primarily by structural alterations due to the extended C-terminus in the human form. The region adjacent to the uridine and ribose moieties of the substrate is more open in hUGDH relative to *SpUGDH*, where the shorter C-terminus packs against this part of the substrate. Both enzymes have similar strategies for stabilizing the uridine but ribose interactions with an arginine residue differ slightly. For hUGDH the hydroxyl group on C2 of the ribose interacts directly with the Arg442 side chain. The arginine in the bacterial form, however, is employed in positioning the Asp402 – the last residue at C-terminus – which forms contacts and stabilizes this part of the substrate UDP-Glc instead.

Detailed analysis of domain closure movement

Comparison the apo and ternary structures of hUGDH revealed the movement of the N-terminal domain towards the fixed C-terminal domain. This motion is accompanied by conformational changes of amino acids adjacent to the NAD⁺ binding pocket in accordance with the presence/absence of the cofactor molecule. Tyr14, Glu161 and Glu165 are of particular interest (see Figure 3B). In the apo form, Tyr14 and Glu161 adopt 'in' positions: the side chain of the Tyr14 and the carboxylate group of Glu161 occupy the NAD⁺ pocket, whereas the Glu165 points outward and its side chain is stabilized by Thr342. The conformations accommodating Tyr14 and Glu161 in close vicinity of the active site significantly generates steric conflict with bringing the nicotinamide ring of the cofactor into hydride transfer position. Therefore, these two residues are observed to twist away in 'out' positions in the ternary complex when the cofactor is present in accordance with stabilization of the carboxylate group of Glu161 by Lys129. In contrast, the Glu165 swings 'in' having its protruding side chain stabilizing the carboxamide group of the nicotinamide ring. Interestingly, in the thiohemiacetal-UDP-Glc intermediate structure in which the cofactor pocket is occupied by a UDP-Glc substrate molecule, Glu165 is in 'out' positions as in the apo form, while the other two residues are floppy and display otherwise two conformational modes. As Tyr14 and the mutated Gln161 would be expected to

be 'in' positions, the presence of UDP-Glc presumably induces 'out' conformations. However, in apo and ternary structures, 'in' modes of Tyr14 and Glu(n)161 would produce steric clashes with the cofactor but not with the substrate. Considering these observations, a regulatory role of these two residues due to their variable conformations in NADH release and NAD⁺ binding is feasible.

Structural evidence of the thiohemiacetal intermediate formation

Assessment of electron density in the active sites of all six molecules in the asymmetric unit of the Glu161Gln UGDH structure reveals a clear additional, incessant density bridging UDP-Glc C6 and Cys276 S γ atoms. Since the O6 atom of the sugar ring is not planar to the C6-S γ bond, the tetrahedral thiohemiacetal intermediate is trapped in the structure due to the catalytic consequences of the mutation.

1. Kratzer, R. & Nidetzky, B. (2005) *Biochem. J.* **389**, 507-515.
2. Nidetzky, B., Klimacek, M., & Mayr, P. (2001) *Biochemistry* **40**, 10371-10381.
3. Jelesarov, I. & Bosshard, H. R. (1999) *J. Mol. Recognit.* **12**, 3-18.
4. Wiseman, T., Williston, S., Brandts, J. F., & Lin, L. N. (1989) *Anal. Biochem.* **179**, 131-137.
5. Niesen, F. H., Berglund, H., & Vedadi, M. (2007) *Nat. Protoc.* **2**, 2212-2221.

III TABLES

Table S1. Primers used for site-directed mutagenesis of UGDH. The oligonucleotides are listed in 5'-3' direction and mutated codons are underlined.

mutation	Oligonucleotides fw and rev 5'-3'
C276A	Fw: GTTGGGTTTGGTGGGAGCGCTTTCCAAAAGGATGTTCTG Rev: TCAGAACATCCTTTTGGAAAGCGCTCCCACCAAACCC
C276S	Fw: GTTGGGTTTGGTGGGAGCTCTTTCCAAAAGGATGTTCTG Rev: TCAGAACATCCTTTTGGAAAGAGCTCCCACCAAACCC
D280A	Fw: GGTGGGAGCTGTTTCCAAAAGGCTGTTCTGAATTTGG Rev: GCTGATAAACCAAATTCAGAACAGCCTTTTGGAAACAGC
K220A	Fw: TGGTCTTCAGAGCTTTCCGCACTGGCAGCAAATGC Rev: AGCATTTGCTGCCAGTGCGGAAAGCTCTGAAGACC
E161Q	Fw: CAGGTGCTGTCCAACCCTCAGTTTCTGGCAGAGGGAACAGCCATC Rev: CCTTGATGGCTGTTCCCTCTGCCAGAACTGAGGGTTGGACAGCACCTG
N224A	Fw: TGGTCTTCAGAGCTTTCCAAACTGGCAGCAGCTGCTTTTCTTGCCCAGAG Rev: GCTTATTCTCTGGGCAAGAAAAGCAGCTGCTGCCAGTTTGGAAAGCTCTG
T131A	Fw: GTGACTGAGAAAAGCGCAGTTCCAGTGCGGG Rev: CCCGCACTGGAAGTGCCTTTTCTCAGTCAC
T131S	Fw: GTGACTGAGAAAAGCTCAGTTCCAGTGCGGG Rev: CCCGCACTGGAAGTGCCTTTTCTCAGTCAC

Table S2. Data Collection and Refinement Statistics.

Complex	UGDH-NADH- UDPGlc	UGDH-NAD- UDPGlcA	Apo UGDH, T131A	UGDH- thiohemiacetal- UDPGlc, E161Q
PDB accession code	2q3e	2qg4	3itk	3khu
Synchrotron beamline	SLS, X10SA	SLS, X10SA	Diamond I03	Diamond I03
Wavelength (Å)	0.95362	1.03315	0.9763	0.9763
Spacegroup	P2 ₁	R3	P2 ₁ 2 ₁ 2 ₁	P2 ₁ 2 ₁ 2
Unit cell dimensions	a=116.0, b=184.1, c=170.9 Å $\alpha = \gamma = 90.0^\circ$ $\beta = 109.2^\circ$	a=b=193.9, c=352.2 Å $\alpha = \beta = 90.0^\circ$ $\gamma = 120.0^\circ$	a= 89.1, b=106.6, c=349.1 Å $\alpha = \beta = \gamma = 90.0^\circ$	a= 203.5, b=207.3, c=93.4 Å $\alpha = \beta = \gamma = 90.0^\circ$
Resolution range ^a (Å)	50.0-2.00 Å (2.11-2.00)	60.00-2.10 Å (2.21-2.10)	52.90-2.40 Å (2.53-2.40)	48.74-2.30 Å (2.42-2.30)
No. unique reflections ^a	452865 (65636)	288088 (42048)	130411 (18766)	175128 (25412)
Completeness ^a (%)	99.6 (99.1)	100.0 (100.0)	99.8 (99.4)	99.8 (100.0)
I/ σ ^a	9.7 (2.0)	7.6 (1.8)	7.9 (2.1)	9.4 (2.0)
R _{merge} ^a (%)	0.089 (0.636)	0.139 (0.711)	0.131 (0.550)	0.106 (0.743)
Redundancy ^a	3.9 (3.9)	3.9(3.8)	4.0 (3.3)	4.3 (4.3)
Refinement				
No. Atoms P/L/O ^b	35787/800/2755	28546/580/3023	21656/0/1321	21866/432/1397
R _{fact} / R _{free} (%)	0.173/ 0.205	0.178/ 0.225	0.199/ 0.241	0.195/0.225
rms bond length ^c (Å)	0.010	0.010	0.016	0.016
rms bond angle ^c (°)	1.234	1.238	1.463	1.438
Bf P/L/O ^b (Å ²)	33.0/25.7/35.0	17.0/15.1/23.9	15.4/-/20.6	23.9/42.9/27.5

^a Values in brackets show the statistics for the highest resolution shells.

^b P/L/O represents protein/ligand/other (water, ion and solvent)

^c rms indicates root-mean-square.

Table S3. Stabilization of hUGDH upon binding of substrate and cofactor using differential scanning fluorimetry. The difference in the melting temperature (T_m) in presence and absence of the compound indicates a stabilized (closed) conformation of the enzyme-substrate-cofactor complex. Measurements were corrected for appropriate blanks if necessary and recorded as triplicate and standard errors on all parameters were $\leq 15\%$.

Compound 1	Compound 2	ΔT_m
NAD ⁺		2
UDP-Glc		2.5
UDP-GlcA		5
UDP-Glc	NADH	16
UDP-GlcA	NAD ⁺	15

Table S4. Kinetic parameters for NAD⁺ dependent UDP-glucose oxidation catalyzed by wild-type UGDH and mutated forms of the enzyme respectively at 25 °C and pH 7.5. Kinetic rate constants refer to conversion of 2 NAD⁺ for one turnover of the enzyme. The steady state was not reached for active site mutant proteins, determined values reflect apparent rate constants. Measurements were corrected for appropriate blanks if necessary and recorded as triplicate and standard errors on all parameters were ≤ 15%.

Enzyme	k_{app} [s ⁻¹]	- fold decrease	K_m UDP-glucose [μM]	K_m NAD ⁺ [mM]
WT	0.80		35	0.7
WT full length	0.75	1	35	1
E161Q	$1.7 \cdot 10^{-3}$	$5 \cdot 10^2$	50	n.s.
C276A	$1.3 \cdot 10^{-4}$	$6 \cdot 10^3$	80	1.3
C276S	$1.4 \cdot 10^{-4}$	$6 \cdot 10^3$	60	1.6
K220A	$5.8 \cdot 10^{-5}$	$1.3 \cdot 10^4$	n.s.	4.1
D280A	$4.9 \cdot 10^{-5}$	$1.6 \cdot 10^4$	70	n.s.
T131A	0.10	7	100	0.8
N224A	0.30	3	180	2.9
T131S	0.45	2	40	0.70

n.s. not saturable

IV FIGURES

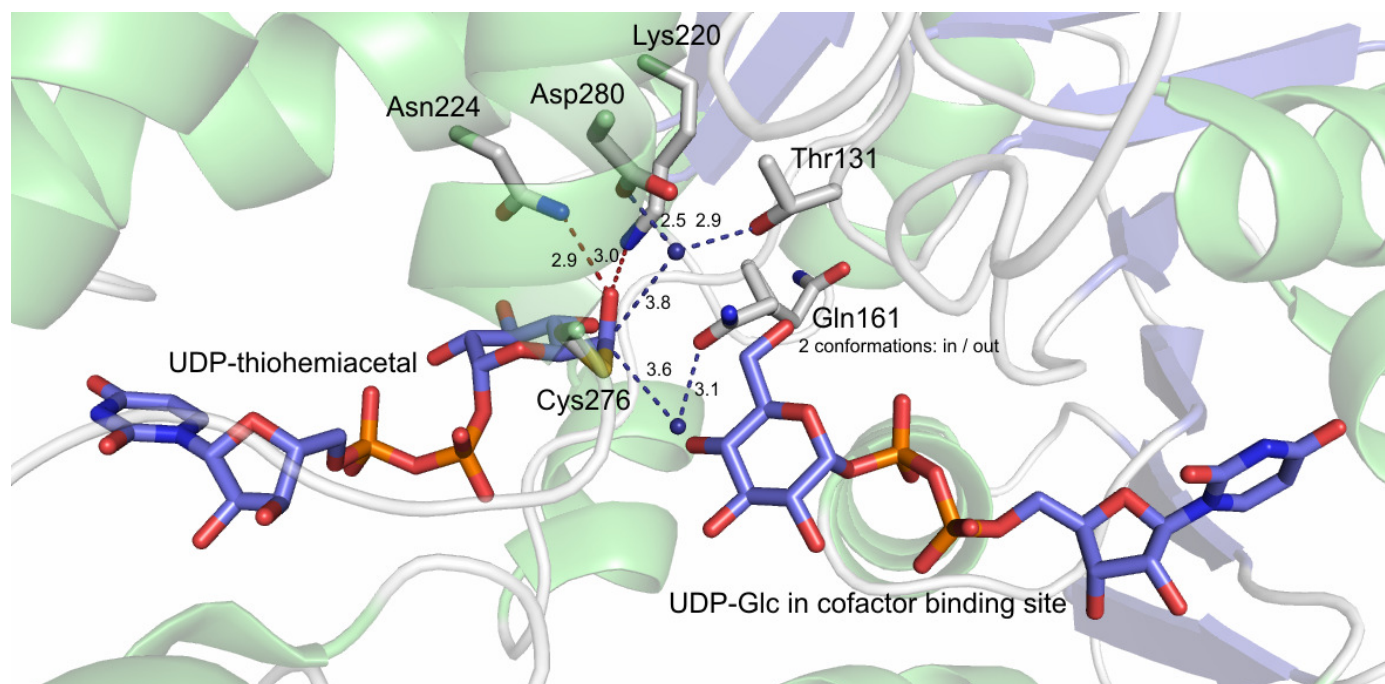


Figure S1. Close up of the active site in the Intermediate structure (PDB: 3KHU). Distances for oxanion stabilization from Lys220 and Asn224 are indicated in red dashed lines. The two water molecules are indicated as blue sphere and corresponding distances to catalytic residues are highlighted as blue dashed lines. A second UDP-Glc molecule occupies the cofactor binding site in all subunits of the hexamer.

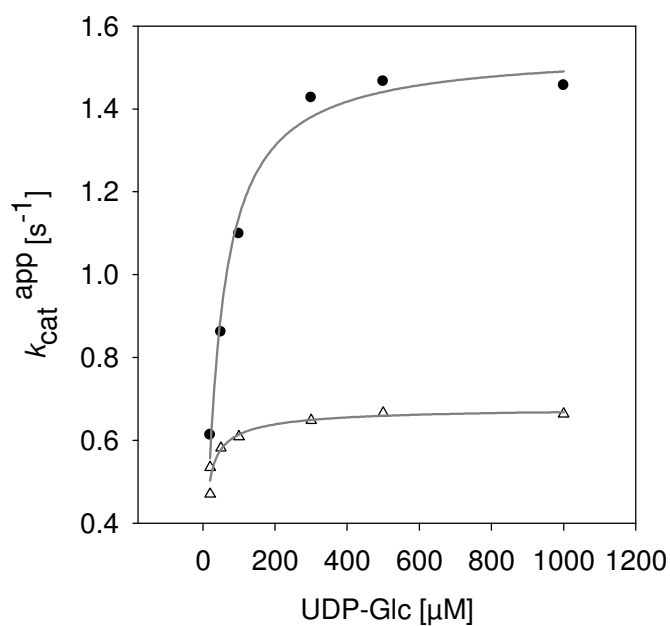


Figure S2: Representative data analysis to determine UDP-Glc Michaelis constant. NAD^+ was saturating under the conditions used (10mM) for black full circles and physiological concentrations (0.5mM) are indicated in triangles. No sigmoidal shape of the curve was observed indicating no cooperative effect within the hUGDH hexamer. Measurements were recorded as triplicates and showed a standard error of $\leq 10\%$.

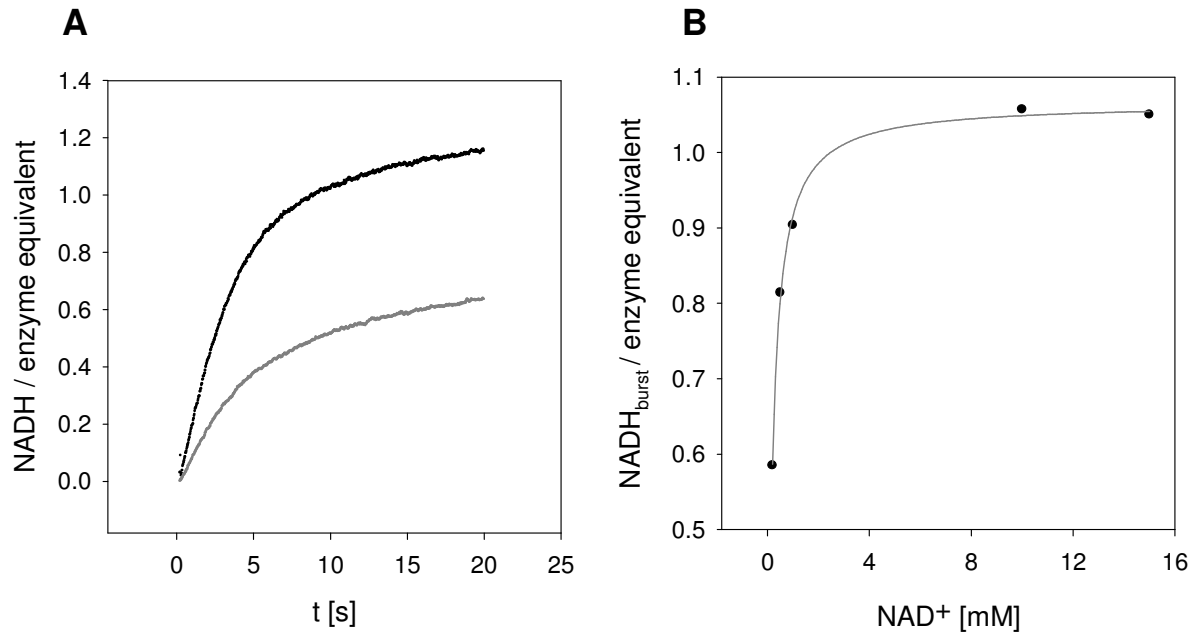


Figure S3. Stopped flow traces of UDP-glucose conversion by UGDH Glu161Gln mutant.
A. Representative traces at different NAD⁺ concentrations: 0.2 mM (red trace) and 15 mM (grey trace) enhance steady state rate constant minimally. However, the initial burst phase separating the ADH from the ALDH reaction is distinct. **B.** Evaluation of stopped flow traces of UDP-glucose conversion by UGDH Glu161Gln: μ M NADH produced during the initial burst phase related to enzyme equivalent present with increasing and saturating concentrations of NAD⁺.

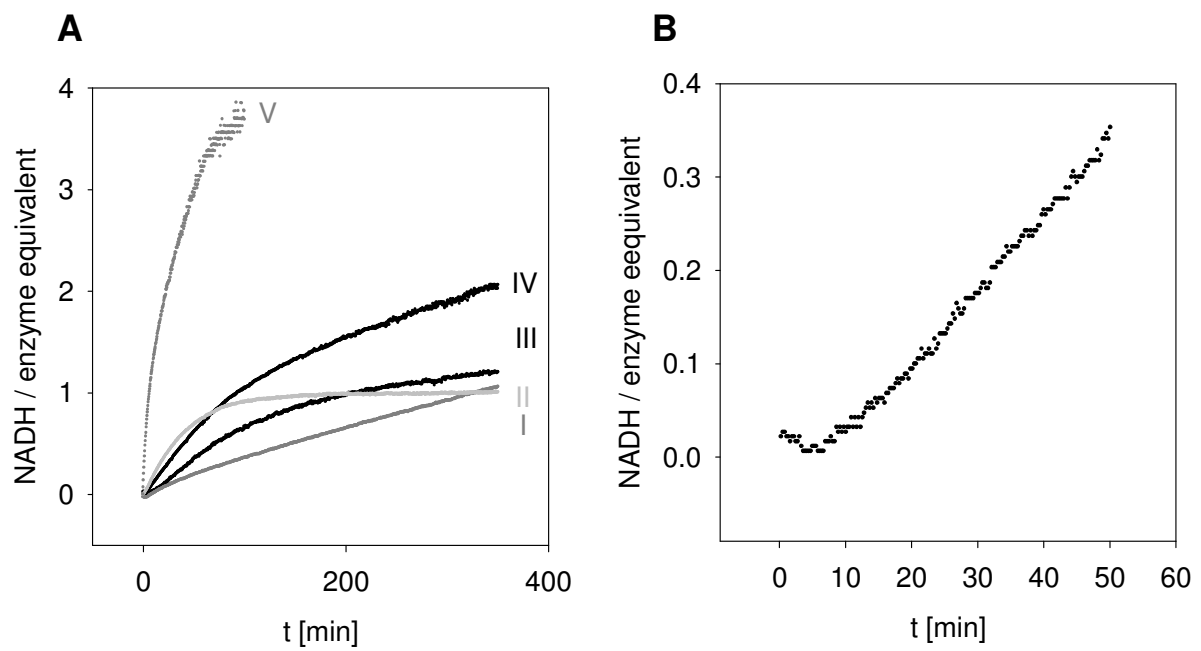


Figure S4. Time course of NADH formation by active site mutants monitored spectrophotometrically: μM NADH produced related to enzyme equivalent present under saturating concentrations of UDP-glc and NAD^+ . **A.** Comparison of traces: Asp280Ala (dark grey (I)), Cys276Ser (grey(II)), Lys220Ala (black (III)), Cys276Ala (black IV)) and rescued Lys220Ala with 500mM methylamine in pH 7.5 (dark grey (V)). **B.** Close up: Lys220Ala mutant shows an initial lag phase

Integration of Enzyme, Strain and Reaction Engineering to Overcome Limitations of Baker's Yeast in the Asymmetric Reduction of α -Keto Esters

Regina Kratzer,^{1,2} Sigrid Egger,² Bernd Nidetzky^{1,2}

¹Research Centre Applied Biocatalysis, Petersgasse 14, A-8010 Graz, Austria; telephone: +43-316-873-8400; fax: +43-316-873-8434; e-mail: bernd.nidetzky@tugraz.at

²Institute of Biotechnology and Biochemical Engineering, Graz University of Technology (TUG), Petersgasse 12/1, A-8010 Graz, Austria

Received 24 January 2008; revision received 3 May 2008; accepted 12 May 2008

Published online 2 June 2008 in Wiley InterScience (www.interscience.wiley.com). DOI 10.1002/bit.21980

ABSTRACT: We report on the development of a whole-cell biocatalytic system based on the popular host *Saccharomyces cerevisiae* that shows programmable performance and good atom economy in the reduction of α -keto ester substrates. The NADPH-dependent yeast reductase background was suppressed through the combined effects of overexpression of a biosynthetic NADH-active reductase (xylose reductase from *Candida tenuis*) to the highest possible level and the use of anaerobic reaction conditions in the presence of an ethanol co-substrate where mainly NADH is recycled. The presented multi-level engineering approach leads to significant improvements in product optical purity along with increases in the efficiency of α -keto ester reduction and co-substrate yield (molar ratio of formed α -hydroxy ester to consumed ethanol). The corresponding α -hydroxy esters were obtained in useful yields (>50%) with purities of $\geq 99.4\%$ enantiomeric excess. The obtained co-substrate yield reached values of greater than 1.0 with acetate as the only by-product formed.

Biotechnol. Bioeng. 2008;101: 1094–1101.

© 2008 Wiley Periodicals, Inc.

KEYWORDS: baker's yeast bioreduction; xylose reductase; *Saccharomyces cerevisiae* strain engineering; co-substrate yield; chiral α -hydroxy ester; whole-cell biocatalysis

Introduction

Asymmetric reduction of ketones is one of the most fundamental processes in the production of chiral secondary alcohols. NAD(P)H-dependent carbonyl reductases are splendid catalysts for this key transformation (Bommarius and Riebel, 2004; Faber, 2000; Hummel, 1997). Because isolated protein preparations are costly and not always stable, it is oftentimes preferred to work with whole cells (Breuer et al., 2004; Gröger et al., 2006; Kataoka et al., 2003; Liese et al., 2006). Whole cells further offer the essential advantage that regeneration of NADPH or NADH is achieved through steps of cellular metabolism (Bommarius and Riebel, 2004; Breuer et al., 2004; Engelking et al., 2006; Faber, 2000; Goldberg et al., 2007; Gröger et al., 2006; Ishige et al., 2005). Recombinant *Escherichia coli* and wild-type or engineered strains of *Saccharomyces cerevisiae* (baker's yeast) have been by far the most popular biocatalytic whole-cell systems (Bertau and Bürli, 2000; Bommarius and Riebel, 2004; Breuer et al., 2004; Faber, 2000; Hummel, 1997; Johanson et al., 2008; Kataoka et al., 2003; Kometani et al., 1996; Liese et al., 2006; Stewart, 2000; Sybesma et al., 1998).

A superior feature of the yeast in comparison to *E. coli* is the relatively high tolerance and robustness to chemicals and organic solvents (Pfruender et al., 2006). However, whole-cell bioreductions in general and those employing baker's yeast in particular oftentimes did not match up with expectations from the performance of isolated reductases (Faber, 2000; Johanson et al., 2005; Kaluzna et al., 2004; Kometani et al., 1996; Stewart, 2000; Sybesma et al., 1998), explicable on account of the presence of multiple, typically NADPH-dependent reductases in the cell that display divergent enantiopreferences (Johanson et al., 2005; Kaluzna et al., 2004; Stewart, 2000; Sybesma et al., 1998).

Regina Kratzer and Sigrid Egger contributed equally to this work.

Correspondence to: B. Nidetzky

Contract grant sponsor: Austrian Science Fund (DK Molecular Enzymology and Hertha-Firnberg)

Contract grant numbers: W901-B05; T350-B09

Adjusting the substrate concentration and structure (Chin-Joe et al., 2002; D'Arrigo et al., 1997; Johanson et al., 2005; Kometani et al., 1993; Nakamura et al., 2003; Rotthaus et al., 1997; Shieh et al., 1985; Sybesma et al., 1998; Zhou et al., 1983) was used to favor acceptance of the target ketone by only a subset of yeast reductases. Strategies to increase the desired activity or to inhibit one or more competing enzymes by genetic overexpression/knock-out approaches (Johanson et al., 2008; Kaluzna et al., 2004; Rodriguez et al., 1999; Sybesma et al., 1998) or by addition of activators and inhibitors (Johanson et al., 2005; Sybesma et al., 1998; Yang et al., 2004) have proven only partially successful.

Another drawback of whole-cell bioreductions is the low atom economy in the utilization of co-substrate for the production of alcohol product. In processes where the central metabolism is employed for cofactor recycling, molar yields of alcohol on co-substrate are typically <0.03 (Faber, 2000; Johanson et al., 2005).

We describe here the results of a multi-level engineering approach to improve optical purity, efficiency and co-substrate yield of ketone reduction by baker's yeast. Scheme 1 summarizes the defining features of the biocatalytic system where transformation of α -keto esters was chosen as a synthetically relevant model reaction. Xylose reductase from *Candida tenuis* (CtXR), a NADH-active reductase catalyzing stereospecific ketone reduction with broad substrate specificity, was overexpressed (Kratzer and Nidetzky, 2007; Kratzer et al., 2006). To suppress the NADPH-dependent reductase background encoded by the host genome (Johanson et al., 2005; Kaluzna et al., 2004; Rodriguez et al., 1999; Sybesma et al., 1998), we selected ethanol as co-substrate and employed anaerobic conditions such that reducing equivalents mainly in the form of NADH were regenerated. The theoretical co-substrate yield was

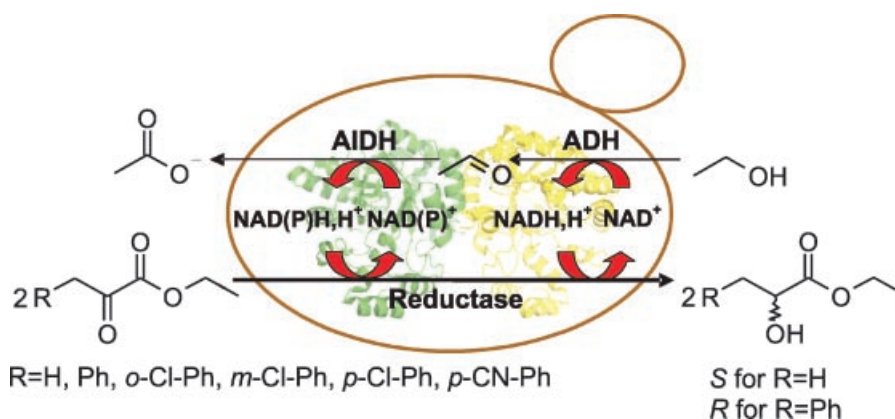
therefore greater than 1 (Kometani et al., 1994) (Scheme 1), and the use of ethanol offered the additional advantage of enhanced substrate solubility.

Materials and Methods

Chemicals and Strains

Ethyl pyruvate, ethyl *R*-lactate, ethyl *S*-lactate, ethyl benzoylformate, ethyl *R*-mandelate, ethyl *S*-mandelate and ethyl 4-cyanobenzoylformate were purchased at Sigma–Aldrich (Vienna, Austria). Racemic ethyl 4-cyanomandelate was from Synthon Chemicals GmbH & Co. KG (Wolfen, Germany). The substrates ethyl 2-chlorobenzoylformate, ethyl 3-chlorobenzoylformate, ethyl 4-chlorobenzoylformate along with the corresponding alcohols ethyl *R*-2-chloromandelate, ethyl *S*-2-chloromandelate, racemic ethyl 3-chloromandelate, ethyl *R*-3-chloromandelate, ethyl *R*-4-chloromandelate and racemic ethyl 4-chloromandelate were synthesized by DSM Fine Chemicals Austria GmbH (Linz, Austria) and obtained as a kind gift from Dr. Wolfgang Skranc. NADH (sodium salt; $\geq 98\%$ pure) and NADPH (sodium salt; $\geq 97\%$ pure) were obtained from Roth (Karlsruhe, Germany).

The microorganisms used in this study were *E. coli* JM109, *S. cerevisiae* CEN.PK 113-7D (MATa MAL2-8c SUC2) (termed *S.c.* wild-type) and *S. cerevisiae* CEN.PK 113-5D (*S. cerevisiae* CEN.PK 113-7D-URA; MATa MAL2-8c SUC2 ura3). *Pfu* DNA polymerase was from Promega (Madison, WI). T4 DNA ligase, restriction enzymes and dNTPs were from MBI Fermentas (Flamborough, ON, Canada). All other chemicals were purchased from Sigma–Aldrich/Fluka (Gillingham, Dorset, UK) or Roth (Karlsruhe, Germany), and were of the highest purity available.



Scheme 1. Optimization of whole-cell bioreduction of α -keto esters through systematic elimination of shortcomings of the wild-type strain of baker's yeast with respect to optical purity of product, conversion efficiency, and economy of co-substrate utilization. The engineered strain overproduces a stereoselective reductase from *C. tenuis* that is active with NADH. The use of anaerobic process conditions in the presence of an ethanol co-substrate promotes regeneration of the reduced coenzyme, mainly in the form of NADH, via the reactions catalyzed by the yeast endogenous alcohol dehydrogenase (ADH) and aldehyde dehydrogenase (AIDH). The co-substrate yield is the molar ratio of α -hydroxy ester produced and ethanol consumed.

Integration of the Gene Encoding Xylose Reductase From *C. tenuis* CBS 4435 Into the Genome of *S. cerevisiae* CEN.PK 113-5D

The gene encoding xylose reductase from *C. tenuis* CBS 4435 was cloned into the multiple cloning site of the plasmid vector pRS416-GPD (Mumberg et al., 1995). This vector contains an expression cassette composed of the strong constitutive glyceraldehyde-3-phosphate dehydrogenase (GPD) promoter, a multiple cloning array based on pBIISK (Stratagene, San Diego, CA), and the *Cyc1* terminator. The expression cassette harboring the CtXR gene was amplified by polymerase chain reaction (PCR) using *Pfu* DNA polymerase. The oligonucleotide primers carried on their 5'-ends *EcoRI* restriction sites that were unique in the yeast integrating plasmid YIp5 (DSMZ, Braunschweig, Germany). These restriction sites were used to subsequently clone the expression cassette into the integrating vector, in analogy to a protocol used by Wang et al. (2004). The transformation of *S. cerevisiae* strain CEN.PK 113-5D with the linearized integrating plasmid was performed by the standard lithium acetate method. The resulting strain was termed *S.c.* XRgenome. The correct integration of the CtXR gene and the absence of misincorporations of nucleotides due to DNA polymerase errors were verified by sequencing.

Cloning the Genes Encoding Wild-Type and W23F Mutant Forms of CtXR Into the Yeast 2 μ Expression Plasmid p426GPD

The p426GPD (Mumberg et al., 1995) vector contains the strong constitutive GPD promoter, a multiple cloning array and the *Cyc1* terminator. The genes encoding wild-type and Trp²³ → Phe mutant forms of CtXR (Kratzer et al., 2006) were amplified by PCR introducing flanking *Bam*HI and *Sal*I restriction sites. Vector and PCR products were cut with the respective restriction enzymes and ligated. After their amplification in *E. coli* JM109 cells, isolated plasmids were sequenced and transformed into *S. cerevisiae* strain CEN.PK 113-5D using the lithium acetate method. The resulting strains were termed *S.c.* XR2 μ and *S.c.* WF2 μ .

Cultivation of Strains

All yeast strains were cultivated at 30°C in 1,000 mL baffled shaken flasks using an agitation rate of 120 rpm. The strains *S.c.* wild-type and *S.c.* XRgenome were grown in YPD medium, containing 20 g/L glucose, 10 g/L yeast extract and 20 g/L peptone at pH 5.6. The strains *S.c.* XR2 μ and *S.c.* WF2 μ were grown in synthetic drop-out medium consisting of the following components: 20 g/L glucose; 1.7 g/L yeast nitrogen base (Sigma product number Y1251) lacking amino acids and (NH₄)₂SO₄; 1.92 g/L yeast synthetic drop out medium lacking uracil; and 5 g/L (NH₄)₂SO₄. The pH of the medium was pH 5.6. The cells were harvested in the early logarithmic growth phase, typically at a concentration of cell

dry weight (cdw) of 0.8 g/L, to prevent the accumulation of glycogen and other intracellular storage material. The yeast cells were collected by centrifugation, washed and suspended in 50 mM potassium phosphate buffer, pH 6.2. Fresh cell preparations were used for bioreduction studies. Final cell suspensions for whole-cell biocatalytic conversions contained an exactly comparable concentration of cdw 5 g_{cdw}/L.

Reductase and Dehydrogenase Activities in the Yeast Cell-Free Crude Extract

Reductase and dehydrogenase activities were assayed spectrophotometrically by monitoring the reduction or oxidation of NAD(P)(H) at 340 nm over a time of 1–5 min (rate of 0.05–0.1 ΔA /min). One unit of enzyme activity refers to 1 μ mol of NAD(P)(H) consumed per minute. All measurements were performed with a Beckman DU-800 spectrophotometer. Alcohol dehydrogenase and α -keto ester reductase activities were determined after disruption of yeast cells with the lysis reagent Y-Per (Pierce, Rockford, IL). The standard assay mixture for α -keto ester reductase activity contained 10 mM ethyl 4-cyanobenzoylformate and 250 μ M NAD(P)H; that for alcohol dehydrogenase activity contained 50 mM ethanol and 1 mM NAD(P)⁺. Reactions were always started by the addition of coenzyme. For determination of acetaldehyde dehydrogenase activity yeast cells were disrupted with a French Press (operated at an applied pressure of 1,000 psi) to prevent inactivation of the enzyme by components of the lysis reagent. A suspension of biomass in 50 mM potassium phosphate buffer, pH 6.2, containing 1 mM dithiothreitol was passed twice through the pressure cell. The standard assay for acetaldehyde dehydrogenase activity contained 1 mM acetaldehyde, 4 mM MgCl₂, 1 mM dithiothreitol and 1 mM NAD(P)⁺. Reactions were started by the addition of acetaldehyde. All enzyme assays were performed in 50 mM potassium phosphate buffer, pH 7.0, at 25°C. Measured rates were corrected for the appropriate blank readings accounting for non-specific oxidation or reduction of NAD(P)(H) by the cell extracts. Protein concentrations were determined with the BCA assay (Pierce) using bovine serum albumin as standard.

General Procedure for Whole-Cell Asymmetric Reduction of α -Keto-Ester Substrate

Bioreduction experiments were carried out by incubating 5 g_{cdw}/L cells suspended in 50 mM potassium phosphate buffer, pH 6.2, in the presence of 10 mM aromatic α -keto ester or 60 mM ethyl pyruvate. Note that optimization of the space-time yield of the bioreductions was not pursued here, hence, the use of a relatively low cell concentration. Unless indicated otherwise, ethanol (1 M) was used as co-substrate. Aerobic conversions were performed in 300 mL baffled flasks with 30 mL working volume that were incubated on an orbital shaker at 25°C and an agitation rate of 140 rpm. Anaerobic assays were done in 1 mL gas-tight reaction tubes

that were incubated at 25°C with an end-over-end rotator at 30 rpm. Homogeneous samples were taken at certain times and analyzed as described under Analytical Methods Section.

Analytical Methods

The concentration of the tested aromatic α -keto esters was 10 mM. Substrate solutions of ethyl pyruvate (60 mM) and ethyl 4-cyanobenzoylformate were monophasic under these conditions, all other substrates (ethyl benzoylformate, ethyl 2-chlorobenzoylformate, ethyl 3-chlorobenzoylformate and ethyl 4-chlorobenzoylformate) formed small droplets in solution. The biphasic samples were diluted with ethanol (1:1) prior to analysis with HPLC or GC. Samples of 500 μ L were taken and centrifuged prior to chromatographic analysis. The stereochemical outcome of the reductions of ethyl pyruvate and ethyl 3-chlorobenzoylformate was determined by chiral GC. The analytes were extracted with CH_2Cl_2 and the organic phase dried with Na_2SO_4 . The samples were analyzed on a Hewlett-Packard 5890 Series II gas chromatograph equipped with a Hewlett-Packard 6890 series injector and a Chrompack 7502 chiral column (coating CP Chirasil-DEX CB, dimensions 25 m \times 0.25 m \times 0.25 μ m). Nitrogen was used as carrier gas with a split ratio of 1:10. The temperature program started with 47°C for 1 min followed by a ramp to a final temperature of 225°C at 10°C min^{-1} . *R*- and *S*-alcohols were separated on the column and detected with a flame ionization detector (FID). HPLC analysis of the aromatic α -hydroxy esters was performed with a reversed phase CHIRALPAK AD-RH column from Daicel (purchased at VWR International, Vienna, Austria) on a LaChrom HPLC system (Merck-Hitachi) equipped with a L-7400 UV-detector (210 nm). Best resolutions of the *R*- and *S*-alcohols were obtained with acetonitrile and water (20:80, by volume) as eluent at a flow rate of 0.5 mL/min and a temperature of 40°C. The absolute configurations of ethyl lactate, ethyl mandelate and ethyl chloromandelates were unambiguously identified by chiral phase GC and HPLC by comparison with authentic standards. Chiral HPLC allowed baseline resolution of a racemic mixture of ethyl 4-cyanomandelate. Assignment of peaks to the ethyl *R*- and *S*-cyanomandelates was done in analogy to elution patterns of other compounds in the series. Standard curves of alcohols were established to assess the degree of conversion.

Analysis of ethanol, its oxidation products (acetaldehyde, acetate) and glucose was performed by HPLC using an Aminex HPX87H column from Bio-Rad on a LaChrom LC system (Merck-Hitachi) equipped with a LaChrom RI Detector L-7490. Five mM H_2SO_4 was used as eluent at a flow rate of 0.6 mL/min, and the operating temperature was 65°C.

Results and Discussion

Strain Engineering

We compared four *S. cerevisiae* strains, including the laboratory strain CEN.PK 113-7D (*S.c.* wild-type) from which all other engineered strains were derived. Strain *S.c.* XRgenome contained the gene encoding xylose reductase from *C. tenuis* integrated into the yeast genome under control of the constitutive glyceraldehyde-3-phosphate (GPD) promoter. Strains *S.c.* XR2 μ and *S.c.* WF2 μ harbored multiple copies of the yeast 2 μ expression vector p426GPD (Christianson et al., 1992; Mumberg et al., 1995) that carried, respectively, the gene for wild-type CtXR and an up to eightfold more active Trp²³ \rightarrow Phe mutant thereof (Kratzer and Nidetzky, 2007; Kratzer et al., 2006). As shown in Table I, the cell-free extract of *S.c.* wild-type displayed 2.9 units of α -keto ester reductase activity (U; $\mu\text{mol/min}$) per g of cell dry weight (g_{cdw}) when using NADPH but lacked the corresponding NADH-dependent activity. The 13-fold higher NADH-dependent activity for *S.c.* XR2 μ in comparison with *S.c.* XRgenome corresponds roughly to the expected B-fold difference in gene copy number for *S.c.* XRgenome (single copy) and *S.c.* XR2 μ (\sim 30 copies, as determined by Christianson et al. (1992), in an otherwise unrelated study of the p426GPD expression vector). The strain *S.c.* WF2 μ yielded eightfold enhancement of NADH-dependent activity in comparison with *S.c.* XR2 μ , roughly as expected from the catalytic efficiencies of purified Trp²³ \rightarrow Phe mutant (955 $\text{M}^{-1} \text{s}^{-1}$) and wild-type CtXR (197 $\text{M}^{-1} \text{s}^{-1}$) (Kratzer and Nidetzky, 2007). Table I also shows that overexpression of the respective CtXR gene caused selective enhancement of the NADH-linked activity, consistent with results of corresponding kinetic assays of highly purified enzymes that revealed 10-fold preference for NADH in both wild-type and mutant CtXR (data not shown). The NADPH-dependent activities of engineered

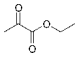
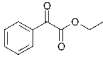
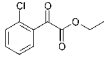
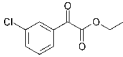
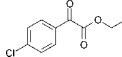
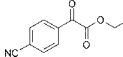
Table I. Comparison of reductase activities* towards ethyl 4-cyanobenzoylformate (10 mM) in cell-free extracts of different strains of *S. cerevisiae*.

<i>S.c.</i> strain	U/ g_{cdw} NADPH	mU/ $\text{mg}_{\text{protein}}$ NADPH	U/ g_{cdw} NADH	mU/ $\text{mg}_{\text{protein}}$ NADH
Wild-type	2.9	15	0	0
XRgenome	4.2	18	2.6	8.0
XR2 μ	7.9	18 ^a	35	36 ^a
WF2 μ	38	62 ^a	280	416 ^a

*Standard errors are \leq 20% ($N=4$).

^aProtein concentration (20 mg/mL) was about twice that of other strains.

Table II. Whole-cell bioreductions of α -keto esters (10 mM)* under anaerobic and aerobic conditions (in parentheses) using 1 M ethanol as co-substrate.**,**

S.c. strain						
Wild-type	7/>99.9S (96.4)	30/98.6R (96.3)	4/84.5R (88.7)	6/>99.9R (88.2)	7/97.2R (91.8)	11/77.2 nd ^a (56.3)
XRgenome	16/>99.9S	37/97.6R	15/90.0R	6/>99.9R	24/96.0R	30/74.0 nd ^a (56.5)
XR2 μ	14/>99.9S	41/99.0R	18/98.6R	6/>99.9R	31/99.3R	21/92.9 nd ^a (84.3)
WF2 μ	13/>99.9S	63/99.4R	28/98.9R	12/>99.9R	56/99.5R	38/96.9 nd ^a (92.4)
WF2 μ Na ₂ SO ₃ (10 mM)	35/>99.9S	80/>99.9R	76/99.6R	14/>99.9R	74/99.9R	100/99.4 nd ^a

*Ethyl pyruvate (60 mM).

**Yield %/ee %; standard errors ($N=3$) are $\leq 20\%$ (yield) and $\leq 6\%$ (concentration of alcohol antipodes); chiral HPLC and GC were used to assign the absolute configurations by comparison with authentic standards.

***Reaction time was 9 h.

^aAbsolute configuration of the alcohol was not determined.

strains in Table I reflect the sum of yeast inherent activities and the NADPH-linked activity of CtXR.

Baker's Yeast Bioreduction of α -Keto Esters

Six representative α -keto esters with aromatic and aliphatic side chains (Table II) were tested as substrates of each yeast strain. Using 1 M of ethanol, biotransformations were carried out under conditions of either surface aeration, where NADPH is efficiently regenerated, or a near complete exclusion of O₂. Kometani et al. (1991) reported that ketone reduction by a wild-type strain of *S. cerevisiae* ceased when the concentrations of the ethanol co-substrate exceeded 400 mM. Note therefore that we did not observe a dependence of α -keto ester conversion rate on the concentration of ethanol in the range 0.2–1 M. Time courses of conversion of ethyl 4-cyanobenzoylformate are shown in Figure 1. The initial rates of ketone reduction varied between 0.058 mmol/g_{cdw} h for *S.c.* wild-type and 0.43 mmol/g_{cdw} h

for the *S.c.* WF2 μ . No ketone conversion was seen under conditions of lacking co-substrate when *S.c.* wild-type was previously depleted of intracellular storage material and the reaction mixture was made completely anaerobic using 10 mM Na₂SO₃. All time courses showed a marked decrease in the initial bioreduction rate after ~ 9 h which limited the final conversion of the substrate, after 43 h, to between 30% and 70%. We incubated ethyl 4-cyanobenzoylformate identically as in Figure 1 but in the absence of yeast as a control and identified spontaneous hydrolysis of substrate as the main reason for low yield and decreased transformation rate (data not shown). Although about 25% of intracellular reductase activity was lost after about 9 h, enzyme inactivation was clearly not a principal factor limiting the efficiency and completeness of substrate conversion.

The results in Table II portray the effects of over-expression of the NADH-active reductase and the exclusion of O₂ on yield and ee of alcohol product. Note that the reported yields were determined by HPLC or GC because product isolation was beyond the scope of this study. Consistent with the Prelog-type stereoselectivity of wild-type and mutant CtXR (Kratzer and Nidetzky, 2007), all recombinant yeast strains preferred formation of ethyl *S*-lactate and ethyl *R*-mandelate (or derivatives thereof). The wild-type strain produced the same alcohol products, however, with a significantly lower optical purity. An increased level of the stereoselective reductase activity resulting from an enhancement of either the gene copy number (XRgenome vs. XR2 μ) or the specific enzyme activity (XR2 μ vs. WF2 μ) caused marked enhancement of yield and ee. Substrate conversion proceeded at a faster rate under aerobic conditions whereas at the same time, ee decreased in response to O₂ availability. Highest ee-values were obtained in the presence of 10 mM Na₂SO₃ probably for two reasons. First, the O₂ scavenger Na₂SO₃ provides strictly anaerobic conditions. Second, formation of an acetaldehyde-SO₂ adduct (Guido et al., 2003) will prevent the NAD(P)⁺-dependent formation of acetate. We confirmed the absence of acetate in bioreductions performed in the presence of Na₂SO₃. Under these conditions, the stereoselectivity of α -keto ester reduction by *S.c.* WF2 μ was comparable to that of the purified enzyme (Table II).

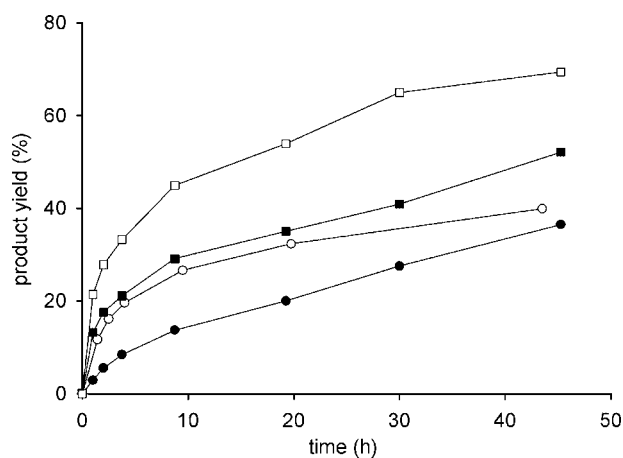
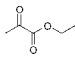
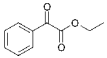
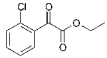
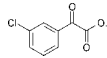
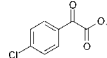
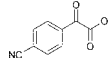


Figure 1. Bioreduction of ethyl 4-cyanobenzoylformate (10 mM), measured as formation of alcohol product, by different strains of *S. cerevisiae* (● *S.c.* wild-type, ○ *S.c.* XRgenome, ■ *S.c.* XR2 μ , □ *S.c.* WF2 μ). [O₂] ≤ 15 μ M.

Table III. Aerobic whole-cell bioreductions of α -keto esters using glucose (300 mM) as co-substrate.***

S.c. strain						
Wild-type	46/>99.9S	52/89.4R	48/91.2R	61/81.7R	83/89.2R	100/65.2 nd ^a

*Yield %/ee %; chiral HPLC and GC were used to assign the absolute configurations by comparison with authentic standards.

**Reaction time was 9 h.

^aAbsolute configuration of the alcohol was not determined.

The product ee was essentially unaffected when glucose replaced ethanol during aerobic conversions by *S.c.* wild-type (Tables II and III). Interestingly, therefore, the rate of co-substrate metabolism, which was about twofold faster for glucose (6.0 mmol/g_{cdw}h) in comparison to ethanol (2.9 mmol/g_{cdw}h), appears to be not a determinant of product enantiomeric purity under aerobic conditions when NADPH is regenerated efficiently.

NAD(P)H Regeneration Rate and Co-Substrate Yield

Comparison of results in Table I and Figure 1 reveals that enhancement of NADH-dependent reductase activity from 0 to 416 mU/mg_{protein} translated into only <7-fold increase in the whole-cell bioreduction rate. In contrast to possible effects of mass transfer which cannot be excluded, activities of ADH (230 mU/mg_{protein}; NAD⁺) and ALDH (64 mU/mg_{protein}; NADP⁺) do not seem to constitute a kinetic bottleneck. We measured by HPLC the formation of acetaldehyde and acetate during the course of conversion of ethyl 4-cyanobenzoylformate (10 mM) and ethyl pyruvate (60 mM) by *S.c.* WF2 μ , as in Figure 1. In the first 20 h, both acetate and acetaldehyde were formed whereas later, acetaldehyde decreased at the expense of accumulation of acetate. The molar ratio of α -hydroxy ester to the sum of acetaldehyde and acetate was 1.4 (\pm 0.3) (Table IV),

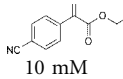
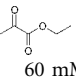
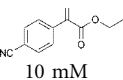
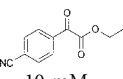
approaching a theoretical value of 2.00 for the oxidation of ethanol into acetate (Scheme 1). The co-substrate yield for bioreductions carried out in the presence of Na₂SO₃ was not determined because the trapped acetaldehyde escaped detection by the analytical methods used.

We analyzed how during bioreduction of ethyl 4-cyanobenzoylformate (10 mM), variations in the reaction conditions affect the molar yield of alcohol on co-substrate consumed (Table IV). Using glucose (300 mM) as co-substrate for aerobic conversions catalyzed by *S.c.* wild-type, 3% of the available carbon source was utilized for biocatalytic synthesis. When ethanol (1 M) was used instead of glucose, the co-substrate yield determined from the amount of acetate produced decreased about twofold to a value of 0.015.

The product yield on the ethanol co-substrate increased to a value of 0.17 in response to an eightfold increase in the biocatalytic reduction rate of 10 mM ethyl 4-cyanobenzoylformate compared to 60 mM ethyl pyruvate. Katz et al. (2003) reported a glucose co-substrate yield of 0.032 for anaerobic ketone reduction by recombinant *S. cerevisiae*. In an engineered yeast strain with reduced glycolytic rate due to knock-out of the gene encoding phosphoglucose isomerase, the co-substrate yield was enhanced to a value of 0.32.

We realize that the overall utilization of ethanol co-substrate during anaerobic α -keto ester reductions (see Table II) requires attention in further process development.

Table IV. Summary of co-substrate yields and conversion rates obtained during whole-cell bioreductions of α -keto esters under different process conditions.*

S.c. strain	Co-substrate	Substrate	O ₂ supply	Co-substrate yield (mM/mM) ^a	Conversion rate (mmol/g _{cdw} h) ^a
WF2 μ	Ethanol 1 M	 10 mM	Anaerobic ^b	1.4	0.10
Wild-type	Ethanol 1 M	 60 mM	Aerobic	0.17	0.42
Wild-type	Ethanol 1 M	 10 mM	Aerobic	0.015	0.050
Wild-type	Glucose 300 mM	 10 mM	Aerobic	0.034	0.22

*Reaction time was 9 h.

^aStandard errors ($N=3$) are \leq 25%. The co-substrate yield is expressed as the molar ratio of alcohol product formed and co-substrate converted. The concentration of ethanol used in the bioconversion equals the sum of the measured concentrations of acetate and acetaldehyde.

^b[O₂] \leq 15 μ M.

A useful option would be to increase the substrate concentration beyond the limit of solubility in the water-ethanol mixture and work in a two-phase system. However, aside from issues of strain viability in the presence of an organic phase (Engelking et al., 2006; Pfruender et al., 2006) balancing the relative rates of α -keto ester reduction and decomposition would constitute an important parameter of process optimization in that case. The use of yeast cell concentrations substantially higher than the 5 g_{cdw}/L employed herein would probably be required. Improvement of ethanol conversion in the bioreduction process was outside the remit of this study and is left for consideration in future work.

Conclusions

The example of α -keto ester reduction by *C. tenuis* xylose reductase was used to develop a general approach with which to improve stereoselectivity in the asymmetric synthesis of alcohols via whole-cell bioreduction of ketone substrates catalyzed by recombinant *S. cerevisiae*. Over-expression of the NADH-active biosynthetic reductase and use of process conditions in which mainly NADH is regenerated lead to an almost complete suppression of the action of endogenous yeast reductases that are NADPH-dependent and show divergent enantiopreferences. Our results furthermore support the notion that optimization of product yield on a metabolizable co-substrate requires careful balancing of the rates of biocatalytic reduction and co-substrate consumption (see also, Johanson et al., 2005, 2008; Katz et al., 2003). The biocatalytic process in Scheme 1 therefore offers the advantage that because acetate is not further fermented, the co-substrate yield is decoupled from the relative conversion rates of substrate and co-substrate and reaches a value greater than 1.00 provided that O₂ is completely excluded from the reaction. Summarizing, the proposed strategy improves a long-known microbial workhorse for the biocatalytic synthesis of chiral α -hydroxy esters and opens up the possibility for application with other reductase-catalyzed conversions that utilize NADH naturally or after suitable engineering of the cofactor specificity of the enzyme.

We thank Dr. Barbara Petschacher (Institute of Biotechnology and Biochemical Engineering, TUG) and Dr. Harald Pichler (Institute of Molecular Biotechnology, TUG) for yeast strains and expression vectors. Financial support from the Austrian Science Fund (project DK Molecular Enzymology W901-B05 and Hertha-Firnberg grant T350-B09) is gratefully acknowledged.

References

Bertau M, Bürli M. 2000. Enantioselective microbial reduction with baker's yeast on an industrial scale. *Chimia* 54:503–507.
 Bommarius AS, Riebel BR. 2004. Production of enantiomerically pure hydrophobic alcohols: Comparison of different process routes and

reactor configurations. In: Bommarius AS, Riebel BR, editors. *Biocatalysis*. Weinheim: Wiley-VCH, p 556–561.
 Breuer M, Ditrich K, Habicher T, Hauer B, Keßler M, Stürmer R, Zelinski T. 2004. Industrial methods for the production of optically active intermediates. *Angew Chem Int Ed* 43:788–824.
 Chin-Joe I, Straathof AJJ, Pronk JT, Jongejan JA, Heijnen JJ. 2002. Effect of high product concentration in a dual fed-batch asymmetric 3-oxo ester reduction by baker's yeast. *Biocatal Biotransform* 20:337–345.
 Christianson TW, Sikorski RS, Dante M, Shero JH, Hieter P. 1992. Multifunctional yeast high-copy-number shuttle vectors. *Gene* 110:119–122.
 D'Arrigo P, Fantoni GP, Servi S, Strini A. 1997. The effect of absorbing resins on substrate concentration and enantiomeric excess in yeast reduction. *Tetrahedron: Asymm* 8:2375–2379.
 Engelking H, Pfaller R, Wich G, Weuster-Botz D. 2006. Reaction engineering studies on β -ketoester reductions with whole cells of recombinant *Saccharomyces cerevisiae*. *Enzyme Microb Technol* 38:536–544.
 Faber K. 2000. Reduction reactions. In: Faber K, editor. *Biotransformations in organic chemistry*. Berlin: Springer, p 177–219.
 Goldberg K, Schroer K, Lütz S, Liese A. 2007. Biocatalytic ketone reduction—A powerful tool for the production of chiral alcohols. Part II. Whole-cell reductions. *Appl Microbiol Biotechnol* 76:249–255.
 Gröger H, Chamouveau F, Orologas N, Rollmann C, Drauz K, Hummel W, Weckbecker A, May O. 2006. Enantioselective reduction of ketones with “designer cells” at high substrate concentrations: Highly efficient access to functionalized optically active alcohols. *Angew Chem Int Ed* 45:5677–5681.
 Guido LF, Fortunato NA, Rodrigues JA, Barros AA. 2003. Voltammetric assay for the aging of beer. *J Agric Food Chem* 51:3911–3915.
 Hummel W. 1997. New alcohol dehydrogenases for the synthesis of chiral compounds. *Adv Biochem Eng/Biotechnol* 58:145–184.
 Ishige T, Honda K, Shimizu S. 2005. Whole organism biocatalysis. *Curr Opin Chem Biol* 9:174–180.
 Johanson T, Katz M, Gorwa-Grauslund MF. 2005. Strain engineering for stereoselective bioreduction of dicarbonyl compounds by yeast reductases. *FEMS Yeast Res* 5:513–525.
 Johanson T, Carlquist M, Olsson C, Rudolf A, Frejd T, Gorwa-Grauslund MF. 2008. Reaction and strain engineering for improved stereoselective whole-cell reduction of a bicyclic diketone. *Appl Microbiol Biotechnol* 77:1111–1118.
 Kaluzna IA, Matsuda T, Sewell AK, Stewart JD. 2004. Systematic investigation of *Saccharomyces cerevisiae* enzymes catalyzing carbonyl reductions. *J Am Chem Soc* 126:12827–12832.
 Kataoka M, Kita K, Wada M, Yasohara Y, Hasegawa J, Shimizu S. 2003. Novel bioreduction system for the production of chiral alcohols. *Appl Microbiol Biotechnol* 62:437–445.
 Katz M, Frejd T, Hahn-Hägerdal B, Gorwa-Grauslund MF. 2003. Efficient anaerobic whole cell stereoselective bioreduction with recombinant *Saccharomyces cerevisiae*. *Biotechnol Bioeng* 84:573–582.
 Kometani T, Kitatsuji E, Matsuno R. 1991. Baker's yeast mediated bioreduction: Practical procedure using EtOH as energy source. *J Ferment Bioeng* 71:197–199.
 Kometani T, Yoshii H, Kitatsuji E, Nishimura H, Matsuno R. 1993. Large-scale preparation of (S)-ethyl 3-hydroxybutanoate with a high enantiomeric excess through baker's yeast-mediated bioreduction. *J Ferment Bioeng* 76:33–37.
 Kometani T, Morita Y, Furui H, Yoshii H, Matsuno R. 1994. NADP(H) regeneration using ethanol as an energy source in baker's yeast-mediated bioreduction. *J Ferment Bioeng* 77:13–16.
 Kometani T, Yoshii H, Matsuno R. 1996. Large-scale production of chiral alcohols with baker's yeast. *J Mol Catal B: Enzym* 1:45–52.
 Kratzer R, Nidetzky B. 2007. Identification of *Candida tenuis* xylose reductase as highly selective biocatalyst for the synthesis of chiral α -hydroxy esters and improvement of its efficiency by protein engineering. *Chem Commun* 10:1047–1049.
 Kratzer R, Leitgeb S, Wilson DK, Nidetzky B. 2006. Probing the substrate binding site of *Candida tenuis* xylose reductase (AKR2B5) with site-directed mutagenesis. *Biochem J* 393:51–58.

- Liese A, Seelbach K, Buchholz A, Haberland J. 2006. Oxireductases. In: Liese A, Seelbach K, Wandrey C, editors. *Industrial biotransformations*. Weinheim: Wiley-VCH, p 153–264.
- Mumberg D, Müller R, Funk M. 1995. Yeast vectors for the controlled expression of heterologous proteins in different genetic backgrounds. *Gene* 156:119–122.
- Nakamura K, Yamanaka R, Matsuda T, Harada T. 2003. Recent developments in asymmetric reduction of ketones with biocatalysts. *Tetrahedron: Asymm* 14:2659–2681.
- Pfruender H, Jones R, Weuster-Botz D. 2006. Water immiscible ionic liquids as solvents for whole cell biocatalysis. *J Biotechnol* 124:182–190.
- Rodriguez S, Kayser M, Stewart JD. 1999. Improving the stereoselectivity of baker's yeast reductions by genetic engineering. *Org Lett* 1:1153–1155.
- Rotthaus O, Krüger D, Demuth M, Schaffner K. 1997. Reductions of keto esters with baker's yeast in organic solvents—A comparison with the results in water. *Tetrahedron* 53:935–938.
- Shieh W-R, Gopalan AS, Sih CJ. 1985. Stereochemical control of yeast reductions. 5. Characterization of the oxidoreductases involved in the reduction of β -keto esters. *J Am Chem Soc* 107:2993–2994.
- Stewart JD. 2000. Organic transformations catalyzed by engineered yeast cells and related systems. *Curr Opin Biotechnol* 11:363–368.
- Sybesma WFH, Straathof AJJ, Jongejan JA, Pronk JT, Heijnen JJ. 1998. Reductions of 3-oxo esters by baker's yeast: Current status. *Biocatal Biotransform* 16:95–134.
- Wang Y, Shi W-L, Liu X-Y, Shen Y, Bao X-M, Bai F-W, Qu Y-B. 2004. Establishment of a xylose metabolic pathway in an industrial strain of *Saccharomyces cerevisiae*. *Biotechnol Lett* 26:885–890.
- Yang Z-H, Yao S-J, Lin D-Q. 2004. Improving the stereoselectivity of asymmetric reduction of 3-oxo ester to 3-hydroxy ester with pretreatments on baker's yeast. *Ind Eng Chem Res* 43:4871–4875.
- Zhou BN, Gopalan AS, VanMiddlesworth F, Shieh W-R, Sih CJ. 1983. Stereochemical control of yeast reductions. 1. Asymmetric synthesis of L-carnitine. *J Am Chem Soc* 105:5925–5926.

Research

Open Access

Whole-cell bioreduction of aromatic α -keto esters using *Candida tenuis* xylose reductase and *Candida boidinii* formate dehydrogenase co-expressed in *Escherichia coli*

Regina Kratzer^{1,2}, Matej Pukl¹, Sigrid Egger¹ and Bernd Nidetzky*^{1,2}

Address: ¹Institute of Biotechnology and Biochemical Engineering, Graz University of Technology (TUG), Petersgasse 12/1, A-8010 Graz, Austria and ²Research Centre Applied Biocatalysis, Petersgasse 14, A-8010 Graz, Austria

Email: Regina Kratzer - regina.kratzer@tugraz.at; Matej Pukl - matejpukl@gmail.com; Sigrid Egger - sigrid.egger@tugraz.at; Bernd Nidetzky* - bernd.nidetzky@tugraz.at

* Corresponding author

Published: 10 December 2008

Received: 31 October 2008

Microbial Cell Factories 2008, **7**:37 doi:10.1186/1475-2859-7-37

Accepted: 10 December 2008

This article is available from: <http://www.microbialcellfactories.com/content/7/1/37>

© 2008 Kratzer et al; licensee BioMed Central Ltd.

This is an Open Access article distributed under the terms of the Creative Commons Attribution License (<http://creativecommons.org/licenses/by/2.0>), which permits unrestricted use, distribution, and reproduction in any medium, provided the original work is properly cited.

Abstract

Background: Whole cell-catalyzed biotransformation is a clear process option for the production of chiral alcohols via enantioselective reduction of precursor ketones. A wide variety of synthetically useful reductases are expressed heterologously in *Escherichia coli* to a high level of activity. Therefore, this microbe has become a prime system for carrying out whole-cell bioreductions at different scales. The limited capacity of central metabolic pathways in *E. coli* usually requires that reductase coenzyme in the form of NADPH or NADH be regenerated through a suitable oxidation reaction catalyzed by a second NADP⁺ or NAD⁺ dependent dehydrogenase that is co-expressed. *Candida tenuis* xylose reductase (CtXR) was previously shown to promote NADH dependent reduction of aromatic α -keto esters with high Prelog-type stereoselectivity. We describe here the development of a new whole-cell biocatalyst that is based on an *E. coli* strain co-expressing CtXR and formate dehydrogenase from *Candida boidinii* (CbFDH). The bacterial system was evaluated for the synthesis of ethyl *R*-4-cyanomandelate under different process conditions and benchmarked against a previously described catalyst derived from *Saccharomyces cerevisiae* expressing CtXR.

Results: Gene co-expression from a pETDuet-I vector yielded about 260 and 90 units of intracellular CtXR and CbFDH activity per gram of dry *E. coli* cell mass (g_{CDW}). The maximum conversion rate (r_s) for ethyl 4-cyanobenzoylformate by intact or polymyxin B sulphate-permeabilized cells was similar (2 mmol/ $g_{CDW}h$), suggesting that the activity of CbFDH was partly rate-limiting overall. Uncatalyzed ester hydrolysis in substrate as well as inactivation of CtXR and CbFDH in the presence of the α -keto ester constituted major restrictions to the yield of alcohol product. Using optimized reaction conditions (100 mM substrate; 40 g_{CDW}/L), we obtained ethyl *R*-4-cyanomandelate with an enantiomeric excess (e.e.) of 97.2% in a yield of 82%. By increasing the substrate concentration to 500 mM, the e.e. could be enhanced to \cong 100%, however, at the cost of a 3-fold decreased yield. A recombinant strain of *S. cerevisiae* converted 100 mM substrate to 45 mM ethyl *R*-4-cyanomandelate with an e.e. of \geq 99.9%. Modifications to the recombinant *E. coli* (cell permeabilisation; addition of exogenous NAD⁺) and addition of a water immiscible solvent (e.g. hexane or 1-butyl-3-methylimidazolium hexafluorophosphate) were not useful. To enhance the overall capacity for NADH regeneration in the system, we supplemented the original biocatalyst

after permeabilisation with also permeabilised *E. coli* cells that expressed solely *CbFDH* (410 U/g_{CDW}). The positive effect on yield (18% → 62%; 100 mM substrate) caused by a change in the ratio of *FDH* to *XR* activity from 2 to 20 was invalidated by a corresponding loss in product enantiomeric purity from 86% to only 71%.

Conclusion: A whole-cell system based on *E. coli* co-expressing *CtXR* and *CbFDH* is a powerful and surprisingly robust biocatalyst for the synthesis of ethyl *R*-4-cyanomandelate in high optical purity and yield. A clear requirement for further optimization of the specific productivity of the biocatalyst is to remove the kinetic bottleneck of *NADH* regeneration through enhancement (≥ 10-fold) of the intracellular level of *FDH* activity.

Background

Enzyme-catalyzed enantioselective reductions of ketones have become quite popular for the production of homochiral alcohols at industrial scale [1]. *NAD(P)H*-dependent reductases catalyze these transformations with exquisite chemo-, regio-, and stereoselectivities such that usually an optically pure product is obtained in high yield. Generally, the biocatalyst employed for ketone reduction can be a whole-cell system or a (partially) purified protein preparation [2-5]. The use of whole cells offers the important advantage of a simple, hence low-cost catalyst preparation. The synthetic reductase is often-times more stable within the cellular environment as compared to the isolated enzyme. Enzymatic reduction of ketones is usually performed in the presence of a substoichiometric amount of coenzyme (*NADH* or *NADPH*), implying that the catalytic reductant must be recycled during the conversion. Cells provide a basal capacity for coenzyme regeneration through the reduction of *NAD*⁺ and *NADP*⁺ in central metabolic pathways. The spatial organisation of the whole-cell system where enzymes and cofactors are encapsulated by the supramolecular structure of the cell membranes potentially improves the efficiency of coenzyme recycling as compared to homogeneous reactors employing "free-floating" biocatalytic components.

Considering the ability of *Escherichia coli* to over-express various synthetically useful ketoreductases to a high level of activity, this organism has become a prime choice for the development of whole-cell bioreduction catalysts. The capabilities of *E. coli* to provide internal cofactor regeneration are, however, oftentimes limiting overall [6-9]. Co-expression of another, *NAD*⁺ or *NADP*⁺-dependent dehydrogenase is therefore used to couple the biosynthetic reduction of the target ketone with the oxidation of a suitable co-substrate. Currently, oxidation of glucose catalyzed by glucose dehydrogenase (*GDH*) is most often used for cofactor regeneration [2,6,9-14]. While the method effectively drives ketone reduction and can be flexibly applied to the recycling of *NADH* and *NADPH*, there is the clear disadvantage that the native glucose uptake system in *E. coli* involves coupled transport and phosphorylation. The resulting glucose 6-phosphate is

not a substrate of *GDH*. To provide glucose efficiently for *GDH*-catalyzed oxidation, one must therefore make the cell membrane just sufficiently permeable for glucose (but not for coenzyme) or engineer the glucose uptake system [15-17]. Formation of gluconic acid as the ultimate oxidation product that is not further used in the reaction has a negative impact on the atom economy of the overall conversion. Moreover it requires that bioprocessing be performed under pH control [6,11,12,14,17]. Addition of concentrated base can lead to local peaks of high pH in imperfectly mixed bioreactors which in turn constitutes a strong factor of enzyme inactivation [18-20]. The use of *GDH* was further invalidated in this work because the ketoreductase employed for synthesis showed weak activity towards reduction of glucose into sorbitol [21].

Therefore, the ideal co-substrate should be readily taken up by the *E. coli* cell. It should not by itself or the product generated from it, inhibit or inactivate the synthetic ketoreductase. Oxidation of the co-substrate should be thermodynamically favoured, and the co-product should be easily removed from the reaction mixture. These demands are widely met by the conversion of formate into carbon dioxide catalyzed by formate dehydrogenase (*FDH*) [7,17,22-26]. *FDH* enzymes from yeast and bacterial sources are typically specific for *NAD*⁺ and can be used in a broad pH range (pH 6.0–9.0; [27]). While many papers have been published on the use of isolated *FDH* for the regeneration of *NADH*, particularly the enzyme from *Candida boidinii* (*CbFDH*), the development of corresponding whole-cell systems is not advancing as quickly. The relatively low specific activity of *CbFDH* (3 U/mg, [28]) is considered a drawback for whole-cell applications of this enzyme.

We describe in this paper the construction of a novel whole-cell biocatalyst that was derived from *E. coli* BL21 (DE3) through co-expression of the genes encoding *Candida tenuis* xylose reductase (*CtXR*) and *CbFDH*. It was shown in previous work that *CtXR* promotes the reduction of aromatic α -keto esters with useful efficiency and excellent stereoselectivity [29]. Here, the synthesis of ethyl *R*-4-cyanomandelate was employed to characterize and

optimize the biocatalytic performance of the recombinant *E. coli* strain (Figure 1). The bacterial whole-cell system was compared with a recently developed strain of *Saccharomyces cerevisiae* that was designed for stereospecific reduction of aromatic α -keto esters through overexpression of the gene encoding *CtXR*.

Results and discussion

Co-expression of *CtXR* and *CbFDH* in *E. coli*

The vector pETDuet-1-XR_FDHD was constructed to enable co-expression of the genes encoding *CtXR* and *CbFDH*. The specific activity of purified *CbFDH* (3 U/mg; [28]) is about 2-fold that of the purified *CtXR* on 10 mM ethyl 4-cyanobenzoylformate (1.8 U/mg). We placed the gene encoding *CbFDH* after the *CtXR* gene with the aim of specifically enhancing the overproduction of the formate dehydrogenase, as recommended by the supplier Novagen.

In a screening for conditions that are suitable for the simultaneous production of *CtXR* and *CbFDH* in *E. coli* BL21 (DE3), we compared low (0.25 mM) and high (1.00 mM) IPTG concentrations in combination with short (5 h) and long (20 h) induction times. The specific activity of *CtXR* in the cell-free extract was not dependent on the IPTG concentration but enhanced from 0.58 U/mg to 0.91 U/mg by using the long induction phase. The specific activity of *CbFDH* (0.18 U/mg) was insensitive to changes in any of the two cultivation parameters. By way of comparison, the specific activity of *CbFDH* in the cell extract of *E. coli* FDH was 1.4 U/mg. The specific activity of *CtXR* in *E. coli* XR_FDHD compares roughly to one of 0.49 U/mg that is obtained when using the expression vector pBE-Act.1i in *E. coli* BL21 (DE3). The results also show that the activity ratio *CtXR*/*CbFDH* in *E. coli* XR_FDHD was ~8-fold higher than expected from the specific activities of the purified enzymes. Therefore, differential overproduction of *CtXR* and *CbFDH* to favour formation of the formate

dehydrogenase did not occur with the expression construct used. We inspected *E. coli* XR_FDHD under the light microscope and observed that a substantial amount of protein inclusion bodies was formed under induction conditions (data not shown). While intracellular precipitation could clearly account for losses of *CbFDH* activity, we considered the examination of folding factors for *CbFDH* in *E. coli* to be outside the scope of this paper. The level of *CbFDH* expression using pETDuet-1-XR_FDHD was comparable to that seen in previous work where *CbFDH* and an alcohol dehydrogenase were co-expressed in *E. coli* BL21 (DE3) from a pACYCDuet-1 vector [23]. Note that the arrangement of genes in the expression construct was similar in both studies.

Table 1 summarizes results of activity measurement for *E. coli* XR_FDHD. To facilitate the comparison of different whole-cell catalysts, we normalized the results using g_{CDW} . The activity of *CtXR* (using xylose as the substrate) in *E. coli* XR_FDHD was about 7 times the corresponding enzyme activity in *S. cerevisiae* XR2 μ . The levels of the enzyme activities exploited in the regeneration of NADH were similar in *E. coli* XR_FDHD and *S. cerevisiae* XR2 μ (alcohol dehydrogenase; ADH). With the assay used [30], the level of NAD⁺-dependent aldehyde dehydrogenase (ALDH) activity in *S. cerevisiae* XR2 μ was below detection limit (< 0.2 U/ g_{CDW}). The wild-type strain of *S. cerevisiae* as well as *E. coli* FDH shows no ethyl 4-cyanobenzoylformate reductase activity in the absence of *CtXR* overexpression.

Whole cell-catalyzed reduction of ethyl 4-cyanobenzoylformate

We compared the initial rates of substrate reduction (r_s) by *E. coli* XR_FDHD, *S. cerevisiae* XR2 μ , and the wild-type strain of *S. cerevisiae*. A low substrate concentration of 10 mM was chosen to decrease toxic effects of ethyl 4-cyanobenzoylformate on the cells (see later). Yeast bioreduction experiments were carried out under anaerobic

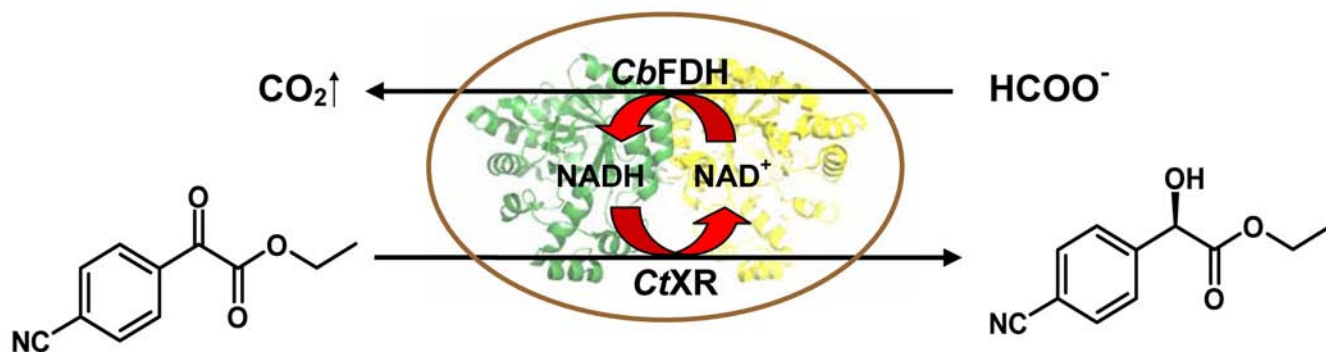


Figure 1
Whole-cell biocatalytic reduction of ethyl 4-cyanobenzoylformate using a recombinant strain of *E. coli* co-expressing *Candida tenuis* xylose reductase (*CtXR*) and *Candida boidinii* formate dehydrogenase (*CbFDH*).

Table 1: Biosynthetic and NADH regenerating enzyme activities in different strains of *E. coli* and *S. cerevisiae*

strain	XR activity [U/g _{CDW}] ¹ NADH-dependent	dehydrogenase activity [U/g _{CDW}] ¹ NADH ⁺ -dependent
<i>E. coli</i> XR_FDHDH	256	85 (FDH)
<i>E. coli</i> FDH	0	408 (FDH)
<i>S. cerevisiae</i> XR2 μ	35	174 (ADH)
<i>S. cerevisiae</i> wild-type	0	112 (ADH)

¹Standard errors \leq 15%.

conditions in the presence of ethanol as co-substrate to promote ADH-catalyzed regeneration of NADH while suppressing at the same time routes that could recycle NADPH. Kratzer et al. [31] have recently shown that reduction of aromatic α -keto esters by *S. cerevisiae* XR2 μ proceeded under these conditions with the near perfect enantioselectivity of isolated CtXR in analogous conversions. Initial rates (r_s) were calculated from linear time courses of substrate conversion in the first \approx 1 h of reaction, and results are summarized in Table 2. r_s -Values for the bacterial strain and *S. cerevisiae* XR2 μ were similar and surpassed that for the wild-type yeast by a factor of 10. The comparison of data in Tables 1 and 2 reveals that the observed pattern of r_s values is not reflected clearly in the activity levels for the biosynthetic and NADH-regenerating enzymes that are present in the different cells. However, we must consider that r_s is a kinetically complex parameter (Figure 1) that is also prone to mass transfer effects.

The e.e. of the alcohol product obtained by using *E. coli* XR_FDHDH was reasonable but not as good as in bioreductions with *S. cerevisiae* XR2 μ or the isolated CtXR (Table 2, [29,31]). This result and evidence presented later indicate that in contrast to the widely held notion [6,7] the effect of the *E. coli* reductase background must not generally be neglected during development of a whole-cell catalyst for reduction of ketones [6,9,14]. The stereochemical outcome of the conversion of ethyl 4-cyanobenzoylformate by *E. coli* XR_FDHDH, however, presented a clear improvement in terms of selectivity as compared to reduction of the same substrate by the wild-type strain of *S. cerevisiae*.

Table 2 also shows the effect of varied substrate and cell concentrations on r_s for *E. coli* XR_FDHDH. At a given concentration of ethyl 4-cyanobenzoylformate, r_s was largely independent of the cell concentration used in the experiment. r_s was doubled in response to an increase in substrate concentration from 10 mM to 100 mM. However, as the solubility of ethyl 4-cyanobenzoylformate was only around 10 mM under the conditions used, the availability

Table 2: Initial rates and ee-values of ethyl 4-cyanobenzoylformate reduction by different whole-cell biocatalysts.

strain	cell dry weight [g/L]	substrate conc.	initial rate [mmol/g h] ¹ /ee ² [%]
<i>E. coli</i> XR_FDHDH	5	10	0.60/97.0 R
<i>E. coli</i> XR_FDHDH	5	100	1.12/99.0 R
<i>E. coli</i> XR_FDHDH	20	100	1.39/99.3 R
<i>E. coli</i> XR_FDHDH	40	100	1.19/98.6 R
<i>E. coli</i> XR_FDHDH	40	500	1.94/99.9 R
<i>S. cerevisiae</i> XR2 μ ³	5	10	0.26/ \geq 99.9 R
<i>S. cerevisiae</i> XR2 μ ³	40	100	1.03/ \geq 99.9 R
<i>S. cerevisiae</i> wild-type ³	5	10	0.06/80.4 R

¹Determined from the time course of substrate conversion between 0 and \leq 1.4 h reaction time; standard errors \leq 20%. ²The detection limit of ethyl 4-cyanomandelate is below 0.01 mM. ³Anaerobic reaction conditions where [O₂] < 15 μ M; ethanol was used as co-substrate.

of substrate at higher concentrations of the keto ester was not clear. The 1.6-fold enhancement in r_s resulting from an increase in substrate concentration from 100 mM to 500 mM is interesting as it seems to imply uptake of ethyl 4-cyanobenzoylformate by the cells directly from the organic phase. The concentration of substrate dissolved in the aqueous phase will be the same irrespective of the total substrate concentration being 100 mM or 500 mM. Another important implication of Table 2 is that e.e. increased as the substrate concentration was raised. The level of substrate that was optimal with respect to maximizing the e.e. was dependent on the cell concentration used. The results suggest that the *E. coli* reductase background which is responsible for the lowering of the optical purity of product was inhibited by high substrate concentrations.

Figure 2 shows the full time courses of substrate conversion by *E. coli* XR_FDHD under the conditions that were used for determination of initial rates in Table 2. In terms of product yield based on substrate used in the overall reaction, the choice of a cell concentration of 40 g_{CDW}/L and a substrate concentration of 100 mM was best and used during further optimization of the whole-cell biotransformation. However, the maximum yield obtained in Figure 2 was significantly below 100%, making it also necessary to examine the factors that limit conversion of ethyl 4-cyanobenzoylformate into product. Note that when using *S. cerevisiae* XR2 μ (40 g_{CDW}/L), the yield from 100 mM ethyl 4-cyanobenzoylformate was 45% (data not shown).

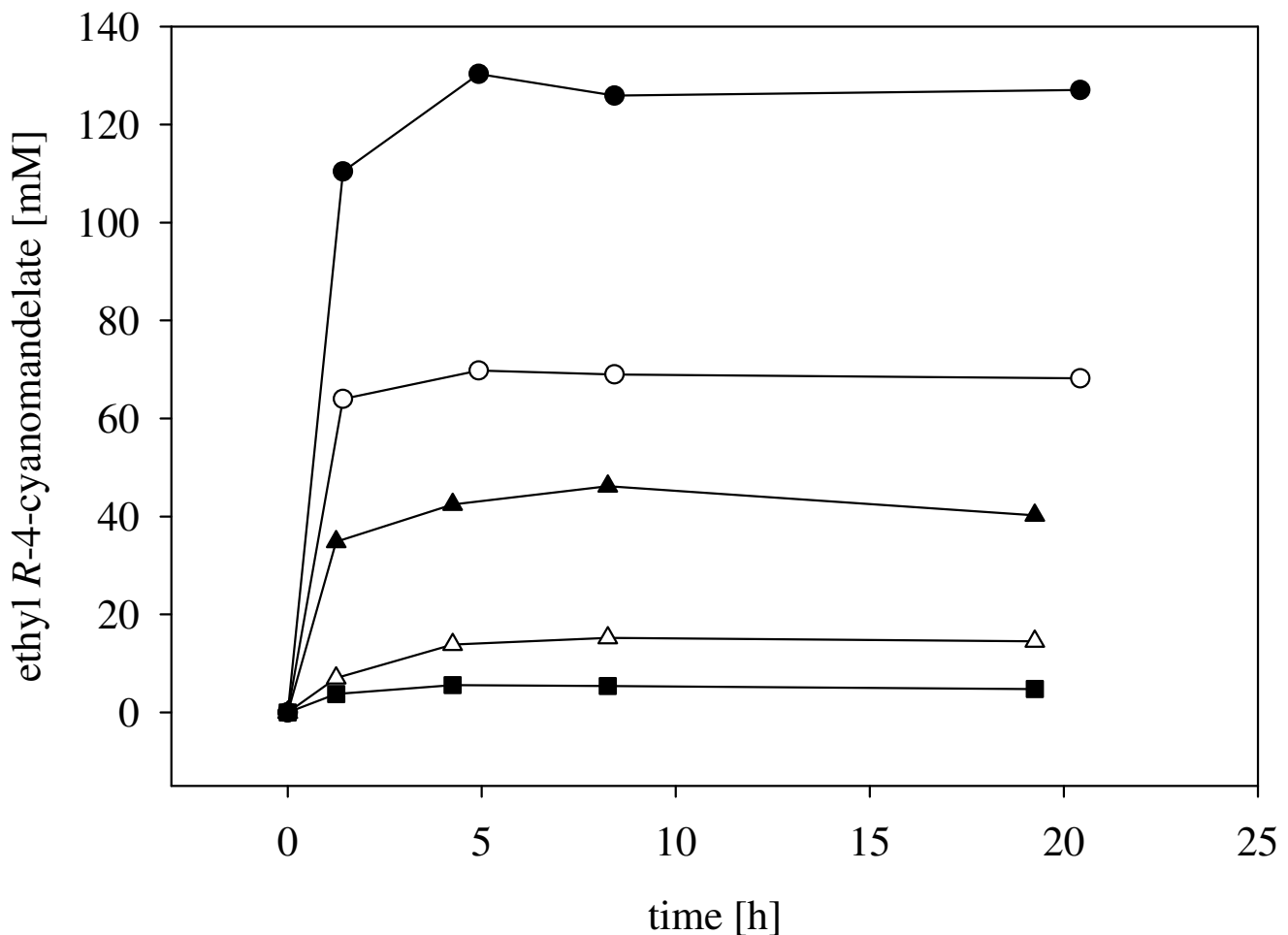


Figure 2

Whole cell-catalyzed reduction of ethyl 4-cyanobenzoylformate by *E. coli* XR_FDHD. The analytical yield is given and expressed as concentration of ethyl 4-cyanomandelate formed from the initial substrate concentration. Conditions are indicated by symbols: ● [substrate] = 500 mM, [cells] = 40 g_{CDW}/L; ○ [substrate] = 100 mM, [cells] = 40 g_{CDW}/L; ▲ [substrate] = 100 mM, [cells] = 20 g_{CDW}/L; △ [substrate] = 100 mM, [cells] = 5 g_{CDW}/L; ■ [substrate] = 10 mM, [cells] = 5 g_{CDW}/L.

Limitations in whole-cell reductions of ethyl 4-cyanobenzoylformate by *E. coli* XR_FDHD and *S. cerevisiae* XR2 μ

Time courses of reduction of ethyl 4-cyanobenzoylformate were characterized by a sharp decrease in the conversion rate which irrespective of the amount of product already formed under the different experimental conditions, occurred at approximately the same time during the initial phase of the transformation (Figure 2). Chemical degradation of substrate and/or product and deactivation of XR and/or enzymes involved in coenzyme regeneration are factors that could account for the observed slowing down of the reaction and hence limit the final yield of alcohol product (Figure 3). We incubated 100 mM ethyl 4-cyanobenzoylformate identically as in Figure 2 but in the absence of biomass as a control and measured sponta-

neous decomposition of the substrate [32], which is most probably due to hydrolysis (Figure 3). Ethyl 4-cyanobenzoylformate was quite unstable, its calculated half-life time being only about 1.4 h. No detectable degradation of the product ethyl 4-cyanomandelate took place under the same conditions during a 6-h long incubation (data not shown). The presence of the α -keto ester substrate (100 mM) had a strong negative impact on the stabilities of XR and FDH in *E. coli* XR_FDHD cells, as shown in Figure 3. The calculated half-life time of XR was 1.4 h, that of FDH was 1.5 h. In the absence of substrate, the two enzymes were fully stable over the period of 6 hs [28]. Therefore, these results imply that reduction of ethyl 4-cyanobenzoylformate is critically limited by substrate as well as biocatalyst stability. In order to obtain high product yield, it would thus be necessary that τ_s is much larger throughout

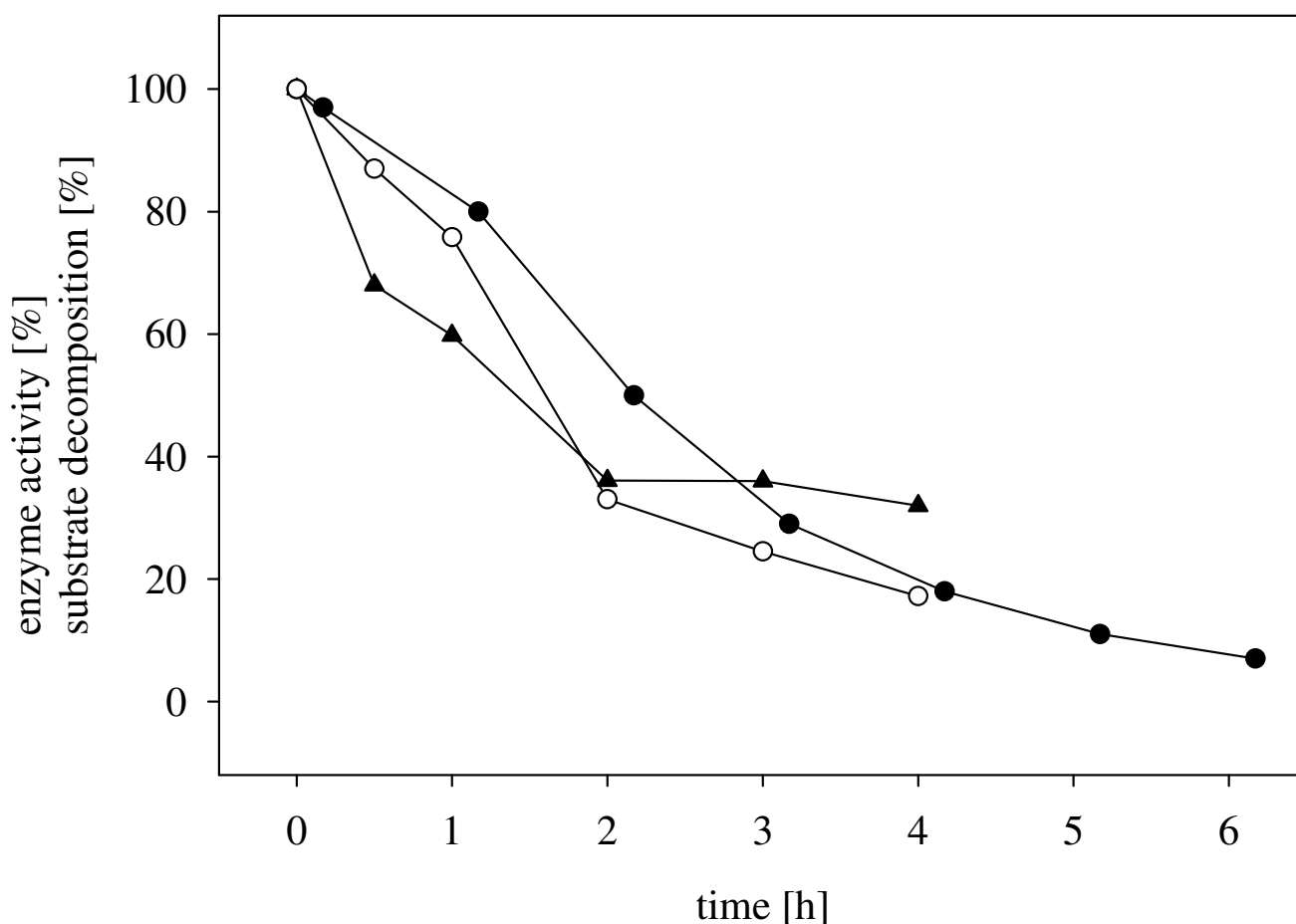


Figure 3

Inactivation of enzymes and spontaneous decomposition of substrate are limiting factors during whole cell-catalyzed reduction of ethyl 4-cyanobenzoylformate by *E. coli* XR_FDHD. Inactivation: *E. coli* XR_FDHD (40 g_{CDW}/L) was incubated in the presence of 100 mM ethyl 4-cyanobenzoylformate and at the indicated times, enzyme activities were measured after cell disruption using B-Per (○ CtXR activity, ▲ CbFDH activity). Substrate decomposition: 100 mM ethyl 4-cyanobenzoylformate was incubated in potassium phosphate buffer 50 mM, pH 7.5, lacking cells, and the concentration of the compound was measured by HPLC in samples taken at the indicated times (●).

than the decomposition rate of the substrate. Likewise, unless stabilized against inactivation by the organic substrate, cells cannot be re-used for multiple rounds of batchwise substrate conversion. Feeding the substrate at a moderately toxic concentration [33] and the use of less toxic organic co-solvents (see later) might be relevant process options with which to enhance both substrate utilization and the total turnover number of the enzymes. The development of a fed-batch process was beyond the scope of this paper.

The half-life time of XR in *S. cerevisiae* XR2 μ was 2.7 h, a \cong 2-fold increase in enzyme stability as compared to the *E. coli* XR_FDHD system. According to literature [34] baker's yeast is more resistant than *E. coli* to the denaturing effects of organic compounds, irrespective of whether they are soluble or present as a second liquid phase. Therefore, this could explain the observed stabilisation of XR. Note that a soluble preparation of XR has a half-life time of 3.7 min when exposed to 100 mM ethyl 4-cyanobenzoylformate, indicating that the whole-cell environment of *S. cerevisiae* or *E. coli* generally provides significant protection to the enzyme. However, with a half-life of only 0.8 h, the stability of ADH appeared to determine overall lifetime of the yeast whole-cell catalyst under the conditions used for α -keto ester reduction.

Effect of organic co-solvents on ethyl 4-cyanobenzoylformate reduction

We considered that a water-immiscible organic co-solvent could, by lowering the substrate concentration in the aqueous phase which contains the whole-cell catalyst, improve the stability of all critical components in the reaction system for ethyl 4-cyanobenzoylformate reduction. A widely held notion is that the toxicity of organic solvents on whole cells decreases as their log*P* value increases. We therefore selected three common solvents covering a log*P* range from 0.68 to 3.5 (ethyl acetate 0.68; butyl acetate 1.7; hexane 3.5) and one ionic liquid (1-butyl-3-methylimidazolium hexafluorophosphate (BMIMPF₆)). The BMIMPF₆ co-solvent was chosen considering the report of Bräutigam et al. [22] where this ionic liquid was described as biocompatible and not damaging to cells. Taking into account the relevant literature (e.g. [22,35,36]), it was unexpected that both *E. coli* XR_FDHD (Table 3) and *S. cerevisiae* XR2 μ (data not shown) displayed a significantly poorer biocatalytic performance in the presence of co-solvent than in the absence thereof. By way of comparison, the use of BMIMPF₆ caused \cong 13-fold enhancement of space-time-yield in the reductive conversion of a β -keto ester catalyzed by whole cells of *E. coli* co-expressing a ketoreductase and bacterial FDH [22]. Therefore, these findings provide a note of caution concerning generalisation of the use of organic co-solvents for whole cell-catalyzed reduction of ketones. They also emphasize that

despite the clear focus on *E. coli* and *S. cerevisiae* in the development of whole-cell biocatalysts [13,37,38], there remains the requirement for case-specific optimization of reaction conditions by medium engineering.

Effect of cell permeabilization and externally added NAD⁺ on ethyl 4-cyanobenzoylformate reduction

Evidence from previous studies of ketone reduction by whole-cell biocatalysts suggests that r_s can in certain cases be enhanced by making the cell wall more easily permeable for low-molecular weight compounds such as substrates, products and if applied, external NAD(P) cofactors [10,39-43]. From the various methods reported for permeabilization of Gram-negative bacteria [44], we selected treatment with the antibiotic polymyxin B sulphate because of its mainly locally disruptive effect on cell wall integrity. Polymyxin B sulphate binds to the lipid A portion of bacterial lipopolysaccharides and induces pore formation in the membrane [45]. Data in Table 3 shows that the chosen permeabilization did not affect the performance of *E. coli* XR_FDHD in the conversion of ethyl 4-cyanobenzoylformate. Likewise, the addition of NAD⁺ (see [6,13,23]) to intact or polymyxin B sulphate-treated cells of *E. coli* XR_FDHD did not enhance the product yield in reactions performed in aqueous buffer. Under conditions where an organic co-solvent or BMIMPF₆ was present, however, the yield was improved up to 9-fold as result of supplementation of the medium with external NAD⁺. Summarizing, the highest yield (\cong 80%) of ethyl *R*-4-cyanomandelate from 100 mM substrate was obtained when using aqueous buffer lacking co-solvents and other additives. Note that conversion of the α -keto ester via enzymatic reduction and the competing route of chemical decomposition was complete in all experiments, implying that \geq 20% of the used substrate was lost to non-enzymatic transformations. The absence of a rate-enhancing effect of external NAD⁺ may be explicable on account of the total intracellular concentration of NAD(H) which is around 1 mM [46]. Considering the *K_m* values of CtXR [47] and CbFDH [23] for NADH and NAD⁺ which are 38 μ M and 90 μ M, respectively, it seems probable that the levels of reduced and oxidized coenzyme in *E. coli* are high enough to saturate the coupled enzyme system. Permeabilization of *S. cerevisiae* XR2 μ was not pursued.

Evidence for limitation of r_s by the activity of FDH

E. coli XR_FDHD showed a XR to FDH activity ratio of 3:1, which may not be optimal for biocatalytic synthesis. The level of FDH activity in *E. coli* FDH was 5 times that of *E. coli* XR_FDHD (Table 1). We therefore used *E. coli* FDH to complement the possible deficit of *E. coli* XR_FDHD with respect to FDH activity. Experiments were performed at a constant XR activity of 1.4 U/mL (equivalent to 5 g_{CDW}/L *E. coli* XR_FDHD) and the activity of FDH was varied at levels of 3, 9 and 27 U/mL. Both *E. coli* strains were permea-

Table 3: Effect of additives and co-solvents on yield and enantiomeric excess of whole-cell bioreduction of ethyl 4-cyanobenzoylformate catalyzed by *E. coli* XR_FDHD.

substrate conc. [mM]	org. co-solvent ¹	additive ^{2,3}	yield [mM] ⁴ /ee [%] ⁵
100			82/97.2 R
100		NAD ⁺	85/97.1 R
100		polymyxin B	75/97.0 R
100		NAD ⁺ , polymyxin B	77/97.2 R
100	ethyl acetate		1/> 99.9 R
100	ethyl acetate	NAD ⁺	9/> 99.9 R
100	hexane		3/> 99.9 R
100	hexane	NAD ⁺	7/> 99.9 R
500			134/> 99.9 R
500		NAD ⁺	136/> 99.9 R
500		polymyxin B	125/> 99.9 R
500		NAD ⁺ , polymyxin B	126/> 99.9 R
500	butyl acetate		9/> 99.9 R
500	butyl acetate	NAD ⁺	35/> 99.9 R
500	BMIMPF ₆		74/> 99.9 R
500	BMIMPF ₆	NAD ⁺	108/> 99.9 R

Conditions: 40 g_{CDW}/L; 8.5 h reaction time. ¹Co-solvents were added in 1:1 volume ratio. ²[NAD⁺] = 490 μM. ³[polymyxin B sulphate] = 144 μM. ⁴Standard errors ≤ 15%. ⁵Detection limit of ethyl 4-cyanomandelate is below 0.01 mM.

bilized using polymyxin B sulphate, and external NAD⁺ was also added. Results are summarized in Table 4. They show that product yield increased markedly (≈ 3.5-fold) in response to a 10-fold increase in FDH activity, demonstrating that r_s of *E. coli* XR_FDHD is limited by NADH regeneration capacity. The presence of external NAD⁺ did not stimulate r_s in the two-strain system, indicating that it is availability of NADH, however not that of total coenzyme that restricts the synthesis rate. Using a comparable system where one *E. coli* strain expressed the synthetic ketoreductase and another GDH for regeneration of NADPH, Xu et al. [9] made the observation that the cellular pools of coenzyme are sufficient to promote ketone reduction. Table 4 reveals that the optical purity of product decreased significantly in response to an increase in the total biomass concentration that was necessary to raise the level of FDH, relative to that of XR, in the reaction. The result provides a note of caution regarding the role of the

E. coli ketoreductase background in the overall conversion of the ketone substrate (see also, [6,9,14]).

Conclusion

A whole-cell system based on *E. coli* co-expressing CtXR and CbFDH is a powerful biocatalyst for the synthesis of ethyl R-4-cyanomandelate in high optical purity and useful yield. The performance of the novel *E. coli* strain in the conversion of 100 mM α-keto ester substrate surpassed that of a yeast strain previously developed for chiral alcohol production using CtXR-catalyzed reduction [31]. Ethyl 4-cyanobenzoylformate was highly "toxic" to the bacterial and yeast biocatalysts, causing rapid inactivation of CtXR and CbFDH in *E. coli* and likewise, CtXR and ADH in *S. cerevisiae*. In the absence of a suitable co-solvent that alleviates the toxic effect, a fed-batch transformation might be the most promising process option for each strain. A clear requirement for further optimization of the

Table 4: Effect of varied activity ratio for CtXR and CbFDH during whole cell-catalyzed reduction of 100 mM ethyl 4-cyanobenzoylformate by a suitable mixture of *E. coli* XR_FDH and *E. coli* FDH.

substrate conc. [mM]	XR : FDH	additive ^{1,2}	yield [mM] ³ /ee [%] ⁴
100	1 : 2	polymyxin B	18/86.1 R
100	1 : 6	polymyxin B	36/74.6 R
100	1 : 20	polymyxin B	62/71.3 R
100	1 : 2	NAD ⁺ , polymyxin B	23/66.8 R
100	1 : 6	NAD ⁺ , polymyxin B	36/64.7 R
100	1 : 20	NAD ⁺ , polymyxin B	64/71.2 R
500	1 : 2	polymyxin B	25/≥ 99.9 R
500	1 : 6	polymyxin B	39/84.6 R
500	1 : 20	polymyxin B	88/73.7 R
500	1 : 2	NAD ⁺ , polymyxin B	29/≥ 99.9 R
500	1 : 6	NAD ⁺ , polymyxin B	42/85.1 R
500	1 : 20	NAD ⁺ , polymyxin B	90/75.5 R

The activity of CtXR was kept constant at 1.4 U/mL throughout.

¹ [NAD⁺] = 490 μM, ² [polymyxin B sulphate] = 144 μM; ³Standard errors ≤ 15%. ⁴Detection limit of ethyl 4-cyanomandelate is below 0.01 mM.

specific productivity of the *E. coli* biocatalyst is to remove the kinetic bottleneck of NADH regeneration through enhancement (≥ 10-fold) of the intracellular level of FDH activity. Because yeast FDHs in their wild-type forms show rather low specific activities [28,48]), powerful expression systems or more active variants of the enzyme [48] should be employed [7,17,22,24].

Methods

Chemicals and strains

Ethyl 4-cyanobenzoylformate was purchased at Sigma-Aldrich (Vienna, Austria). Racemic ethyl 4-cyanomandelate was from Synthon Chemicals GmbH & Co. KG (Wolfen, Germany). NADH (sodium salt; ≥ 98% pure), NAD⁺ (free acid; ≥ 97.5% pure) and NADPH (sodium salt; ≥ 97% pure) were obtained from Roth (Karlsruhe, Germany).

The microorganisms used were *E. coli* JM109, *E. coli* BL21 (DE3), *S. cerevisiae* CEN.PK 113-7D (MATa MAL2-8c SUC2) (termed *S. c.* wild-type) and *S. cerevisiae* CEN.PK 113-5D (*S. cerevisiae* CEN.PK 113-7D – URA; MATa MAL2-8c SUC2 *ura3*). *Pfu* DNA polymerase was from Promega (Madison, WI, USA). dNTPs, T4 DNA ligase, and

restriction enzymes were from MBI Fermentas (Flamborough, ON, Canada). The ionic liquid 1-butyl-3-methylimidazolium hexafluorophosphate (BMIMPF₆) was from Sigma-Aldrich (product number 18122). All other chemicals were purchased from Sigma-Aldrich/Fluka (Gillingham, Dorset, U.K.) or Roth (Karlsruhe, Germany), and were of the highest purity available.

Strain construction

All DNA manipulations and bacterial transformations were carried out according to standard protocols. Cloning of the *CbFDH* gene (from strain *C. boidinii* ATCC 18810) into the plasmid vector pBTac1 (pBTac1-FDH) was described previously [49]. The strain *E. coli* JM109 harbouring pBTac1-FDH was termed *E. coli* FDH. The pET-Duet-1 vector from Novagen (VWR International GmbH, Vienna Austria) was used for co-expression of the genes encoding CtXR and CbFDH. This vector contains two multiple cloning sites, each of which is preceded by a T7 promoter/lac operator and an optimal ribosome binding site for high level protein expression [50]. The vector also carries a ColE1 replicon, the *lacI* gene and an ampicillin resistance gene. The gene encoding CtXR (from *C. tenuis* CBS 4435) was amplified from the plasmid pBEAct.1i

[51] by a PCR using *Pfu* DNA polymerase and the following pair of oligonucleotide primers which provided *PagI* (compatible ends to *NcoI*) and *HindIII* restriction sites.

forward primer: 5'- GGTGTTCATGAGCGCAAGTATCC-3',

reverse primer: 5'- ACCACCAAGCTTTTAAACGAAGATT-GGAATG -3'.

These restriction sites were used subsequently to clone the gene into the first multiple cloning site of pETDuet-1 (*NcoI*, *HindIII*), yielding pETDuet-1-XR. The *CbFDH* gene was likewise amplified from pBTac1-FDH using the oligonucleotide primers listed below.

forward primer: 5'- GGAATTCCATATGAAGATCGTTTTAG-3',

reverse primer: 5'- ACCACCCCTAGGTTATTTCTTATCGT-GTTTAC -3'.

The primers provided *NdeI* and *AvrII* restriction sites which were used subsequently to clone the *CbFDH* gene into the second multiple cloning site of pETDuet-1-XR, yielding pETDuet-1-XR_FDHD. *E. coli* B121 (DE3) was transformed with pETDuet-1-XR_FDHD using a standard electroporation method. The correct integration of the genes for *CtXR* and *CbFDH* and the absence of misincorporations of nucleotides due to DNA polymerase errors were verified by sequencing. The resulting strain was termed *E. coli* XR_FDHD. Construction of the strain *S. cerevisiae* XR2 μ was described previously [31]. The strain was derived from *S. cerevisiae* CEN.PK 113-5D and harbours the yeast 2 μ expression plasmid p426GPD that contains the gene for *CtXR* under control of the strong constitutive glyceraldehyde-3-phosphate dehydrogenase (GPD) promoter.

Cultivation of strains

E. coli strains were grown in 1000 mL baffled shaken flasks containing 200 mL of LB media supplemented with 115 mg/L ampicillin. A Certomat[®] BS-1 incubator from Sartorius was used at a constant agitation rate of 120 rpm. Recombinant protein production used a standard procedure in which cultures were cooled from 37°C to 25°C when an optical density of 1.1 (\pm 10%) was reached. Iso-propylthio- β -D-galactoside (IPTG) was added in a concentration of 0.25 or 1.0 mM, and the cultivation time after induction was 5 or 20 h. Cells were harvested by centrifugation and broken up with the lysis reagent B-Per (Pierce, Rockford, IL, USA). *S. cerevisiae* XR2 μ was grown and processed as described recently [31].

Enzyme activity measurements in the cell-free extracts

Reductase and dehydrogenase activities were assayed spectrophotometrically at 25°C, monitoring the reduction or oxidation of NAD(P)(H) at 340 nm over a time of 1–5 min. Typically, rates of 0.05 – 0.10 ΔA /min were measured. One unit of enzyme activity refers to 1 μ mol of NAD(P)(H) consumed per minute. All measurements were performed with a Beckman DU-800 spectrophotometer using 50 mM potassium phosphate buffer, pH 7.5. The standard assay for *CtXR* contained 10 mM ethyl 4-cyanobenzoylformate and 250 μ M NAD(P)H; that for *CbFDH* contained 200 mM sodium formate and 2 mM NAD⁺. Five % (v/v) ethanol was added to the buffer to enhance the solubility of ethyl 4-cyanobenzoylformate. Reactions were always started by the addition of coenzyme. Measured rates were corrected for appropriate blank readings accounting for non-specific oxidation or reduction of NAD(P)(H) by the cell extracts. Protein concentrations were determined with the BCA assay (Pierce) using bovine serum albumin as a standard. Determination of the activities of *CtXR*, ADH, and ALDH in the cell-free extract of *S. cerevisiae* was described previously [31].

Enzyme stability measurements

Reaction mixtures (1 mL total volume) containing 40 g_{CDW}/L *E. coli* XR_FDHD and 100 mM ethyl 4-cyanobenzoylformate in 100 mM potassium phosphate buffer, pH 7.5, were incubated in 1.5 mL Eppendorf tubes at 30°C. Tubes were incubated for 0.5, 1, 2, 3 or 4 h. The reaction mixture was diluted 20-fold with buffer such that no organic phase (from insoluble substrate) remained, and cells were then collected by centrifugation. After cell lysis using B-Per, enzyme activities were assayed as described above.

Whole-cell bioreduction of ethyl 4-cyanobenzoylformate

Experiments were carried out at 30 (\pm 1) °C using 2-mL Eppendorf reaction tubes that were incubated in an end-over-end rotator (SB3 from Stuart) at 30 rpm. Cells in a concentration between 5 and 80 g_{CDW}/L were suspended in 100 mM potassium phosphate buffer, pH 7.5. Ethyl 4-cyanobenzoylformate is a liquid and was added in a concentration between 10 and 500 mM as indicated. Because the solubility of ethyl 4-cyanobenzoylformate was only 10 mM under the conditions used, reactions with substrate concentrations of > 10 mM, took place in an aqueous-organic two-phase system. The concentration of sodium formate always exceeded that of the ketone substrate by 50 mM (minimum 150 mM). The total reaction volume was 1 mL, and conversions were started through addition of substrate. In reactions where a water-immiscible organic co-solvent (ethyl acetate, butyl acetate, hexane) or ionic liquid (BMIMPF₆) was used, the substrate was dissolved in the co-solvent first and added to the aqueous phase containing the cells in a 1:1 v/v ratio. A

potassium phosphate buffer solution was used as control under otherwise identical conditions. 1 mL samples were taken at certain times, typically every hour, and analyzed as described under Analytical methods.

Procedures used in whole-cell reductions catalyzed by *S. cerevisiae* XR2 μ were described in a recent paper [31].

Analytical methods

Samples were diluted with ethanol as required to obtain a homogeneous liquid phase. Cells were then separated by centrifugation. The supernatant was analyzed by chiral HPLC using a LaChrom HPLC system (Merck-Hitachi) equipped with a reversed phase CHIRALPAK AD-RH column from Daicel (purchased at VWR International, Vienna, Austria) and an L-7400 UV-detector. Detection was at 210 nm. Baseline separation of the *R* and *S* antipode in a racemic mixture of ethyl 4-cyanomandelate was obtained when using acetonitrile and water (20:80, by volume) as eluent at a flow rate of 0.5 mL/min and a temperature of 40°C. Authentic (relevant) standards were used for peak identification, and quantification was based on peak area that was suitably calibrated with standards of known concentration. Reported yields of product on substrate consumed are always from analytical data because product isolation (and determination of the overall yield) was beyond the scope of this study.

Competing interests

The authors declare that they have no competing interests.

Authors' contributions

RK has made substantial contributions to conception, design of experiments and acquisition of data. Carried out analysis, interpreted the data and has been involved in drafting the manuscript. MP contributed to acquisition of data. SE carried out the molecular genetic work. BN has made substantial contributions to conception, design of experiments, interpretation of data and has drafted the manuscript. All authors read and approved the final manuscript.

Acknowledgements

The financial support from the Austrian Science Fund (FWF; project DK Molecular Enzymology W901-B05 and Hertha-Firnberg grant T350-B09) is gratefully acknowledged.

References

- Moore JC, Pollard DJ, Kosjek B, Devine PN: **Advances in the enzymatic reduction of ketones.** *Acc Chem Res* 2007, **40**:1412-1419.
- Goldberg K, Schroer K, Lütz S, Liese A: **Biocatalytic ketone reduction—a powerful tool for the production of chiral alcohols—part II: Whole cell reductions.** *Appl Microbiol Biotechnol* 2007, **76**:249-255.
- Goldberg K, Schroer K, Lütz S, Liese A: **Biocatalytic ketone reduction—a powerful tool for the production of chiral alcohols—part I: Processes with isolated enzymes.** *Appl Microbiol Biotechnol* 2007, **76**:237-248.
- Faber K: **Reduction Reactions.** In *Biotransformations in Organic Chemistry* 4th edition. Edited by: Faber K. Berlin: Springer; 2000:177-219.
- Bommarius AS, Riebel BR: **Production of enantiomerically pure hydrophobic alcohols: Comparison of different routes and reactor configurations.** In *Biocatalysis* 1st edition. Edited by: Bommarius AS, Riebel BR. Weinheim: Wiley-VCH; 2004:456-569.
- Ema T, Yagasaki H, Okita N, Takeda M, Sakai T: **Asymmetric reduction of ketones using recombinant *E. coli* cells that produce a versatile carbonyl reductase with high enantioselectivity and broad substrate specificity.** *Tetrahedron* 2006, **62**:6143-6149.
- Ernst M, Kaup B, Müller M, Bringer-Meyer S, Sahm H: **Enantioselective reduction of carbonyl compounds by whole cell biotransformation, combining a formate dehydrogenase and a (R)-specific alcohol dehydrogenase.** *Appl Microbiol Biotechnol* 2005, **66**:629-634.
- Kataoka M, Rohani LPS, Yamamoto K, Wada M, Kawabata H, Kita K, Yanase H, Shimizu S: **Enzymatic production of ethyl (R)-4-chloro-3-hydroxybutanoate: Asymmetric reduction of ethyl 4-chloro-3-oxobutanoate by an *Escherichia coli* transformant expressing the aldehyde reductase gene from yeast.** *Appl Microbiol Biotechnol* 1997, **48**:699-703.
- Xu Z, Liu Y, Fang L, Jiang X, Jing K, Cen P: **Construction of a two-strain system for asymmetric reduction of ethyl 4-chloro-3-oxobutanoate to (S)-4-chloro-3-hydroxybutanoate ethyl ester.** *Appl Microbiol Biotechnol* 2006, **70**:40-46.
- Zhang J, Witholt B, Li Z: **Coupling of permeabilized microorganisms for efficient enantioselective reduction of ketone with cofactor recycling.** *Chem Commun* 2006, **4**:398-400.
- Gröger H, Chamouleau F, Orologas N, Rollmann C, Drauz K, Hummel W, Weckbecker A, May O: **Enantioselective reduction of ketons with 'designer cells' at high substrate concentrations: Highly efficient access to functionalized optically active alcohols.** *Angew Chem Int Ed* 2006, **45**:5677-5681.
- Ema T, Okita N, Ide S, Sakai T: **Highly enantioselective and efficient synthesis of methyl (R)-o-chloromandelate with recombinant *E. coli* : Toward practical and green access to clopidogrel.** *Org Biomol Chem* 2007, **5**:1175-1176.
- Kataoka M, Kita K, Wada M, Yasohara Y, Hasegawa J, Shimizu S: **Novel bioreduction system for the production of chiral alcohols.** *Appl Microbiol Biotechnol* 2003, **62**:437-445.
- Yun H, Choi H-L, Fadnavis NW, Kim B-G: **Stereospecific synthesis of (R)-2-hydroxy carboxylic acids using recombinant *E. coli* BL21 overexpressing YiaE from *Escherichia coli* K12 and glucose dehydrogenase from *Bacillus subtilis*.** *Biotechnol Prog* 2005, **21**:366-371.
- De Anda R, Lara AR, Hernández V, Hernández-Montalvo V, Gosset G, Bolívar F, Ramírez OT: **Replacement of the glucose phosphotransferase transport system by galactose permease reduces acetate accumulation and improves process performance of *Escherichia coli* for recombinant protein production without impairment of growth rate.** *Metab Eng* 2006, **8**:281-290.
- Wong MS, Wu S, Causey TB, Bennett GN, San K-Y: **Reduction of acetate accumulation in *Escherichia coli* cultures for increased recombinant protein production.** *Metab Eng* 2008, **10**:97-108.
- Kaup B, Bringer-Meyer S, Sahm H: **Metabolic engineering of *Escherichia coli* : Construction of an efficient biocatalyst for D-mannitol formation in a whole-cell biotransformation.** *Appl Microbiol Biotechnol* 2004, **64**:333-339.
- Nordkvist M, Nielsen PM, Villadsen J: **Oxidation of lactose to lactobionic acid by a *Microdochium nivale* carbohydrate oxidase: Kinetics and operational stability.** *Biotechnol Bioeng* 2007, **97**:694-707.
- Nidetzky B, Neuhauser W, Haltrich D, Kulbe KD: **Continuous enzymatic production of xylitol with simultaneous coenzyme regeneration in a charged membrane reactor.** *Biotechnol Bioeng* 1996, **52**:387-396.
- Nidetzky B, Furlinger M, Gollhofer D, Scopes RK, Haltrich D, Kulbe KD: **Improved operational stability of cell-free glucose-fructose oxidoreductase from *Zymomonas mobilis* for the efficient synthesis of sorbitol and gluconic acid in a continuous ultrafiltration membrane reactor.** *Biotechnol Bioeng* 1997, **53**:623-629.

21. Nidetzky B, Mayr P, Hadwiger P, Stütz AE: **Binding energy and specificity in the catalytic mechanism of yeast aldose reductase.** *Biochem J* 1999, **344**:101-107.
22. Bräutigam S, Bringer-Meyer S, Weuster-Botz D: **Asymmetric whole cell biotransformations in biphasic ionic liquid/water-systems by use of recombinant *Escherichia coli* with intracellular cofactor regeneration.** *Tetrahedron: Asymm* 2007, **18**:1883-1887.
23. Weckbecker A, Hummel W: **Improved synthesis of chiral alcohols with *Escherichia coli* cells co-expressing pyridine nucleotide transhydrogenase, NADP⁺-dependent alcohol dehydrogenase and NAD⁺-dependent formate dehydrogenase.** *Biotechnol Lett* 2004, **26**:1739-1744.
24. Yamamoto H, Mitsuhashi K, Kimoto N, Kobayashi Y, Esaki N: **Robust NADH-regenerator: Improved α -haloketone-resistant formate dehydrogenase.** *Appl Microbiol Biotechnol* 2005, **67**:33-39.
25. Menzel A, Werner H, Altenbuchner J, Gröger H: **From enzymes to 'designer bugs' in reductive amination: A new process for the synthesis of L-tert-leucine using a whole cell-catalyst.** *Eng Life Sci* 2004, **4**:573-576.
26. Gröger H, Hummel W, Rollmann C, Chamouleau F, Hüsken H, Werner H, Wunderlich C, Abokitse K, Drauz K, Buchholz S: **Preparative asymmetric reduction of ketones in a biphasic medium with (S)-alcohol dehydrogenase under in situ-cofactor-recycling with formate dehydrogenase.** *Tetrahedron* 2004, **60**:633-640.
27. Mesentsev AV, Lamzin VS, Tishkov VI, Ustinnikova TB, Popov VO: **Effect of pH on kinetic parameters of NAD⁺-dependent formate dehydrogenase.** *Biochem J* 1997, **321**:475-480.
28. Slusarczyk H, Felber S, Kula MR, Pohl M: **Stabilization of NAD-dependent formate dehydrogenase from *Candida boidinii* by site-directed mutagenesis of cysteine residues.** *Eur J Biochem* 2000, **267**:1280-1289.
29. Kratzer R, Nidetzky B: **Identification of *Candida tenuis* xylose reductase as highly selective biocatalyst for the synthesis of chiral α -hydroxy esters and improvement of its efficiency by protein engineering.** *Chem Comm* 2007, **10**:1047-1049.
30. Meaden PG, Dickinson FM, Mifsud A, Tessier W, Westwater J, Bussey H, Midgley M: **The *ALD6* gene of *Saccharomyces cerevisiae* encodes a cytosolic, Mg²⁺-activated acetaldehyde dehydrogenase.** *Yeast* 1997, **13**:1319-1327.
31. Kratzer R, Egger S, Nidetzky B: **Integration of enzyme, strain and reaction engineering to overcome limitations of baker's yeast in the asymmetric reduction of α -keto esters.** *Biotechnol Bioeng* 2008, **101**:1094-1101.
32. Kaluzna IA, Matsuda T, Sewell AK, Stewart JD: **Systematic investigation of *Saccharomyces cerevisiae* enzymes catalyzing carbonyl reductions.** *J Am Chem Soc* 2004, **126**:12827-12832.
33. Modig T, Almeida JRM, Gorwa-Grauslund MF, Lidén G: **Variability of the response of *Saccharomyces cerevisiae* strains to lignocellulose hydrolysate.** *Biotechnol Bioeng* 2008, **100**:423-429.
34. Pfruender H, Ross J, Weuster-Botz D: **Water immiscible ionic liquids as solvents for whole cell biocatalysis.** *J Biotechnol* 2006, **124**:182-190.
35. Kim P-Y, Pollard DJ, Woodley JM: **Substrate supply for effective biocatalysis.** *Biotechnol Prog* 2007, **23**:74-82.
36. Li Y-N, Shi X-A, Zong M-H, Meng C, Dong Y-Q, Guo Y-H: **Asymmetric reduction of 2-octanone in water/organic solvent biphasic system with baker's yeast FD-12.** *Enzyme Microb Technol* 2007, **40**:1305-1311.
37. Sybesma WFH, Straathof AJJ, Jongejan JA, Pronk JT, Heijnen JJ: **Reductions of 3-oxo esters by baker's yeast: Current status.** *Biocatal Biotransform* 1998, **16**:95-134.
38. Johanson T, Katz M, Gorwa-Grauslund MF: **Strain engineering for stereoselective bioreduction of dicarbonyl compounds by yeast reductases.** *FEMS Yeast Res* 2005, **5**:513-525.
39. Andersson M, Holmberg H, Adlercreutz P: **Evaluation of *Alcaligenes eutrophus* cells as an NADH regenerating catalyst in organic-aqueous two-phase system.** *Biotechnol Bioeng* 1998, **57**:79-86.
40. Andersson M, Otto R, Holmberg H, Adlercreutz P: ***Alcaligenes eutrophus* cells containing hydrogenase, a coenzyme regenerating catalyst for NADH-dependent oxidoreductases.** *Biocatal Biotransform* 1997, **15**:281-296.
41. Adlercreutz P: **Novel biocatalyst for the asymmetric reduction of ketones: Permeabilized cells of *Gluconobacter oxydans*.** *Enzyme Microb Technol* 1991, **13**:9-14.
42. Felix H, Brodelius P, Mosbach K: **Enzyme activities of the primary and secondary metabolism of simultaneously permeabilized and immobilized plant cells.** *Anal Biochem* 1981, **116**:462-470.
43. Honorat-Pascal A, Monot F, Ballerini D: **Comparative study of the enzymatic synthesis of L-valine by purified enzymes, crude extract, intact or permeabilized cells from *Bacillus megaterium*.** *Appl Microbiol Biotechnol* 1990, **34**:236-241.
44. Cánovas M, Torroglosa T, Iborra JL: **Permeabilization of *Escherichia coli* cells in the biotransformation of trimethylammonium compounds into L-carnitine.** *Enzyme Microb Technol* 2005, **37**:300-308.
45. Tsubery H, Ofek I, Cohen S, Fridkin M: **Structure-function studies of polymyxin B nonapeptide: Implications to sensitization of gram-negative bacteria.** *J Med Chem* 2000, **43**:3085-3092.
46. Walton AZ, Stewart JD: **Understanding and improving NADPH-dependent reactions by non-growing *Escherichia coli* cells.** *Biotechnol Progr* 2004, **20**:403-411.
47. Kratzer R, Kavanagh KL, Wilson DK, Nidetzky B: **Study of the enzymic mechanism of *Candida tenuis* xylose reductase (AKR2B5): X-ray structure and catalytic reaction profile for the HI 13A mutant.** *Biochemistry* 2004, **43**:4944-4954.
48. Tishkov VI, Popov VO: **Protein engineering of formate dehydrogenase.** *Biomol Eng* 2006, **23**:89-110.
49. Krahulec S, Armao GC, Weber H, Klimacek M, Nidetzky B: **Characterization of recombinant *Aspergillus fumigatus* mannitol-1-phosphate 5-dehydrogenase and its application for the stereoselective synthesis of prolio and deuterio forms of D-mannitol 1-phosphate.** *Carbohydr Res* 2008, **343**:1414-1423.
50. Novy R, Yaeger K, Held D, Mierendorf R: **Coexpression of multiple target proteins in *E. coli*.** *Innovations* 2002, **15**:2-6.
51. Häcker B, Habenicht A, Kiess M, Mattes R: **Xylose utilisation: Cloning and characterisation of the xylose reductase from *Candida tenuis*.** *Biol Chem* 1999, **380**:1395-1403.

Publish with **BioMed Central** and every scientist can read your work free of charge

"BioMed Central will be the most significant development for disseminating the results of biomedical research in our lifetime."

Sir Paul Nurse, Cancer Research UK

Your research papers will be:

- available free of charge to the entire biomedical community
- peer reviewed and published immediately upon acceptance
- cited in PubMed and archived on PubMed Central
- yours — you keep the copyright

Submit your manuscript here:
http://www.biomedcentral.com/info/publishing_adv.asp



Enzyme identification and development of a whole-cell biotransformation for asymmetric reduction of *o*-chloroacetophenone

Regina Kratzer*^{1,2}, Matej Pukl¹, Sigrid Egger¹, Michael Vogl³, Lothar Brecker³ and Bernd Nidetzky*^{1,2}

¹Institute of Biotechnology and Biochemical Engineering, Graz University of Technology, Petersgasse 12, A-8010 Graz, Austria.

²Research Centre Applied Biocatalysis, Petersgasse 14, A-8010 Graz, Austria

³Institute of Organic Chemistry, University of Vienna, Währinger Straße 38, A-1090 Wien, Austria

*Corresponding authors

Fax: +43 316 873 8434; Tel: +43 316 873 8408 (R.K.); +43 316 873 8400 (B.N.); E-mail: regina.kratzer@tugraz.at, bernd.nidetzky@tugraz.at

KEYWORDS: *S*-1-(*o*-Chlorophenyl)-ethanol; PLK1 inhibitors; *Candida tenuis* xylose reductase; whole-cell catalyst; *E. coli*; *S. cerevisiae*; enantioselective carbonyl reduction

Abstract

Chiral 1-(*o*-chlorophenyl)-ethanols are key intermediates in the synthesis of PLK1 (polo-like kinase 1) inhibitors, which constitute an emerging class of chemotherapeutic substances. Enantioselective reduction of *o*-chloro-acetophenone is a preferred method of production but well investigated chemo- and biocatalysts for this transformation are currently lacking. Based on the discovery that *Candida tenuis* xylose reductase converts *o*-chloroacetophenone with useful specificity ($k_{\text{cat}}/K_{\text{m}} = 580 \text{ M}^{-1}\text{s}^{-1}$) and perfect *S*-stereoselectivity, we developed whole-cell catalysts from *Escherichia coli* and *Saccharomyces cerevisiae* co-expressing recombinant reductase and a suitable system for recycling of NADH. Unlike often observed, product chiral purity was not compromised by the use of either cell type. *E. coli* surpassed *S. cerevisiae* sixfold concerning catalytic productivity (3 mmol/g dry cells/h) and total turnover number (1.5 mmol substrate/g dry cells). Considering its high hydrophobicity ($\log P = 2.1$), *o*-chloroacetophenone was unexpectedly “toxic”, and catalyst half-life times of only 20 min (*E. coli*) and 30 min (*S. cerevisiae*) in the presence of 100 mM substrate restricted the time of batch processing to maximally ~5 h. Systematic reaction optimization was used to enhance the product yield ($\leq 60\%$) of *E. coli* catalyzed conversion of 100 mM *o*-chloro-acetophenone which was clearly limited by catalyst instability. Supplementation of external NAD^+ (0.5 mM) to cells permeabilized with Polymyxin B sulphate (0.14 mM) was most effective in enhancing the conversion rate (r_s) relative to r_s of untreated cells, thereby alleviating the regime of catalyst inactivation and providing 98 mM *S*-1-(*o*-chlorophenyl)-ethanol. The strategies considered for optimization of r_s should be generally useful, however, especially under process conditions that promote fast loss of catalyst activity.

Introduction

The serine-threonine kinase PLK1 (polo-like kinase 1) is a key regulator of mitotic progression and cell division in eukaryotes. It is highly expressed in tumor cells and considered a potential target for cancer therapy. *In vivo* studies have shown that competitive inhibition of PLK1 has good antitumor efficacy in xenograft tumor models (Santamaria et al., 2007; Sato et al., 2009). Thiophene-benzimidazole and -imidazopyridine are currently among the most promising PLK1 inhibitor candidates, and *S*-1-(*o*-chlorophenyl)-ethanol is used as chiral key intermediate in their synthesis (Rheault et al., 2008; Sato et al., 2009; Stengel et al., 2009). The pharmaceutical industry therefore strives for “green chemical” methods for production of enantiopure 1-*o*-chlorophenyl-ethanols. Asymmetric reduction of the ketone precursor *o*-chloroacetophenone (Scheme 1A) is a preferred synthetic route towards chiral alcohol product.

A wide range of chemo-catalysts have been explored for *o*-chloroacetophenone conversion. However, except for very few examples (Baratta et al., 2008; Evans et al. 2003; Zeror et al., 2008), use of these catalysts was prohibited by insufficient enantioselectivity. Extensive screening of microbes isolated from environmental samples has provided a relatively limited selection of strains capable of *o*-chloroacetophenone reduction (Andrade et al, 2005, 2009; Kagohara et al., 2008; Kurbanoglu et al., 2007a,b, 2010; Nakamura and Matsuda, 1998; Ou et al., 2008; Salvi and Chattopadhyay, 2008; Xie et al., 2006). Despite these efforts, the number of isolated reductases exhibiting useful activity towards *o*-chloroacetophenone is still very small (Abokitse and Hummel, 2003; Itoh et al., 1999; Yang et al., 2007; Zhu et al., 2006), and none of the reported enzymes was characterized in more detail. This presents reaction engineering with a serious

limitation because kinetic properties and stability of the biocatalyst are parameters needed for defining a usable window of process operation (Burton et al., 2002).

We report herein on the identification of xylose reductase from the yeast *Candida tenuis* CBS4435 (CtXR) as a practical catalyst for the synthesis of *S*-1-(*o*-chlorophenyl)-ethanol. It was known from previous studies of the structurally and biochemically well characterized enzyme (Kratzer et al., 2006b) that its substrate scope includes electronically activated ketones such as aromatic α -keto esters that are chemically reactive towards hydride reduction by NADH. However, according to a reactivity scale established for a series of ketones converted by CtXR (Kratzer et al., 2006a), *o*-chloroacetophenone was not a likely substrate of the enzyme. Notwithstanding, NADH-dependent reduction of target ketone by CtXR proceeded with high activity and almost perfect *S*-enantioselectivity as shown later. Robust catalysts for reduction of α -keto-esters have previously been developed by overexpressing the CtXR gene in the two most common hosts for whole-cell biotransformations, *E. coli* and *S. cerevisiae*. Design of the *E. coli* catalyst involved co-expression of the gene encoding formate dehydrogenase from *Candida boidinii* ATCC 18810 (CbFDH) for the purpose of regeneration of NADH. In *S. cerevisiae*, endogenous metabolic sequences such as anaerobic oxidation of ethanol to acetate were used for NADH recycling. Both whole-cell systems retained the splendid stereoselectivity of the isolated reductase in conversion of substituted ethyl benzoylformates and proved useful in the production of enantiopure ethyl *R*-mandelate and derivatives thereof (Kratzer et al., 2008a,b).

Herein, we would therefore like to communicate results of a reaction engineering study in which systematic comparison of *E. coli* and *S. cerevisiae* whole-cell catalysts for synthesis of *S*-1-(*o*-chlorophenyl)-ethanol has been carried out. The reported findings are of general relevance because a key task of reaction

optimization was to (partly) overcome the pronounced “toxicity” of the hydrophobic substrate, a problem often encountered in the field of whole-cell (oxidoreductive) biotransformations. Catalyst half-life times of just about 30 min in the presence of 100 mM *o*-chloroacetophenone limited the time of batch processing with either cell type to maximally a few hours. The regime of catalyst inactivation was best alleviated by enhancing the activity of *E. coli* cells using permeabilization and cofactor supplementation such that enantiopure product (~100 mM) was obtained in almost quantitative yield. Our findings support the notion from a recent article of Gorwa-Grauslund and coworkers (Parachin et al., 2009) that emphasizes the importance of host selection (*E. coli*, *S. cerevisiae*) in development of a whole-cell bioreduction catalyst.

Materials and Methods

Chemicals, strains, and assays

All chemicals used were described elsewhere (Kratzer et al. 2008a,b). The strains *E. coli* BL21 (DE3), *E. coli* JM109, and *S. cerevisiae* CEN.PK 113-5D were employed. *E. coli*_XR is the parent BL21 (DE3) strain harboring plasmid vector pBeact.li (pet11a_XR) that encodes wild-type CtXR (Häcker et al., 1999). *E. coli*_FDH is also the JM109 strain containing plasmid vector pBTac1 (pBTac1-FDH) that encodes CbFDH (Krahulec et al., 2008). *E. coli* XR_FDH is a BL21 (DE3) strain containing the plasmid vector pETDuet-1 (pETDuet_XR_FDH) that is used for co-expression of the genes encoding CtXR and CbFDH (Kratzer et al., 2008b). *S. cerevisiae* XR2 μ is the parent CEN.PK strain harboring the yeast 2 μ expression plasmid p426GPD that contains the gene for CtXR under control of the constitutive glyceraldehyde-3-phosphate dehydrogenase (*TDH3*) promoter (Kratzer et al., 2008a). All strains were cultivated using the conditions described in the given references. Crude cell extract

from *E. coli* and *S. cerevisiae* biomass was prepared by reported methods. Assays used for determination of relevant enzyme activities (xylose reductase, formate dehydrogenase, alcohol dehydrogenase) were described by Kratzer et al. (2008a,b).

Enzyme studies

A highly purified preparation of recombinant CtXR was obtained using reported methods of enzyme production in *E. coli*_XR and chromatographic isolation (Mayr et al., 2000). Enzyme muteins having Trp23 replaced by Phe or Tyr (Kratzer and Nidetzky, 2007) were prepared using analogous procedures. Xylose reductase activity and protein concentration were determined as described previously (Kratzer et al. 2008a,b). Initial rates of *o*-chloroacetophenone reduction by isolated CtXR were acquired spectrophotometrically by absorbance at 340 nm. Reactions were performed at 25 °C in 50 mM potassium phosphate buffer, pH 7.0, using different concentrations of soluble ketone in the range 0.1 – 10 mM. The substrate was dissolved in ethanol and diluted into buffer to give a final ethanol concentration of maximally 5 % (by weight). It was shown in earlier work that this level of ethanol does not interfere with CtXR activity and stability (Kratzer and Nidetzky, 2007).

Synthesis of 1-(*o*-chlorophenyl)-ethanol was performed at 25 °C using 10 mM *o*-chloroacetophenone and 11 mM NADH. The enzyme concentration was 0.3 mg/mL, equivalent to about 1.5 U/mL ketone reductase activity. Substrate conversion was monitored spectrophotometrically as depletion of NADH. The reaction completed to > 90 % in 10 min and was analyzed by chiral HPLC.

Whole-cell bioreduction of *o*-chloroacetophenone

Experiments were carried out at 30 (\pm 1) °C using 2-mL Eppendorf reaction tubes that were incubated in an end-over-end rotator (model SB3, Stuart, VWR, Austria) at

30 rpm. *E. coli* cells were suspended in a concentration between 5 and 40 g cell dry weight (g_{CDW})/L in 100 mM potassium phosphate buffer, pH 7.5, containing 150 mM sodium formate. *o*-Chloroacetophenone dissolved in ethanol was added to give final substrate concentrations of 10 or 100 mM. The ethanol concentration in the reaction was 5 % (by weight). The total volume of the reaction including biomass was 1 mL. Conversion was started by substrate addition. In reactions where a water-immiscible organic co-solvent such as butyl acetate, hexane or the ionic liquid 1-butyl-3-methylimidazolium hexafluorophosphate (BMIMPF₆) was used, *o*-chloroacetophenone was dissolved in the co-solvent first and added in a 1:1 volumetric ratio to the aqueous phase containing the cells. For stopping reactions containing two liquid phases, ethanol was added as required to obtain a homogeneous liquid phase. As in reactions performed in buffer, cells were then removed by centrifugation and the supernatant was used for further analysis.

Conversions catalyzed by *S. cerevisiae* XR2 μ were carried out exactly as described above, except that no sodium formate was present and a 50 mM potassium phosphate buffer, pH 6.2, containing 10 mM Na₂SO₃ was used (Kratzer et al. 2008a). Note: Na₂SO₃ was added to trap the acetaldehyde that is produced by the yeast through NAD⁺-dependent oxidation of ethanol. Kratzer et al. (2008a) have shown that under anaerobic reaction conditions in which “metabolism” of ethanol is essentially limited to a two-step oxidation into acetate, formation of the acetaldehyde-sulfite adduct pulls the conversion of ethanol to completion. It furthermore restricts the coenzyme regeneration capacity of the yeast to formation of NADH because reaction of the NAD(P)⁺-dependent acetaldehyde dehydrogenase is effectively prohibited.

Preparative work-up of 1-(*o*-chlorophenyl)-ethanol used a sample obtained by exhaustive conversion of 100 mM *o*-chloroacetophenone in the presence of *E. coli*

XR_FDH (40 g_{CDW}/L). The biocatalytic synthesis was performed in a total volume of 10 mL, and the reaction mixture contained 0.5 mM NAD⁺ and 0.14 mM Polymyxin B sulfate (see later). After removal of cells, 1-(*o*-chlorophenyl)-ethanol was extracted thrice with 10 mL CH₂Cl₂. Phase separation was done by centrifugation, the organic phases were united, dried with brine, and CH₂Cl₂ was evaporated under reduced pressure. An oily product was obtained with 66 and 68 % of isolated yields of 1-(*o*-chlorophenyl)-ethanol (experiments run in duplicate).

Evaluation of substrate “toxicity”

Loss of relevant enzyme activities in crude *E. coli* or *S. cerevisiae* cell extract was measured in dependence of the time of incubation in the presence of 100 mM *o*-chloroacetophenone. Cell suspensions had a total liquid volume of 1 mL and contained 40 g_{CDW}/L *E. coli* XR_FDH or *S. cerevisiae* XR2 μ . pH, buffer concentrations, temperature and co-substrates were adjusted as in whole cell bioreductions. Incubations were stopped after 0.5, 1, 2, 3 or 4 h by a 20-fold dilution with buffer such that no organic phase from substrate and product remained. Cells were recovered by centrifugation and subjected to chemical lysis using Y-Per (*S. cerevisiae* XR2 μ) or B-Per (*E. coli* XR_FDH). Activities of XR, FDH, and alcohol dehydrogenase (ADH) were assayed as described previously (Kratzer et al., 2008a,b).

Analytical methods

Chiral HPLC. This was performed on a LaChrom HPLC system (Merck-Hitachi) equipped with an L-7400 UV-detector and a thermo-stated column oven. A reversed phase CHIRALPAK AD-RH column from Daicel (purchased at VWR International, Vienna, Austria) was used and detection was at 210 nm absorbance (Kratzer and

Nidetzky, 2007). Best resolution of the *R*- and *S*-alcohol was obtained with acetonitrile and water (20:80, by volume) as eluent at a flow rate of 0.5 mL/min and a temperature of 40 °C. Under these conditions, baseline separation of the *R*- and *S*-antipodes in a racemic mixture of 1-(*o*-chlorophenyl)-ethanols was obtained. The detection limits of *o*-chloroacetophenone and 1-(*o*-chlorophenyl)-ethanols were below 0.005 mM.

Optical rotation. This was measured using a PerkinElmer Automatic Polarimeter 241 (PerkinElmer Austria GesmbH, Vienna, Austria). Data were recorded at the sodium D line using a 100 mm path length cell. Results are reported as $[\alpha]_D^{T \text{ } ^\circ\text{C}}$, concentration (g/100 mL, solvent).

Preparation of the MTPA ester and ¹H NMR thereof. Both *R*- α -methoxy- α -(trifluoromethyl)-phenylacetyl ester and *S*- α -methoxy- α -(trifluoromethyl)-phenylacetyl ester were prepared using the respective MTPA chlorides (0.02 mmol, 5.5 mg), Et₃N (0.02 mmol, 2.0 mg), 4-*N,N*-dimethylaminopyridine (DMAP, 0.001 mmol, 0.12 mg), which have been added to solutions of 1-(*o*-chlorophenyl)-ethanol (0.0175 mmol, 2.73 mg) in CH₂Cl₂. The two solutions were stirred at room temperature for 12 h, then washed with 5 % HCl and saturated aqueous NaHCO₃. CH₂Cl₂ was evaporated under reduced pressure and the remaining product was purified by flash chromatography on silica gel (CH₂Cl₂) (Dale and Mosher, 1973). ¹H NMR spectra were recorded on a DRX-400 Avance spectrometer (Bruker, Rheinstetten, Germany), equipped with an x-gradient inverse probe. ¹H irradiation and measurement frequency was 400.13 MHz, and the sample temperature was 300.2 K. All spectra were processed with the Topspin 1.3 software. Spectra were recorded with an acquisition of 32,768 data points, a relaxation delay of 1.0 s, and 64 scans. After zero filling to 65,536 data points the free induction decays were directly Fourier

transformed to spectra with 8000 Hz (^1H). All spectra were recorded in CDCl_3 and referenced on internal CHCl_3 (δ ^1H : 7.24 ppm).

Results and Discussion

CtXR: an unexpected, yet useful *o*-chloroacetophenone reductase

A screening in which a variety of ketones were assessed with respect to NADH-dependent reduction by CtXR revealed *o*-chloroacetophenone as candidate substrate of the enzyme. Using a ketone concentration of 10 mM, which corresponds roughly to the solubility limit of *o*-chloroacetophenone in phosphate buffer at 30 °C, purified CtXR showed a specific activity of 4.5 U/mg. This value can be compared with a specific activity of 12 U/mg for reduction of xylose. Steady-state kinetic analysis revealed that the rate of ketone reduction displayed a weakly hyperbolic dependence on the concentration of *o*-chloroacetophenone in the range 0.4 – 10 mM. From a nonlinear fit of the data with the Michaelis-Menten equation we obtained a K_m of 6.2 (\pm 1.5) mM and a k_{cat} of 3.6 (\pm 2.1) s^{-1} . Note: the molar concentration of CtXR was determined from the protein concentration, using a molecular mass of 36.02 kDa for the enzyme subunit. The k_{cat}/K_m for reduction of *o*-chloroacetophenone ($580 \text{ M}^{-1}\text{s}^{-1}$) was \sim 4.3 times that for conversion of xylose. It can be compared to catalytic efficiencies for enzymatic reaction with aromatic α -keto ester substrates that are best preferred by CtXR (Scheme 1B): ethyl 2-chlorobenzoylformate ($576 \text{ M}^{-1}\text{s}^{-1}$), ethyl 4-cyanobenzoylformate ($2211 \text{ M}^{-1}\text{s}^{-1}$) (Kratzer and Nidetzky, 2007). Interestingly, therefore, two muteins of CtXR that had shown up to 8-fold increased efficiency towards the above α -keto ester substrates as compared to the corresponding k_{cat}/K_m values of the wild-type enzyme (Kratzer and Nidetzky, 2007) did not display enhanced performance in reduction of *o*-chloroacetophenone

(Trp²³→Phe: 405 M⁻¹s⁻¹; Trp²³→Tyr: 235 M⁻¹s⁻¹). This result is a useful piece of structure-function information on CtXR because it indicates that accommodation of the relatively bulky ethoxycarbonyl side chain of ethyl 2-chlorobenzoylformate benefits more from site-directed substitution of Trp²³ than does accommodation of the methyl side chain of *o*-chloroacetophenone.

By comparison to the parent ketone acetophenone, which according to $k_{\text{cat}}/K_{\text{m}}$ ($= 0.5 \text{ M}^{-1}\text{s}^{-1}$) is a very poor substrate of CtXR, *o*-chloroacetophenone was converted with remarkable specificity. We were therefore interested to place *o*-chloroacetophenone into a broader structure-activity relationship for ketone substrates of CtXR. A correlation of logarithmic catalytic efficiency with the net electron-withdrawing ability of the ketone side chains is shown in Figure 1 for NADH-dependent reduction of a series of carbonyl substrates of CtXR. A reasonably linear relationship ($r^2 = 0.86$; slope = 1.62; Kratzer et al., 2006a) was obtained over the series of ketones tested whereby $\log(k_{\text{cat}}/K_{\text{m}})$ increased strongly in response to a increase in substituent electron-withdrawing character. Being about two orders of magnitude higher than expected from the structure-activity relationship analysis, the observed reactivity of *o*-chloroacetophenone presents a clear (positive) outlier from the linear correlation. Interestingly, acetophenone and derivatives thereof harbouring the chloro substituent in *para* and *meta* position on the aromatic ring showed poor $k_{\text{cat}}/K_{\text{m}}$ values of 6.6 and 0.8 M⁻¹s⁻¹, respectively, thereby fitting the linear trend in Figure 1 ($r^2 = 0.79$; slope = 1.64). The unusually high $k_{\text{cat}}/K_{\text{m}}$ of CtXR for *o*-chloroacetophenone reduction is therefore ascribed to an effect of the *ortho*-chloro substituent in a type of substrate-assisted catalysis (Zhu et al., 2005). The underlying molecular mechanism is left for consideration in future work.

CtXR displays splendid stereoselectivity for reduction of *o*-chloroacetophenone. Supplementary Figure 1 shows a representative absorbance

trace for elution in reversed phase chiral HPLC of a sample containing about 10 mM of 1-(*o*-chlorophenyl)-ethanol, obtained by exhaustive enzymatic conversion of the same concentration of ketone. The sample gave only a single alcohol peak that co-eluted with one of the peaks associated with a racemic 1-(*o*-chlorophenyl)-ethanol standard. It will be shown later that *S*-alcohol was synthesized. The ee-value of the product was > 99.9 %. The result is in excellent agreement with the proposed catalytic mechanism of ketone reduction by CtXR (Kratzer and Nidetzky, 2007) in which the NADH hydride is transferred to the *re* side of the reactive carbonyl group of the substrate (Scheme 1C).

Whole-cell catalysts for *o*-chloroacetophenone reduction

Table 1 summarizes *o*-chloroacetophenone reductase activities, measured in cell extract and normalized on g_{CDW} , for *E. coli* XR_FDHD and *S. cerevisiae* XR2 μ . Enzyme activities promoting regeneration of NADH in these strains are also shown. *E. coli*_FDHD and *S. cerevisiae* wild-type (CEN.PK 113-7D) were examined as the respective reference. Neither strain contained *o*-chloroacetophenone reductase activity.

The activity of XR in *E. coli*_XR_FDHD was 730 U/ g_{CDW} and 9-fold the activity of FDHD. Therefore, the FDHD activity in *E. coli*_XR_FDHD was just one-fifth that of the reference strain, *E. coli* FDHD. It was previously shown by us (Kratzer et al. 2008b) and others (Weckbecker and Hummel, 2004) that functional expression of the CbFDHD gene in *E. coli* is markedly attenuated by co-expression of another (reductase) gene. XR activity in *S. cerevisiae* XR2 μ was 91 U/ g_{CDW} and half of the appendant ADH activity. The levels of reductase and dehydrogenase activities were better balanced than they were in *E. coli* XR_FDHD. One generally prefers to have the enzyme responsible for regeneration of NADH in excess because this is expected to

provide “kinetic push” to the synthetic reaction of the reductase. However, as will be shown later, NADH recycling is not a kinetic bottleneck for the conversion of *o*-chloroacetophenone by *E. coli* XR_FD_H.

Table 2 shows *o*-chloroacetophenone reduction rates (r_s) for whole cells of *E. coli* XR_FD_H and *S. cerevisiae* XR2 μ recorded under different reaction conditions. r_s values were obtained from measurements of product formation after 30 min. As expected from the absence of the requisite reductase activity in crude cell extracts, whole cells of *E. coli*_FD_H and *S. cerevisiae* wild-type were unable to synthesize appreciable amounts of 1-(*o*-chlorophenyl)-ethanol ($r_s < 0.4$ U/g_{CDW}). Using the same concentration of *o*-chloroacetophenone that was employed for activity measurement in crude cell extracts (Figure 2), we obtained r_s values of 5 – 6 U/g_{CDW} for both *E. coli* XR_FD_H and *S. cerevisiae* XR2 μ . The limiting value of r_s expected from the corresponding enzyme activities (CbFDH in *E. coli* XR_FD_H; CtXR in *S. cerevisiae* XR2 μ) is ~90 U/g_{CDW}. The apparent, ≥ 15 -fold loss of activity for whole cells as compared to free enzymes could be complex manifestation of various limitations, kinetic and otherwise, present in the whole-cell system (Walton and Stewart, 2004). Interestingly, therefore, r_s of *E. coli* XR_FD_H increased about 4.5-fold in response to an increase in substrate concentration from 10 to 100 mM. Considering the solubility limit of *o*-chloroacetophenone in buffer (~10 mM), this change of r_s is not immediately explained by enhancement of substrate availability in solution (~10 mM, see later). In *S. cerevisiae* XR2 μ , the same increase in substrate concentration was without significant effect on r_s (data not shown). According to Kotyk and Alonso (1985) who reported a high diffusivity of ethanol in biological membranes, the supply of ethanol as co-substrate for regeneration of NADH by ADH should hardly be limiting for r_s . Using a biphasic system containing 100 mM substrate, r_s of *E. coli* XR_FD_H was further increased about twofold to a value of 50 U/g_{CDW} when the cell concentration

was raised from 5 to 40 g_{CDW}/L. A similar role of the cell concentration on enhancing r_s was not seen with *S. cerevisiae* XR2 μ (Table 2).

Time course analysis for whole cell-catalyzed reduction of *o*-chloroacetophenone: the regime of enzyme inactivation

Figure 2 shows time courses of formation of 1-(*o*-chlorophenyl)-ethanol catalyzed by *E. coli* XR_FD H under conditions in which the *o*-chloroacetophenone concentration and the cell loading was varied. All time courses were characterized by a strong decrease in r_s that took place after a reaction time of ~5 h and limited the level of substrate conversion attainable in the respective experiment. Experiments performed with *S. cerevisiae* XR2 μ under otherwise identical conditions gave similar results, except that the amount of alcohol product formed from 100 mM *o*-chloroacetophenone by the yeast was substantially (~6-fold) lower than the corresponding *E. coli* reference value (data not shown). Because the onset of the drop in r_s for either cell type appeared to be completely unrelated to the extent of substrate depletion at this point, we examined loss of whole-cell catalytic activity in the course of the reaction.

Figure 3 summarizes results of measurement of the relevant enzyme activities in crude cell extracts prepared after incubation of *E. coli* XR_FD H or *S. cerevisiae* XR2 μ in the presence of 100 mM *o*-chloroacetophenone for the times given. The substrate was unusually denaturing (“toxic”) to CtXR in both whole-cell systems, and it likewise caused very rapid inactivation of CbFDH in *E. coli* XR_FD H and ADH in *S. cerevisiae* XR2 μ . The decrease in r_s for *E. coli* XR_FD H (Figure 2) appears to occur in parallel with activity loss in CtXR, CbFDH or both (Figure 3). Data suggest that denaturation of CtXR and CbFDH comes to a stop at ~20 % of the original activity. Notwithstanding, whatever level of activity remains for each of the two enzymes in *E.*

E. coli XR_FDHD, it was clearly too low to promote conversion of *o*-chloroacetophenone after ~5 h of incubation time (see Figure 3). Activity of CtXR in *S. cerevisiae* XR2 μ was slightly more stable than it was in *E. coli* XR_FDHD. In yeast cells, therefore, the activity of the relatively less stable ADH may become limiting for *o*-chloroacetophenone conversion (Figure 3). Table 3 lists enzyme half-life times for each whole-cell system and compares the data to relevant half-life times of isolated CtXR. Although entrapment of CtXR in the cellular environment of *E. coli* XR_FDHD and *S. cerevisiae* XR2 μ provided substantial stabilization to the *o*-chloroacetophenone reductase activity as compared to the free enzyme, it is also clear from the data in Figure 3 and Table 2 that batch wise whole cell-catalyzed conversion of ketone substrate (Figure 3) takes place completely under the regime of enzyme inactivation. Enhancement of r_s was considered as a strategy to shift the kinetic regime from inactivation to reaction.

Optimization of r_s to overcome limitation by enzyme stability

Effect of high cell concentration. Figure 3 shows that the product yield obtained from conversion of 100 mM *o*-chloroacetophenone by *E. coli* XR_FDHD was strongly enhanced, from 5 to 60 %, by increasing the cell concentration from 5 to 40 g_{CDW}/L. The effect on yield in Figure 2 is reasonably explained by the ~12-fold increase in overall ketone reduction rate at high cell concentration which results not only because of the increased loading (per volume) of whole-cell catalyst but also because the specific rate (r_s) was enhanced ~2-fold under these conditions (Table 2). Note: About 15 % of total reaction volume is taken by the cells at 40 g_{CDW}/L. Further increase in cell concentration was therefore not considered in order to avoid problems during work-up of the product (see later).

Because loss of activity in the presence of *o*-chloroacetophenone is so fast, the value of r_s is probably affected by whole-cell catalyst stability. It is known from previous studies (Sikkema et al., 1994) that hydrophobic substrates dissolve in cellular membranes, causing breakdown of cells when the membrane concentration exceeds ~300 mM. A high biomass concentration may therefore be stabilizing by simply increasing the available membrane phase, thereby reducing the substrate concentration in it. Furthermore, the toxicity of undissolved hydrophobic compounds increases with droplet size (Uribe and Peña, 1990). Aono and Kobayashi (1997) demonstrated that *n*-octane droplets recombine in buffer, but are kept small in the presence of *E. coli*. Decreased-size droplet formation at high cell concentration might contribute to reducing the toxicity of *o*-chloroacetophenone and therefore contribute to enhancement of r_s .

S. cerevisiae XR2 μ (40 g_{CDW}/L) performed much less efficiently in *o*-chloroacetophenone conversion than *E. coli* XR_FD_H. The maximum product yield obtained from 100 mM ketone substrate was just 10 %. Co-solvent addition strategies described below for *E. coli* XR_FD_H were unsuccessful in enhancing the yield to a value greater than ~20 % (data not shown). Yeast bioreduction of *o*-chloroacetophenone was therefore not further pursued. Note, however, that like in the experiments described above for *E. coli* XR_FD_H (Figure 2), only a single enantiomeric product was formed during *o*-chloroacetophenone reduction by *S. cerevisiae* XR2 μ .

Co-solvent addition. To decrease the effective concentration of *o*-chloroacetophenone and its corresponding alcohol, a second organic phase was examined as an *in situ* extracting agent (Figure 4; Halling 1987; Stark and von Stockar, 2003). However, hexane and the ionic liquid BMIMPF₆ did not improve alcohol yields as compared to the yield of the reference reaction lacking the organic

phase. Using *n*-butyl acetate, the alcohol yield from 100 mM *o*-chloroacetophenone was only ~7 %. Considering literature where both *n*-butyl acetate and BMIMPF₆ are reported to provide substantial yield enhancement to reduction of α -keto esters by *E. coli* whole-cell catalysts (Kizaki et al., 2001; Bräutigam et al., 2007), we would like to make a note of caution concerning the generalization of the effect of organic co-solvents in these bioconversions.

Permeabilization and supplementation of external NAD⁺. It was previously shown by us (Kratzer et al., 2008b) and others (Zhang et al., 2006) that supply of NAD⁺ to suitably permeabilized *E. coli* cells is a potentially useful approach with which to increase r_s . Figure 4 shows that 100 mM *o*-chloroacetophenone was converted in near complete yield (~98 %) under conditions in which NAD⁺ (0.5 mM) and permeabilizing agent (Polymyxin B sulphate; 0.14 mM) were added to the reaction system. The presence of organic substrate and/or co-solvent is expected to also bring about some permeabilization of *E. coli* cells. Interestingly, therefore, NAD⁺ supply did enhance product yield under all reaction conditions used except for the system containing BMIMPF₆ (Figure 4). The effect of NAD⁺ in the reaction containing *n*-butyl acetate was remarkable, leading to a sevenfold improved yield. However, complete conversion was accomplished only when using the treatment with Polymyxin B sulphate.

Enhancing the activity of CbFDH. Results in Table 1 suggest that the level of CbFDH activity could be a limiting factor for the overall conversion efficiency of *E. coli* XR_FDH. Using conditions in which NAD⁺ was supplied to cells permeabilized with Polymyxin B sulphate, we examined the effect of complementation of *E. coli* XR_FDH with *E. coli* FDH. The addition of *E. coli* FDH was used to enhance the activity of FDH in the reaction system while at a constant concentration of *E. coli* XR_FDH (5 g_{CDW}/L), the volumetric activity of XR remained invariant (3 U/mL).

However, change of the activity ratio FDH:XR between values of 1, 3, and 9 did not affect the maximum product amount (11 mM) obtained from 100 mM *o*-chloroacetophenone as compared to the reference reaction in which just *E. coli* XR_FDHDH was used, the corresponding FDH:XR ratio being 0.11. These findings together with the evidence from Figure 4 suggest that availability of coenzyme, however, not the level of FDH activity is a limiting factor for *o*-chloroacetophenone reduction by *E. coli* XR_FDHDH.

Synthesis of S-1-(*o*-chlorophenyl)-ethanol

A preparative synthesis was performed in which 0.4 g_{CDW} of permeabilized *E. coli* XR_FDHDH were incubated with 1 mmol *o*-chloroacetophenone in a total volume of 10 mL. A 100 mM potassium phosphate buffer, pH 7.5, containing 150 mM sodium formate was used. Ketone conversion was complete ($\geq 97\%$; N = 2) within 5 h. The product solution contained a single enantiomer of 1-(*o*-chlorophenyl)-ethanol, concentrated above its solubility limit of ~ 80 mM. The emulsion was dissolved by addition of the solvent mediator ethanol (10 mL), cell debris was centrifuged (18000 g, 10 min) from the homogenous solution and the remaining ethanol was evaporated at reduced pressure. Product isolation was done by two steps of extraction, using each time 10 mL of CH₂Cl₂. Organic-aqueous phase separation was strongly impeded by cellular residues, such as coagulated proteins, unless a g-force of 18000 g (10 min) was applied. However, cell sludge accumulated at the liquid-liquid interface, capturing around 20% of the total volume of the organic phase and therefore causing substantial loss of product. The potential benefit resulting from enhancement of r_s when working at cell concentrations greater than 40 g_{CDW}/L might be completely offset by the concomitant decrease in yield for the downstream processing. The withdrawn organic phases were united, dried with brine, and CH₂Cl₂

was evaporated under reduced pressure. The 1-(*o*-chlorophenyl)-ethanol product was obtained as a colorless liquid in an isolated yield of 66 – 68%. Strategies to enhance the isolated yield for alcohol product could involve extra filtration steps to remove biomass prior to extraction (Gröger et al., 2006) or the use of a larger organic to aqueous volume ratio (Ema et al., 2007).

Absolute configuration of isolated 1-(*o*-chlorophenyl)-ethanol was determined by comparing product chiroptical data with literature and by ¹H NMR of the corresponding *R*- and *S*-MTPA esters. The optical rotation ($[\alpha]_D^{20}$ (c 1.12, CHCl₃) = \sim 58°) assigns the alcohol to *S*-1-(*o*-chlorophenyl)-ethanol (Salvi and Chattopadhyay, 2008, $[\alpha]_D^{27}$ (c 1.46, CHCl₃) = \sim 57.75°). ¹H NMR shift of the CH₃-group in the *R*-MTPA ester [δ 1.59 (d, *J* = 6.6 Hz, 3H)] was shifted downfield as compared to the corresponding *S*-MTPA ester [δ 1.54 (d, *J* = 6.6 Hz, 3H)]. Concomitantly, the chemical shift of the remaining *ortho*-proton in the *o*-chlorophenyl-group was shifted upfield in the *R*-MTPA ester [δ 7.14 (m, 1H)] compared to the *S*-MTPA ester [δ 7.39 (m, 1H)]. This orientation of contrary up- and downfield shifts is excellent agreement with *R,S*- and *S,S*-diastereomeric configurations of the esters, which clearly confirm the alcohol to be *S*-1-(*o*-chlorophenyl)-ethanol. The relative proximity of the phenyl group in the *R*- and *S*-MTPA esters to the methyl-group and to the *o*-chlorophenyl group, respectively, explain the contrary up- and downfield shifts and are shown in Figure 2 of Supplementary Information (Dale and Mosher, 1973). These findings support the stereochemical course of *o*-chloroacetophenone reduction by CtXR shown in Scheme 1C.

CONCLUSIONS

Whole-cell bioreductions in general and those catalyzed by *S. cerevisiae* in particular are often confronted with the problem of “background activity” due to host-inherent

reductases. The complete absence of *o*-chloroacetophenone reductase activity in *E. coli* as well as the very low acceptance by *S. cerevisiae* confirms literature in indicating a generally low abundance of *o*-chloroacetophenone reductases. Xylose reductase from *Candida tenuis* is therefore a rare and unexpectedly powerful catalyst for the reduction of *o*-chloroacetophenone, and it does so with absolute *S*-stereochemical selectivity. Complete conversion of 100 mM *o*-chloroacetophenone through optimized *E. coli* XR_FDHD-catalyzed transformation facilitated work-up and provided *S*-1-(*o*-chlorophenyl)-ethanol in useful yield and excellent purity. The combination of full conversion and absolute enantioselectivity (> 99 %) is hardly found in chemical catalysis (Zeror et al., 2008). Moreover, there is very limited availability of alternative bioreduction systems that could be applied for production of optically pure *S*-1-(*o*-chlorophenyl)-ethanol on preparative scale (Gröger et al., 2006). The high toxicity of *o*-chloroacetophenone/1-(*o*-chlorophenyl)-ethanol constituted the main obstacle for efficient ketone conversion by *E. coli* XR_FDHD and the applied strategies considered for optimization of r_s in order to eliminate the regime of enzyme inactivation should be generally useful. *E. coli* XR_FDHD could be of interest in production of chiral phenylethanols as compounds of pPLK1 inhibitor libraries.

Acknowledgements

Financial support from the Austrian Science Fund (Hertha-Firnberg grant T350-B09 and project DK Molecular Enzymology W901-B05) is gratefully acknowledged.

References

- Abokitse K, Hummel W. 2003. Cloning, sequence analysis, and heterologous expression of the gene encoding a (S)-specific alcohol dehydrogenase from *Rhodococcus erythropolis* DSM 43297. *Appl Microbiol Biotechnol* 62:380-386.
- Andrade LH, Comasseto JV, Rodrigues DF, Pellizari VH, Porto ALM. 2005. Enantioselective reduction of *ortho*-substituted acetophenones by bacterial strains isolated from medium enriched with biphenyl or diesel fuel. *J Mol Catal B: Enzym* 33:73-79.
- Andrade LH, Piovan L, Pasquini MD. 2009. Improving the enantioselective bioreduction of aromatic ketones mediated by *Aspergillus terreus* and *Rhizopus oryzae*: The role of glycerol as a co-solvent. *Tetrahedron: Asymmetry* 20:1521-1525.
- Aono R, Kobayashi H. 1997. Cell surface properties of organic solvent-tolerant mutants of *Escherichia coli* K-12. *Appl Environ Microbiol* 63: 3637-3742.
- Baratta W, Ballico M, Baldino S, Chelucci G, Herdtweck E, Siega K, Magnolia S, Rigo P. 2008. New benzo[*h*]quinoline-based ligands and their pincer Ru and Os complexes for efficient catalytic transfer hydrogenation of carbonyl compounds. *Chem-A Eur J* 14:9148-9160.
- Bräutigam S, Bringer-Meyer S, Weuster-Botz D. 2007. Asymmetric whole cell biotransformations in biphasic ionic liquid/water-systems by use of recombinant *Escherichia coli* with intracellular cofactor regeneration. *Tetrahedron: Asymmetry* 18: 1883-1887.
- Burton SG, Cowan DA, Woodley JM. 2002. The search for the ideal biocatalyst. *Nat Biotechnol* 20:37-45.
- Dale JA, Mosher HS. 1973. Nuclear magnetic resonance enantiomer reagents. Configurational correlations via nuclear magnetic resonance chemical shifts of

diastereomeric mandelate, O-methylmandelate, and α -methoxy- α -trifluoromethylphenylacetate (MTPA) esters. *J Am Chem Soc* 95:512-519.

Ema T, Okita N, Ide S, Sakai T. 2007. Highly enantioselective and efficient synthesis of methyl (*R*)-*o*-chloromandelate with recombinant *E. coli*: Toward practical and green access to clopidogrel. *Org Biomol Chem* 5:1175-1176.

Evans DA, Michael FE, Tedrow JS, Campos KR. 2003. Application of chiral mixed phosphorus/sulfur ligands to enantioselective rhodium-catalyzed dehydroamino acid hydrogenation and ketone hydrosilylation processes. *J Am Chem Soc* 125:3534-3543.

Gröger H, Chamouleau F, Orogas N, Rollmann C, Drauz K, Hummel W, Weckbecker A, May O. 2006. Enantioselective reduction of ketons with 'designer cells' at high substrate concentrations: Highly efficient access to functionalized optically active alcohols. *Angew Chem Int Ed* 2006, 45:5677-5681.

Häcker B, Habenicht A, Kiess M, Mattes R. 1999. Xylose utilisation and characterisation of the xylose reductase from *Candida tenuis*. *Biol Chem*, 380:1395-1403.

Halling PJ. 1987. Biocatalysis in multi-phase reaction mixtures containing organic liquids. *Biotechnol Adv* 5:47-84.

Itoh N, Mizuguchi N, Mabuchi M. 1999. Production of chiral alcohols by enantioselective reduction with NADH-dependent phenylacetaldehyde reductase from *Corynebacterium strain*, ST-10. *J Mol Catal B* 6:41-50.

Kagohara E, Pellizari VH, Comasseto JV, Andrade LH, Porto ALM. 2008. Biotransformations of substituted phenylethanols and acetophenones by environmental bacteria. *Food Technol Biotech* 46:381-387.

Kizaki N, Yasohara Y, Hasegawa J, Wada M, Kataoka M, Shimizu S. 2001. Synthesis of optically pure ethyl (*S*)-4-chloro-3-hydroxybutanoate by *Escherichia coli*

transformant cells coexpressing the carbonyl reductase and glucose dehydrogenase genes. *Appl Microbiol Biotechnol* 55:590-595.

Kotyk A, Alonso A. 1985. Transport of ethanol in baker's yeast. *Folia Microbiol* 30:90-91.

Krahulec S, Armao GC, Weber H, Klimacek M, Nidetzky B. 2008. Characterization of recombinant *Aspergillus fumigatus* mannitol-1-phosphate 5-dehydrogenase and its application for the stereoselective synthesis of *protio* and *deuterio* forms of D-mannitol 1-phosphate. *Carbohydr Res*, 343:1414-1423.

Kratzer R, Leitgeb S, Wilson DK, Nidetzky B. 2006a. Probing the substrate binding site of *Candida tenuis* xylose reductase (AKR2B5) with site-directed mutagenesis. *Biochem J* 393: 51-58.

Kratzer R, Wilson DK, Nidetzky B. 2006b. Catalytic mechanism and substrate selectivity of aldo-keto reductases: Insights from structure-function studies of *Candida tenuis* xylose reductase. *IUBMB Life* 58:499-507.

Kratzer R, Nidetzky B. 2007. Identification of *Candida tenuis* xylose reductase as highly selective biocatalyst for the synthesis of chiral α -hydroxy esters and improvement for its efficiency by protein engineering. *Chem Commun* 10:1047-1049.

Kratzer R, Egger S, Nidetzky B. 2008a. Integration of enzyme, strain and reaction engineering to overcome limitations of baker's yeast in the asymmetric reduction of α -keto esters. *Biotechnol Bioeng* 101:1094-1101.

Kratzer R, Pukl M, Egger S, Nidetzky B. 2008b. Whole-cell bioreduction of aromatic α -keto esters using *Candida tenuis* xylose reductase and *Candida boidinii* formate dehydrogenase co-expressed in *Escherichia coli*. *Microb Cell Fact* 7:37-48.

Kurbanoglu EB, Zilbeyaz K, Kurbanoglu NI, Kilic H. 2007a. Enantioselective reduction of substituted acetophenones by *Aspergillus niger*. *Tetrahedron: Asymmetry* 18:1159-1162.

Kurbanoglu EB, Zilbeyaz K, Kurbanoglu NI, Kilic H. 2007b. Asymmetric reduction of acetophenone analogues by *Alternaria alternata* using ram horn peptone. *Tetrahedron: Asymmetry* 18:2332-2335.

Kurbanoglu EB, Zilbeyaz K, Ozdal M, Taskin M, Kurbanoglu NI. 2010. Asymmetric reduction of substituted acetophenones using once immobilized *Rhodotorula glutinis* cells. *Bioresource Technol* 101:3825-3829.

Nakamura K, Matsuda T. 1998. Asymmetric reduction of ketones by the acetone powder of *Geotrichum candidum*. *J Org Chem* 63:8957-8964.

Mayr P, Brüggler K, Kulbe KD, Nidetzky B. 2000. D-Xylose metabolism by *Candida intermedia*: Isolation and characterisation of two forms of aldose reductase with different coenzyme specificities. *J Chromatogr B* 737:195-202.

Ou Z, Wu J, Yang L, Cen P. 2008. Asymmetric reduction of chloroacetophenone to produce chiral alcohols with microorganisms. *Korean J Chem Eng* 25:124-128.

Parachin NS, Carlquist M, Gorwa-Grauslund MF. 2009. Comparison of engineered *Saccharomyces cerevisiae* and engineered *Escherichia coli* for the production of an optically pure keto alcohol. *Appl Microbiol Biotechnol* 84:487-497.

Rheault TR, Cheung M, Alberti JGB, Donaldson KH. PCT Int. Appl. WO 2008070354 A2 20080612, 2008.

Salvi NA, Chattopadhyay S. 2008. Asymmetric reduction of halo-substituted arylalkanones with *Rhizopus arrhizus*. *Tetrahedron: Asymmetry* 19:1992-1997.

Santamaria A, Neef R, Eberspächer U, Eis K, Husemann M, Mumberg D, Prechtel S, Schulze V, Siemeister G, Wortmann L, Barr FA, Nigg EA. 2007. Use of the novel Plk1 inhibitor ZK-Thiazolidinone to elucidate functions of Plk1 in early and late stages of mitosis. *Mol Biol Cell* 18:4024-4036.

Sato Y, Onozaki Y, Sugimoto T, Kurihara H, Kamijo K, Kadowaki C, Tsujino T, Watanabe A, Otsuki S, Mitsuya M, Iida M, Haze K, Machida T, Nakatsuru Y,

Komatani H, Kotani H, Iwasawa Y. 2009. Imidazopyridine derivatives as potent and selective Polo-like kinase (PLK) inhibitors. *Bioorg Med Chem Lett* 19: 4673-4678.

Sikkema J, de Bont JA, Poolman B. 1994. Interactions of cyclic hydrocarbons with biological membranes. *J Biol Chem* 269:8022-8028.

Stark D, von Stockar U. 2003. *Process integration in biochemical engineering*. Berlin/Heidelberg:Springer. 150 p.

Stengel T, Schmidt M, Weinbrenner S, Weber A, Gimmnich P, Gekeler V, Beckers T, Zimmermann A, Maier T, Schmidt B, Dehmel F. PCT Int. Appl. WO 2009003911 A1 20090108, 2009.

Uribe S, Pena A. 1990. Toxicity of allelopathic monoterpene suspensions on yeast dependence on droplet size. *J Chem Ecol.* 16:1399-1408.

Walton AZ, Stewart JD. 2004. Understanding and improving NADPH-dependent reactions by non-growing *Escherichia coli* cells. *Biotechnol Progr* 20:403-411.

Weckbecker A, Hummel W. 2004. Improved synthesis of chiral alcohols with *Escherichia coli* cells co-expressing pyridine nucleotide transhydrogenase, NADP⁺-dependent alcohol dehydrogenase and NAD⁺-dependent formate dehydrogenase. *Biotechnol Bioeng*, 26:1739-1744.

Xie Q, Wu J, Xu G, Yang L. 2006. Asymmetric reduction of *o*-chloroacetophenone with *Candida pseudotropicalis* 104. *Biotechnol Prog* 5:1301-1304.

Yang Y, Zhu D, Piegata TJ, Hua L. 2007. Enzymatic ketone reduction: Mapping the substrate profile of a short-chain alcohol dehydrogenase (YMR226c) from *Saccharomyces cerevisiae*. *Tetrahedron: Asymmetry* 18:1799-1803.

Zeror S, Collin J, Fiaud, J-C, Zouioueche LA. 2008. Evaluation of ligands for ketone reduction by asymmetric hydride transfer in water by multi-substrate screening. *Adv Synth Catal* 350:197-204.

Zhang J, Witholt B, Li Z. 2006. Coupling of permeabilized microorganisms for efficient enantioselective reduction of ketone with co-factor recycling. *Chem Commun* 4:398-400.

Zhu D, Rios BE, Rozzell JD, Hua L. 2005. Evaluation of substituent effects on activity and enantioselectivity in the enzymatic reduction of aryl ketones. *Tetrahedron: Asymmetry* 16: 1541-1546.

Zhu D, Malik HT, Hua L. 2006. Asymmetric ketone reduction by a hyperthermophilic alcohol dehydrogenase. The substrate specificity, enantioselectivity and tolerance of organic solvents. *Tetrahedron: Asymmetry* 17:3010-3014.

Table 1: Biosynthetic and NADH regenerating enzyme activities in different whole cell biocatalysts.

Strain	XR activity ¹ [U/g _{CDW}] NADH	Dehydrogenase activity ² [U/g _{CDW}] NADH
<i>E. coli</i> XR_FDHDH	730	FDH 85
<i>E. coli</i> FDH	0	FDH 408
<i>S. cerevisiae</i> XR2 μ	91	ADH 174
<i>S. cerevisiae</i> wild-type	0	ADH 112

¹Determined with 10 mM *o*-chloroacetophenone and 250 μ M NADH. ²FDH activity determined with 200 mM sodium formate and 2 mM NAD⁺; ADH activity determined with 50 mM ethanol and 1 mM NAD⁺. Standard errors \leq 15 %.

Table 2: Initial rates and ee-values of *o*-chloroacetophenone reduction by different whole-cell biocatalysts.

Strain	Cell dry weight [g/L]	Substrate conc. [mM]	Initial rate [U/g _{CDW}] ¹ / ee [%]
<i>E. coli</i> XR_FDHDH	5	10	6 / > 99.9 S
<i>E. coli</i> XR_FDHDH	5	100	27 / > 99.9 S
<i>E. coli</i> XR_FDHDH	20	100	33 / > 99.9 S
<i>E. coli</i> XR_FDHDH	40	100	50 / > 99.9 S
<i>S. cerevisiae</i> XR2μ ²	5	10	5 / > 99.9 S
<i>S. cerevisiae</i> XR2μ ²	40	100	8 / > 99.9 S

¹Determined from the time course of substrate conversion between 0 and 30 min reaction time; standard errors ≤ 20 %. ²Anaerobic reaction conditions where [O₂] < 15 μM.

Table 3: Half-life times ($T_{1/2}$ ¹) of three different reductase systems based on CtXR under process conditions as compared to buffered, aqueous solutions.

Reductase system	$T_{1/2}$	$T_{1/2}$ process conditions ²
Isolated CtXR (2 μ M) pH 7.0; 25 °C	11 d	< 3 min
<i>E. coli</i> XR_FDHDH (40 g _{CDW} /L) pH 7.5; 30 °C	2.5 d	20 min
<i>S. cerevisiae</i> XR2 μ (40 g _{CDW} /L) pH 6.2, 30 °C	3.5 d	46 min (ADH 31 min)

¹Exponential decay; standard errors \leq 15 %; ²100 mM *o*-chloroacetophenone, 5 % ethanol, co-substrate, 30 °C.

Scheme 1. General scheme of stereoselective ketone reduction by CtXR. Sparsely activated *o*-chloroacetophenone (A), highly activated α -keto esters (B), general, Prelog-type stereoselectivity of CtXR (C) (Kratzer and Nidetzky, 2007).

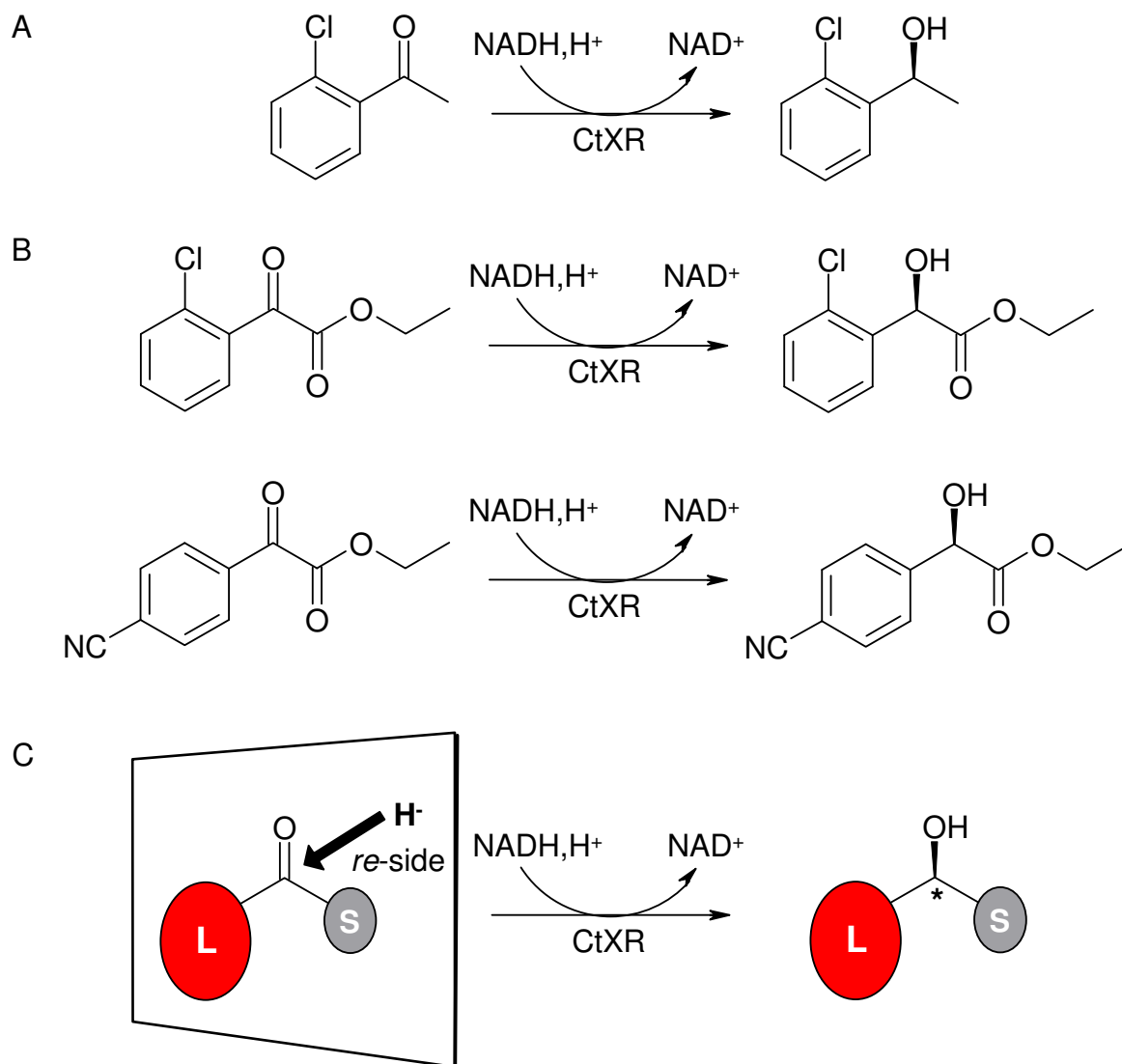
Figure 1. Catalytic efficiencies of NADH-dependent ketone reduction catalysed by CtXR as function of Taft factors (σ^* ; corrected for molecular volumes, logmv). Black circles show data points obtained with 4-hydroxybutan-2-one (σ^* 0.21), acetoin (σ^* 0.46), acetylacetone (σ^* 0.60), acetophenone (σ^* 0.60), ethyl acetoacetate (σ^* 0.82), diacetyl (σ^* 1.65), oxopantoyl-lactone (σ^* 1.81), ethyl 4-chloroacetoacetate (σ^* 1.83), ethyl pyruvate (σ^* 2.26), ethyl benzoylformate (σ^* 2.86) (Kratzer et al., 2006); this work: *p*-chloroacetophenone (σ^* 0.75), *m*-chloroacetophenone (σ^* 0.85). The continuous line shows bivariate regression analysis of black circles.

Figure 2. Whole cell-catalyzed reduction of *o*-chloroacetophenone by *E. coli* XR_FDHD. The analytical yield is given and expressed as concentration of *S*-1-(*o*-chlorophenyl)-ethanol formed from the initial substrate concentration. Conditions are indicated by symbols: ● [substrate] = 100 mM, [cells] = 40 g_{CDW}/L; ○ [substrate] = 100 mM, [cells] = 20 g_{CDW}/L; ▲ [substrate] = 100 mM, [cells] = 5 g_{CDW}/L; Δ [substrate] = 10 mM, [cells] = 5 g_{CDW}/L.

Figure 3. Catalyst inactivations during whole cell-catalyzed reductions of *o*-chloroacetophenone by *E. coli* XR_FDHD and *S. cerevisiae* XR2 μ . Inactivation: Cells (40 g_{CDW}/L) were incubated in the presence of 100 mM *o*-chloroacetophenone and at the indicated times, enzyme activities were measured after cell disruption using B-Per (*E. coli* XR_FDHD: ● XR activity, ○ FDH activity; *S. cerevisiae* XR2 μ : ▲ XR activity, Δ ADH activity).

Figure 4. Effect of organic solvents, cell permeabilisation and externally added NAD⁺ on yields of 100 mM *o*-chloroacetophenone bioreductions catalyzed by *E. coli* XR_FDHD. Black bars: Control (experiment in buffer); PM B (buffer, Polymyxin B

sulfate [0.14 mM]); butyl acetate (1:1 v/v buffer); hexane (1:1 v/v buffer); BMIMPF₆ (1:1 v/v buffer). Grey bars: with additional NAD⁺ [0.5 mM]. Conditions: 40 g_{CDW}/L, 6 h reaction time. Standard errors ≤ 15 %.



Scheme 1.

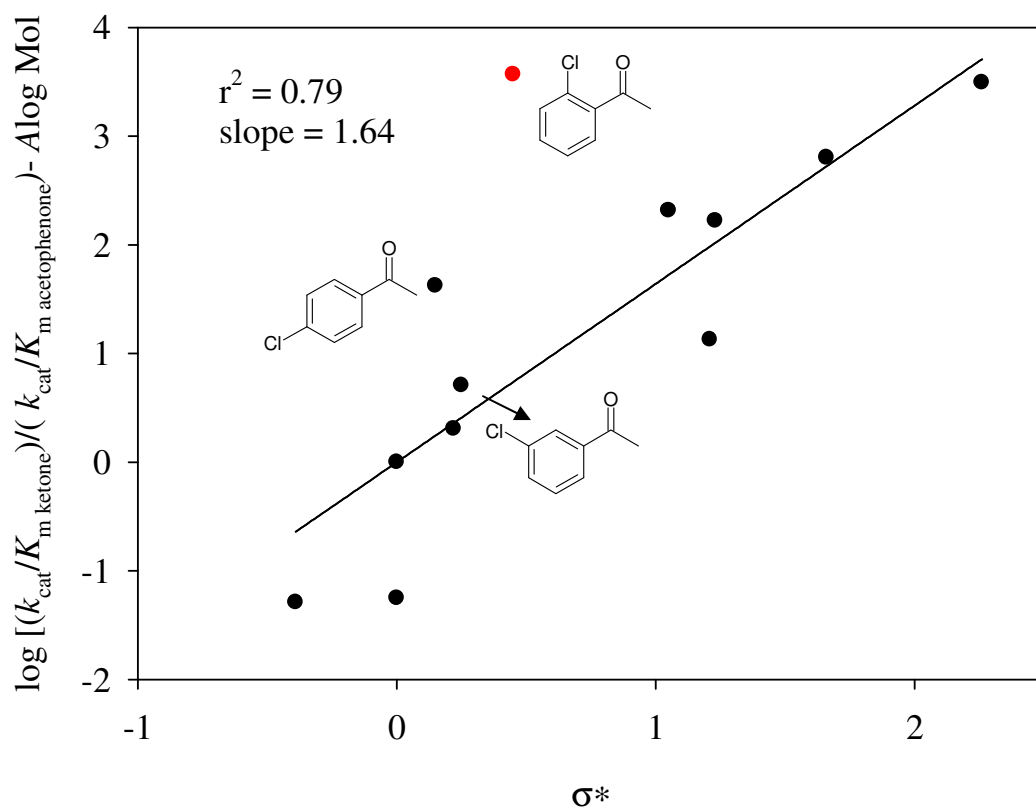


Figure 1.

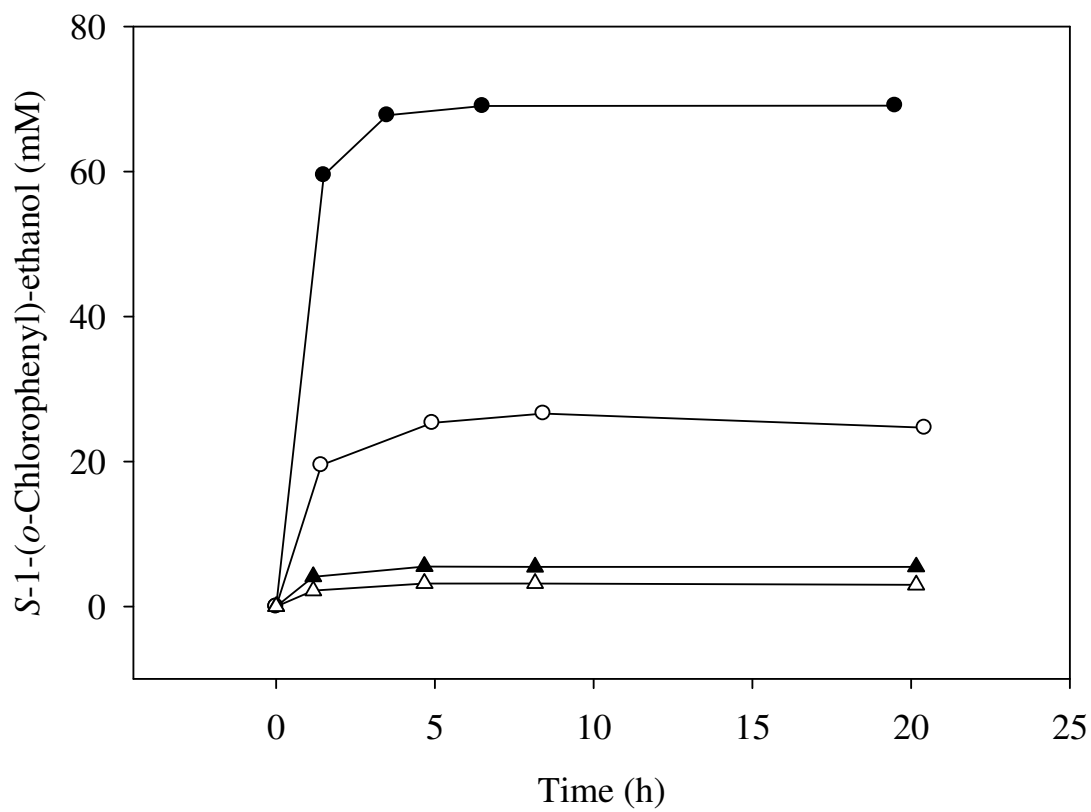


Figure 2.

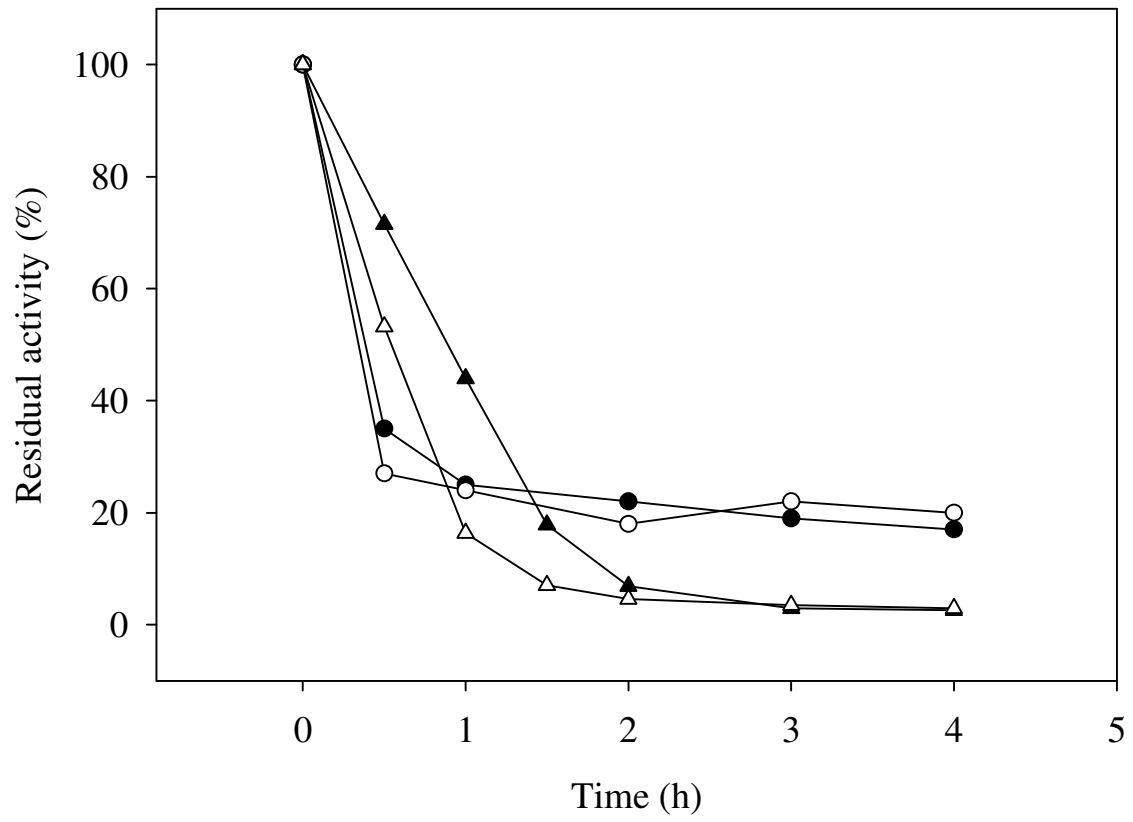


Figure 3.

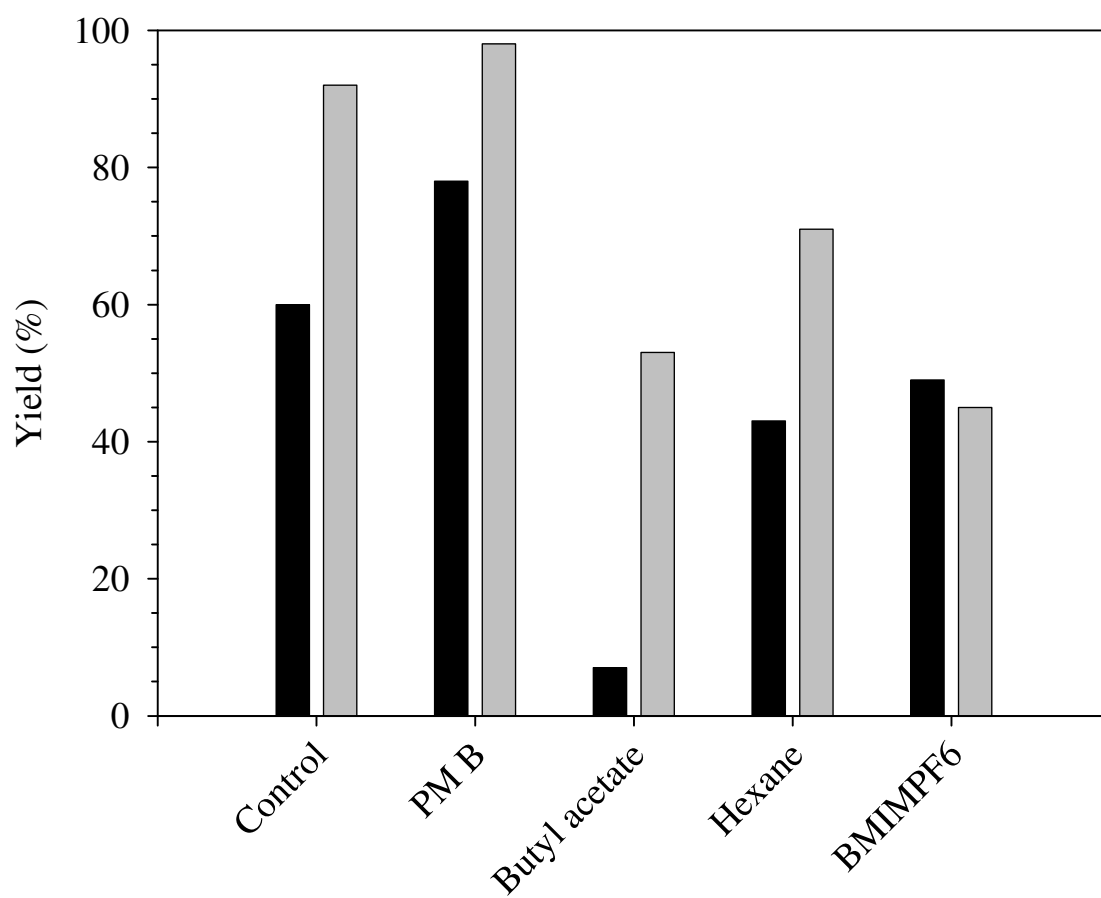


Figure 4.

Enzyme identification and development of a whole-cell biotransformation for asymmetric reduction of *o*-chloroacetophenone

Regina Kratzer*^{1,2}, Matej Pukl¹, Sigrid Egger¹, Michael Vogl³, Lothar Brecker³ and Bernd Nidetzky*^{1,2}

¹Institute of Biotechnology and Biochemical Engineering, Graz University of Technology, Petersgasse 12, A-8010 Graz, Austria.

²Research Centre Applied Biocatalysis, Petersgasse 14, A-8010 Graz, Austria

³Institute of Organic Chemistry, University of Vienna, Währinger Straße 38, A-1090 Wien, Austria

*Corresponding authors

Fax: +43 316 873 8434; Tel: +43 316 873 8408 (R.K.); +43 316 873 8400 (B.N.); E-mail: regina.kratzer@tugraz.at (R.K.), bernd.nidetzky@tugraz.at (B.N.)

Supporting Information

Figure S1

Figure S2

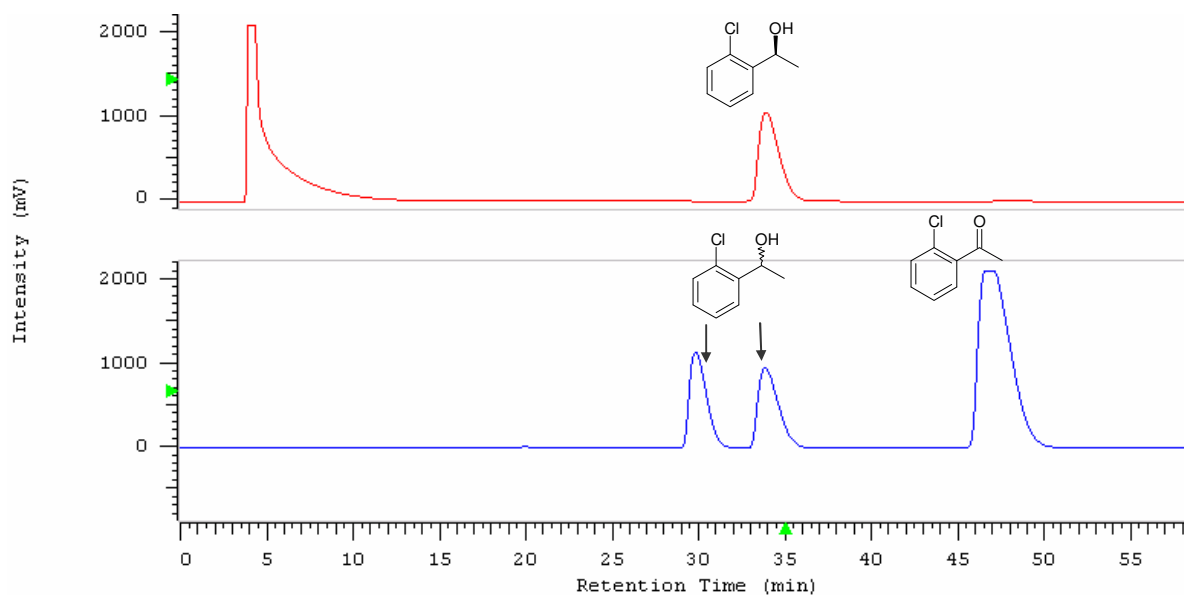


Figure S1. Reversed phase chiral HPLC of a sample containing *S*-1-(*o*-chlorophenyl)-ethanol, obtained by complete conversion of 10 mM ketone by CtXR (red trace). Standard containing 16 mM racemic 1-(*o*-chlorophenyl)-ethanol and 15 mM *o*-chloroacetophenone (blue trace). Traces were detected by UV-absorbance at 210 nm, detection limit was below 5 μ M.

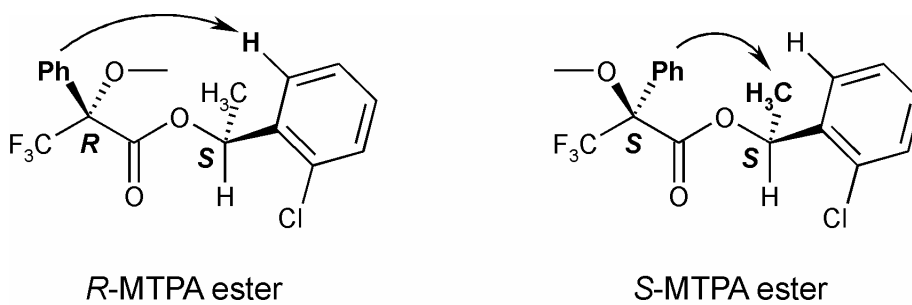


Figure S2. Influence of the phenylring in MTPA onto chemical shifts of methyl group and *o*-chlorophenyl group in the *S*-1-(*o*-chlorophenyl)-ethanol side chains of diastereomeric MTPA esters.

CURRICULUM VITAE

Dipl.Ing. Sigrid Egger

Steyrergasse 61 / 2, 8010 Graz
Phone: +43 650 9251931; email: sigrid.egger@tugraz.at

PERSONAL DATA:

Date of Birth: April 20th, 1979
Place of Birth: Klagenfurt, Austria
Nationality: Austrian



EDUCATION:

01.11.2008 – 15.08.2009 **Research stay at University of Oxford**, Structural genomics consortium (SGC), group of Prof. Udo Oppermann

03. – 13. 09. 2007 Research stay at BOKU Vienna (University of Natural Resources and Applied Life Sciences), Dr. Roland Ludwig

Since June 2006 **PhD student “DK Molecular Enzymology” at the Institute of Biotechnology and Biochemical Engineering, Graz University of Technology:** *“From molecular mechanism to biocatalytic applications of sugar oxidoreductases: Structure and catalytic mechanism of human UDP-glucose dehydrogenase and development of whole-cell catalysts for enantioselective synthesis of chiral alcohols”*

May 2006 Selected in the hearing “DK Molecular Enzymology” as PhD student

February – May 2006 Project collaborator at the Institute of Biotechnology and Biochemical Engineering, Graz University of Technology

November 2005 **Final examination for academic degree (Dipl. Ing.) passed with distinction**

Sept. 2004 – Nov. 2005 Diploma student of Dr. Grit Straganz and Prof. Bernd Nidetzky at the Institute of Biotechnology and Biochemical Engineering, Graz University of Technology in the field of structure-function relationships explored by site-directed mutagenesis and tutor of lab course.

Oct. 1998 – Nov. 2005 Undergraduate education, Graz University of Technology, Technical Chemistry - Biotechnology, Biochemistry and Food Chemistry

Oct. 1997 - June 1998 Undergraduate education, Karl Franzens University, Graz, Biology

June 1997 **University-entrance certificate, passed with distinction**

1990 - 1997 BG/BRG Europagymnasium Klagenfurt, emphasis on foreign languages

CURRICULUM VITAE

Dipl.Ing. Sigrid Egger

*Steyrergasse 61 / 2, 8010 Graz
Phone: +43 650 9251931; email: sigrid.egger@tugraz.at*

FURTHER EDUCATION / COURSES:

2009/2010 TU Graz:	Leading technical teams; Technology transfer; Leading, delegation and motivation; Conflict management
24. - 28.09.2007	DK Molecular Enzymology Summer School for Research and Transferable Skills Training. Graz, Austria.
June 2006	PhD Course Metabolic Engineering and Systems Biology, Lyngby, Denmark, DTU

EXPERTISES AND SKILLS:

- Gene cloning and site-directed mutagenesis (*E. coli* and *S. cerevisiae*)
- Recombinant protein production (*E. coli* and *S. cerevisiae*)
- Protein purification strategies (Affinity chromatography, Size exclusion, Ion exchange....)
- Enzyme kinetic studies (Steady state and transient kinetic analysis)
- Biophysical methods (ITC, DLS, protein crystallization)
- High throughput methods e.g. Differential Scanning Fluorimetry (DSF)
- Analytical chemistry (Methods for GC, HPLC, TLC, MS)
- Process engineering for whole-cell biocatalysis
- Excellent presentation skills
- Excellent verbal and written communication skills in English

SOFT SKILLS:

- Teamwork: fruitful collaboration with colleagues of any educational level
- Lead skills: supervising students
- Taking responsibility and informed decisions for efficient project planning
- Communication and professional presentation of the work
- Motivation and problem solving competence

SCIENTIFIC INTEREST:

- High throughput screening systems in chemical biology
- Evolution and engineering of enzyme structure and function
- Drug discovery and design
- Process and strain engineering
- Interaction and close collaboration with experts

CURRICULUM VITAE

Dipl.Ing. Sigrid Egger

*Steyrergasse 61 / 2, 8010 Graz
Phone: +43 650 9251931; email: sigrid.egger@tugraz.at*

LANGUAGE SKILLS:

- German: mother tongue
- English: fluent written and spoken
- Italian: fluent
- Spanish, French: basics

COMPUTER SKILLS:

- MS Office (Word, Powerpoint, Excel)
- Sigma Plot, Origin
- Isis Draw / Chem Draw
- Endnote
- Pymol, Isee, Vector NTI

PERSONAL INTERESTS:

- Friends and family
- Sports: Yoga, horseback riding, skiing, mountainbiking, swimming
- Travelling
- Literature and music

INDUSTRIAL EXPERIENCE:

07-08 in 2000 - 2003	Industrial project Infineon Austria Technologies AG, Villach Research and Development Center
1998 - 2005	Promotion T-Mobile Austria

RECOMMENDATION:

Prof. Dr. Bernd Nidetzky	bernd.nidetzky@tugraz.at	TU Graz, Institute of Biotechnology and Biochemical Engineering
Prof. Udo Oppermann	udo.oppermann@sgc.ox.ac.uk	University of Oxford, SGC, UK

CURRICULUM VITAE

Dipl.Ing. Sigrid Egger

Steyrergasse 61 / 2, 8010 Graz
Phone: +43 650 9251931; email: sigrid.egger@tugraz.at

SCIENTIFIC PUBLICATIONS:

Egger S., Chaikuad A., Nidetzky B. UDP-glucose dehydrogenase *Minireview Biochem. Soc. Transact. (Conference Biochemical Society, invited). Submitted.*

Egger S., Chaikuad A., Kavanagh, K.L., Oppermann U., Nidetzky B.: Elucidating the mechanism of human UDP-glucose dehydrogenase - structural and kinetic analysis. *Manuscript in preparation.*

Egger, S., Kratzer, R., Nidetzky, B. Integration of enzyme, strain and reaction engineering to overcome limitations of baker's yeast in the asymmetric reduction of α -keto esters. *Biotechnol Bioeng* 2008, 101:1094-1101.

Kratzer, R., Pukl, M., Egger, S., Vogl, M., Brecker, L., and Nidetzky, B. Enzyme identification and development of a whole-cell biotransformation for asymmetric reduction of *o*-chloroacetophenone. *Biotechnol Bioeng. Submitted.*

Kratzer, R., Pukl, M., Egger, S., Nidetzky, B. Whole-cell bioreduction of aromatic α -keto esters using *Candida tenuis* xylose reductase and *Candida boidinii* formate dehydrogenase co-expressed in *Escherichia coli*, *Microbial Cell Factories* 2008, 7:37.

Straganz G.D., Diebold, A.R., Egger, S., Nidetzky, B., Solomon, E.I. Kinetic and CD/MCD Spectroscopic Studies of the Atypical, 3-His Ligated, Non-heme Fe²⁺ Center in Diketone Dioxygenase: the Role of Hydrophilic Outer Shell Residues in Catalysis, *Biochemistry*. 2010 Feb 9; 49(5):996-1004.

Straganz G.D. Egger S., Aquino, G., D'Auria, S., Nidetzky, B. Exploring the cupin-type-metal coordinating signature of acetylacetonate dioxygenase Dke1 with site-directed mutagenesis: Catalytic reaction profile and Fe²⁺ binding stability of Glu-69→Gln mutant, *Journal of Molecular Catalysis B: Enzymatic*, 2006, 39, 1-4, 171-178.

PDB: 3KHU: Crystal structure of human UDP-glucose dehydrogenase Glu161Gln, in complex with thiohemiacetal intermediate: Chaikuad, A., Egger, S., et al.(SGC) Deposition: 30.10.2009

PDB: 3ITK: Crystal structure of human UDP-glucose dehydrogenase Thr131Ala, apo form: Chaikuad, A., Egger, S., et al. (SGC) Deposition: 28.09.2009

CURRICULUM VITAE

Dipl.Ing. Sigrid Egger

Steyrergasse 61 / 2, 8010 Graz
Phone: +43 650 9251931; email: sigrid.egger@tugraz.at

CONFERENCES:

- | | |
|---------------------|---|
| 30. – 31.03.2010 | Structural glycobiology and human health - Biochemical Society, London, (UK) |
| 21. - 25.02.2010 | 238 th ACS National meeting 2010 San Francisco, CA (USA)
Division: Carbohydrate, general papers |
| 11.02.2010 | 14. Austrian Carbohydrate Workshop (Vienna, Austria) |
| 18. - 21.01.2010 | COST workshop Biocatalysis and Medicinal Chemistry: Crossroads and Synergies, Semmering (Austria) |
| 08. - 09.12.2009 | 1 st RSC/SGC Symposium on Chemical Biology for drug discovery (University of Oxford, UK) |
| 13. - 14.11.2008 | Epigenetic mechanisms in health and disease – from Biology to Medicine (University of Oxford, UK) |
| 17. - 21.08.2008 | 236 th ACS National meeting 2008 Philadelphia, PA (USA)
Division: Carbohydrate based drugs |
| 21.02.2008 | 12. Austrian Carbohydrate Workshop (Vienna, Austria) |
| 30.01. - 05.02.2007 | Linz winter school and winter workshop on biological single molecule research and nano-science |
| 03. - 08.07.2005 | Biotrans 2005 7 th International Symposium on Biocatalysis and Biotransformations (Delft, NL) |

TALKS:

Human UDP-Glucose Dehydrogenase: The potential of structural and molecular enzymology as tools for cancer therapy, Structural glycobiology and human health - Biochemical Society, 30. - 31.03.2010, London, (UK).

Structural, kinetic and mutational insights along the reaction coordinate of human UDP-glucose dehydrogenase, American Chemical Society Meeting 2010, 21. - 25.03.2010, Division Carbohydrate: General Papers, San Francisco, CA (USA).

Structure and function of human UDP-glucose dehydrogenase, 14. Österr. Kohlenhydrat workshop, 11.02.2010, BOKU Vienna, (Austria).

Structure and function of human UDP-glucose dehydrogenase, COST workshop Biocatalysis and Medicinal Chemistry: Crossroads and Synergies, 18. - 21.01.2010, Semmering, (Austria).

Elucidating the mechanism of human UDP-glucose dehydrogenase using kinetic, mutational and structural studies, 236th American Chemical Society Meeting 2008, 17. - 21.08.2008, Division: Carbohydrate based drugs, Philadelphia, PA (USA).